Biogeosciences, 23, 4379–4445, 2026
https://doi.org/10.5194/bg-23-4379-2026

Biogeosciences Open Access EGU

A cross-site comparison of ecosystem- and plot-scale methane fluxes across multiple timescales

Tiia Määttä[1], Ankur R. Desai[2], Masahito Ueyama[3], Rodrigo Vargas[4], Eric J. Ward[5,6], Zhen Zhang[7], Gil Bohrer[8], Kyle Delwiche[9], Etienne Fluet-Chouinard[10], Järvi Järveoja[11], Sara H. Knox[12], Lulie Melling[13], Mats B. Nilsson[11], Matthias Peichl[11], Angela Che Ing Tang[14], Eeva-Stiina Tuittila[15], Jinsong Wang[16], Sheel Bansal[17], Sarah Feron[18], Manuel Helbig[19,20], Aino Korrensalo[21,22], Ken W. Krauss[23], Gavin McNicol[24], Shuli Niu[16], Zutao Ouyang[25], Kathleen Savage[26], Oliver Sonnentag[27], Robert Jackson[28,29], and Avni Malhotra[1,30]

[1]Department of Geography, Faculty of Science, University of Zürich, Winterthurerstrasse 190, 8057 Zürich, Switzerland
[2]Atmospheric and Oceanic Sciences, University of Wisconsin-Madison, Madison, WI 53706, USA
[3]Graduate School of Agriculture, Osaka Metropolitan University, Sakai, 599-8531, Japan
[4]School of Life Sciences, Arizona State University, Tempe, AZ 85287, USA
[5]University of Maryland, Earth System Science Interdisciplinary Center, College Park, MD, USA
[6]NASA Goddard Space Flight Center, Biospheric Sciences Laboratory, Greenbelt, MD, USA
[7]National Tibetan Plateau Data Center (TPDC), State Key Laboratory of Tibetan Plateau Earth System, Environment and Resource (TPESER), Institute of Tibetan Plateau Research, Chinese Academy of Sciences, Beijing, 100101, China
[8]Department of Civil, Environmental & Geodetic Engineering, The Ohio State University, Columbus, OH 43210, USA
[9]Department of Environmental Science, Policy & Management, UC Berkeley, Berkeley, CA, USA
[10]Earth System Sciences Division, Pacific Northwest National Laboratory, Richland, WA, USA
[11]Department of Forest Ecology and Management, Swedish University of Agricultural Sciences, Umeå, Sweden
[12]Department of Geography, McGill University, Montreal, Canada
[13]UN Sustainable Development Solutions Network, Asia Headquarters, Sunway University, 47500 Bandar Sunway, Selangor, Malaysia
[14]Department of Environmental Sciences, University of Toledo, Toledo, OH, USA
[15]School of Forest Sciences, Joensuu campus, University of Eastern Finland, Joensuu, Finland
[16]Key Laboratory of Ecosystem Network Observation and Modeling, Institute of Geographic Sciences and Natural Resources Research, Chinese Academy of Sciences, Beijing, 100101, China
[17]U.S. Geological Survey, Northern Prairie Wildlife Research Center, Jamestown, ND, USA
[18]University of Groningen, Leeuwarden, the Netherlands
[19]GFZ Helmholtz Centre for Geosciences, Potsdam, Germany
[20]Department of Physics and Atmospheric Science, Dalhousie University, Halifax, Canada
[21]Department of Environmental and Biological Sciences, University of Eastern Finland, Kuopio, Finland
[22]Natural Resources Institute Finland, Joensuu, Finland
[23]Louisiana Universities Marine Consortium (LUMCON), Chauvin, LA 70344, USA
[24]Department of Earth and Environmental Sciences, University of Illinois Chicago, Chicago, IL, USA
[25]College of Forestry, Wildlife and Environment, Auburn University, Auburn, AL, USA
[26]Woodwell Climate Research Center, Falmouth, USA
[27]Université de Montréal, Département de géographie, Montréal, QC, Canada
[28]Department of Earth System Science, Stanford University, Stanford, 94305, USA
[29]Woods Institute for the Environment and Precourt Institute for Energy, Stanford University, Stanford, 94305, USA
[30]Biological Sciences Division, Pacific Northwest National Laboratory, 902 Battelle Boulevard, Richland, WA, USA

Correspondence: Tiia Määttä (tiia.maatta@geo.uzh.ch)

Published by Copernicus Publications on behalf of the European Geosciences Union.

Received: 10 October 2025 – Discussion started: 27 October 2025
Revised: 23 April 2026 – Accepted: 15 May 2026 – Published: 3 July 2026

Abstract. Wetland and upland ecosystems play significant but opposing roles in the global methane (CH_4) budget, acting as natural sources and sinks, respectively. Two of the most common approaches for measuring CH_4 fluxes (FCH_4) are chambers, which measure fluxes at fine spatial scales (ca. $1\,m^2$), and eddy covariance (EC) towers, which integrate fluxes across larger footprints (ca. $100–10\,000\,m^2$). Although chamber and EC observations have been combined in various syntheses and databases to estimate CH_4 budgets, a unified cross-site evaluation of FCH_4 estimates at plot and ecosystem scales is lacking. As a first step toward a systematic spatiotemporal scaling of EC tower and chamber footprints, we quantified differences in site-level aggregate FCH_4 between EC and chamber measurements (ΔFCH_4) across ten wetland and upland sites at half-hourly, hourly, daily, weekly, monthly, and annual timescales. We found that ecosystem-scale median FCH_4 was consistently higher than plot-scale FCH_4 at all temporal scales, with the smallest difference at the daily timescale (multi-site median ΔFCH_4: $1.36\,nmol\,m^{-2}\,s^{-1}$; median ecosystem-scale $FCH_4 = 1.56\,nmol\,m^{-2}\,s^{-1}$, median plot-scale $FCH_4 = 0.06\,nmol\,m^{-2}\,s^{-1}$) and the largest at annual scales ($2.58\,nmol\,m^{-2}\,s^{-1}$; median ecosystem-scale $FCH_4 = 25.91\,nmol\,m^{-2}\,s^{-1}$, median plot-scale $FCH_4 = 6.55\,nmol\,m^{-2}\,s^{-1}$). In general, the agreement between ecosystem- and plot-scale FCH_4 decreased with finer temporal resolution (from Spearman $\rho = 0.95$ at the annual scale to $\rho = 0.65$ at the half-hourly scale), while ΔFCH_4 variation was greatest at daily-to-annual scales. Key environmental predictors of ΔFCH_4 across the ten sites included plot-scale spatial heterogeneity, dominant vegetation type, vapor pressure deficit, atmospheric pressure, and friction velocity at the daily and monthly scales. Wind direction was a significant predictor only at the monthly scale, suggesting EC footprint effects at these sites. These findings suggest that accounting for variability in EC footprint extent, chamber measurement placement, and measurement artifacts is key to reconciling multi-scale FCH_4 observations across diverse ecosystems and refining CH_4 budgets.

1 Introduction

Methane (CH_4), a potent greenhouse gas, is produced in wetlands and consumed in upland soils- respectively the largest natural CH_4 sources and sinks globally. However, the magnitude of these fluxes remains highly uncertain (IPCC, 2023; Saunois et al., 2025). Field measurements of CH_4 fluxes (FCH_4) are often conducted using enclosed chamber systems or eddy covariance (EC) towers (Bansal et al., 2023b). Chambers are typically deployed at point scale ($<1\,m^2$) to capture plot-scale spatial heterogeneity in CH_4 source-sink dynamics within the study area (Livingston and Hutchinson, 1995; Morin et al., 2017; Virkkala et al., 2018). Chamber measurements can be manual or automated. Manual measurements are more labor-intensive and therefore result in a temporally sporadic sampling pattern (typically few per month). Automated chambers offer more consistent finer-scale temporal sampling (typically half-hourly over seasons) but high instrumentation cost can restrict their spatial coverage. Thus, chamber measurements generally involve a trade-off between temporal resolution and spatial representation of the ecosystem (Barba et al., 2018; McGuire et al., 2012; Morin et al., 2014, 2017).

In contrast, EC towers continuously measure FCH_4 with high temporal resolution (typically half-hourly) over seasons and years (Morin, 2019; Morin et al., 2017). The EC technique is based on the principle that the measured FCH_4 originating from the tower footprint area ($100–10\,000\,m^2$) is carried upwards and outward toward the sensor by turbulent diffusion (Aubinet et al., 2012; Morin et al., 2014). Therefore, a single half-hourly EC measurement represents a mixed observation at the ecosystem scale located over a somewhat uncertain footprint area. The EC footprint changes from one observation to the other and may include a mixture of distinctly different ecosystem and hydrological patches, contributing to the EC FCH_4 uncertainties (Chu et al., 2021; Xu et al., 2018). At the ecosystem subtype scale (i.e., plot scale), chamber measurements represent fixed sampling points with well-defined spatial location but limited areal extent. Averaging multiple chamber observations from the same plot (defined as spatial replicates) increases the area representation of the chamber observation, but it is still several orders of magnitude smaller than EC measurements. While both approaches provide complementary perspectives on ecosystem FCH_4, the data provided by each method pose different challenges for model parameterization or evaluation of relevant ecosystem FCH_4 processes across spatial and temporal scales.

Many global and regional FCH_4 models are parameterized using EC FCH_4 data because of its consistent temporal sampling and because the EC reporting standard include environmental covariates (e.g., McNicol et al., 2023; Oikawa et al., 2024; Peltola et al., 2019; Ueyama et al., 2023b). Community-contributed datasets, such as FLUXNET-CH_4 (Delwiche et al., 2021; Knox et al., 2019), offer unprecedented opportunity to access EC FCH_4 data from around the globe. However, even large collaborations such as FLUXNET-CH_4 only cover a relatively small number of

locations globally and are missing important coverage in key ecosystems (e.g., tropics; Delwiche et al., 2021; Zhu et al., 2024). FCH_4 data from manual chamber campaigns are cheaper and simpler to deploy and are, therefore, implemented in a larger number of sites globally. Thus, sites with chambers provide a greater global measurement coverage than EC sites and could fill the missing data gaps. As a result, data from EC and chamber methods are sometimes compiled to augment syntheses and budget estimations (Hill and Vargas, 2022b; Kuhn et al., 2021; Yuan et al., 2024). Integration of plot-scale chamber FCH_4 data into ecosystem-scale EC datasets poses several challenges due to methodological differences (Hill and Vargas, 2022b). These challenges also apply to carbon dioxide (CO_2) measurements: studies have noted significant discrepancy in CO_2 fluxes between EC and chambers, partly due to manual chambers (and sometimes EC) often lacking nighttime measurements (Barba et al., 2018; Phillips et al., 2017). Chamber and EC FCH_4 measurements also contain different uncertainties due to varying methods for measuring chamber gas concentration (e.g., gas chromatography vs high-precision CH_4 analyzers) and different EC and chamber instrument makes and models (Christiansen et al., 2015; Peltola et al., 2014; Pihlatie et al., 2013). To our knowledge, a systematic comparison of FCH_4 from these different scales across multiple sites, has not been conducted (but see Davidson et al., 2017).

Plot- and ecosystem-scale FCH_4 can differ due to different FCH_4 source areas, measurement artifacts, uncertainties of the chamber and EC methods, and differences in their response to environmental FCH_4 drivers. In many comparison studies conducted in wetland and upland ecosystems, chamber FCH_4 is higher than EC FCH_4 (Chaichana et al., 2018; Clement et al., 1995; Davidson et al., 2017; Krauss et al., 2016; Marushchak et al., 2016; Meijide et al., 2011; Morin et al., 2017; Riutta et al., 2007), although some studies report the opposite (Budishchev et al., 2014; Forbrich et al., 2011; Hill and Vargas, 2022b; Schrier-Uijl et al., 2010; Wang et al., 2013) and others find that the direction of the difference varies between years (Korrensalo et al., 2018). Since the attribution of surface cover type and location is better defined in chamber measurements, chamber FCH_4 sampling can offer more representative estimates of FCH_4 variability within a site (Bansal et al., 2023a). However, chambers capture a small portion of the landscape, are often placed in high-emitting hotspots, do not sample over tall vegetation patches, and may incorporate sampling location biases (Bansal et al., 2023b). This can lead to higher observed fluxes at the sampled plots, than the mean ecosystem-scale FCH_4 as measured by EC (but see Voigt et al., 2023). For example, placing chambers over CH_4-emitting hollows in a peatland could bias ecosystem FCH_4 estimates, as the lower FCH_4 in other peatland microtopographic forms and margins may not be captured (e.g., Bubier, 1993, 1995; Juselius-Rajamäki et al., 2025; Waddington and Roulet, 2000).

The EC method integrates FCH_4 over the constantly moving and often spatially heterogeneous footprint, and the surface cover types within the footprint differ substantially in FCH_4. For example, in wetlands, the EC footprint may include non-flooded areas where FCH_4 is expected to be near zero (Kutzbach et al., 2004; Riutta et al., 2007; Sha et al., 2011), which can also introduce significant bias to ecosystem FCH_4 estimates (Morin et al., 2017). Environmental variables that influence FCH_4 variability, such as soil temperature, water table level, and net ecosystem CO_2 exchange, could also predict cross-scale FCH_4 differences given the different processes influencing FCH_4 across spatial and temporal scales (Knox et al., 2021; Morin et al., 2014; Turetsky et al., 2014). EC observations are sensitive to environmental variables, such as wind speed and direction, that affect the extent and location of the observation footprint, while chamber measurements should likely be unaffected by these (Wang et al., 2013). While some studies have evaluated EC-chamber FCH_4 differences with spatially explicit FCH_4 upscaling or downscaling, many of these studies have been conducted in individual sites (e.g., Budishchev et al., 2014; Marushchak et al., 2016; Morin et al., 2017; Schrier-Uijl et al., 2010). Thus, an exploration of bulk-scale FCH_4 differences between ecosystem- and plot-scale FCH_4 (based on spatiotemporal aggregations) and their controls across multiple sites can help in directing future research efforts utilizing EC footprint modeling to reconcile cross-scale FCH_4 differences.

Here, we explore the differences between ecosystem and plot-scale FCH_4 (ΔFCH_4) measured by EC and chamber systems, respectively, and identify the time scales and environmental conditions at which the two data types agree best. We (1) compared co-located and contemporaneous EC and chamber FCH_4 rates across multiple sites and examined how the differences ranged across temporal scales (half-hourly to annual), and (2) investigated the potential predictors of ΔFCH_4 at these sites. To achieve this, we utilized FCH_4 data commonly used by the FCH_4 community, i.e., gap-filled EC data and chamber data quality-controlled in different ways by data providers. We hypothesized that plot-scale FCH_4 would be higher than ecosystem-scale FCH_4 as chambers often selectively target FCH_4 hotspots and manual chamber measurements are often conducted at warmer daytime conditions. We also expected that ΔFCH_4 is highest during daytime when most chamber measurements are conducted and plant activity is high, the latter of which is fully captured by towers but not always by manual chambers (Knox et al., 2021; Yu et al., 2013).

We hypothesized that larger variance (suggesting higher spatiotemporal heterogeneity) observed in chambers and EC measurements would increase ΔFCH_4, and that the different temporal resolutions of manual and automated chambers would further contribute to ΔFCH_4. Finally, we expected that the temporal scale of data aggregation could influence the magnitude of ΔFCH_4, and we hypothesized that ΔFCH_4 would be lower at coarser (seasonal to annual) than at finer

(hourly to daily) temporal aggregations. This comparison of bulk FCH_4 rates is a key first step toward standardized harmonization of EC tower and chamber footprints to account for spatiotemporal heterogeneity across multiple sites.

2 Methods

2.1 Study sites

We compiled ecosystem-scale (EC) and plot-scale (chamber) FCH_4 data from ten sites, representing different climatic conditions and ecosystem types (two uplands and eight wetlands; Fig. 1, Table 1). Each site differed in the number of days with both chamber and EC measurements ($n = 5$–759), the number of chambers used ($n = 3$–18), the year of observations (range across sites: 2012–2020), and whether the chambers were automated or manual (Table C1 and Fig. B1). The site selection was based on the availability of coincident EC and chamber FCH_4 data. EC data were obtained from the FLUXNET-CH_4 database (Delwiche et al., 2021; Knox et al., 2019) and chamber data were provided by site principal investigators in response to a call for data via the FLUXNET-CH_4 network. The sites are located in China, Finland, Sweden and the USA. Most sites have a humid continental ($n = 3$) or subarctic climate ($n = 3$), with others located in humid subtropical ($n = 3$) and cold subtropical highland ($n = 1$) regions (Table 1).

2.2 Datasets and data compilation

2.2.1 Chamber and EC CH_4 flux data

The FCH_4 data were selected based on coincident plot- and ecosystem-scale FCH_4 observations. The plot-scale chamber FCH_4 data for each site were obtained from the site principal investigators. Each dataset included FCH_4 (varying units) and additional environmental variables, such as soil temperature and water table level. Chamber datasets comprised measurements from both manual ($n = 6$ sites; taken 1–3 times per month) and automated chamber methods ($n = 4$ sites; taken at half-hourly or hourly intervals, see Table C1; Subke et al., 2021). Chamber fluxes for all sites were calculated by the data providers using linear regression of change in CH_4 concentration over time. None of the chamber FCH_4 data were gap-filled, and in some cases ($n = 4$ sites), ebullition events had been filtered out by the data providers (Table C2). The decision to utilize chamber FCH_4 data with differing ebullition removal protocols across data providers was intended to reflect the way ebullition data are dropped in chamber studies. Typically, FCH_4 measurements are excluded from analyses when linear regressions between timepoints fall below a user-defined R^2 threshold (Jentzsch et al., 2025). These data exclusions may contribute to differences between bulk ecosystem- and plot-scale FCH_4 estimates. We designated CH_4 emission with positive, and CH_4 uptake with negative signs.

The ecosystem-scale EC datasets for each site (except US-StJ, see below) were obtained from the FLUXNET-CH_4 database (Delwiche et al., 2021; Knox et al., 2019). These data include both gap-filled and non-gap-filled FCH_4 values ($\mathrm{nmol\,m^{-2}\,s^{-1}}$) at a half-hourly resolution along with various meteorological and environmental variables. We used gap-filled EC FCH_4 in the analyses but excluded data during long data gaps (>2 months) when the gap-filled values may be a significant source of uncertainty (Delwiche et al., 2021). Gap-filling was performed using artificial neural networks (ANN; Knox et al., 2019) which have shown good performance for FCH_4 data gap-filling (Irvin et al., 2021; Knox et al., 2016, 2019).

CN-Hgu EC FCH_4 data showed anomalous extreme CH_4 uptake and isolated extreme positive FCH_4 spikes. Therefore, we filtered out EC FCH_4 values where (1) CH_4 uptake exceeded $-100\,\mathrm{nmol\,m^{-2}\,s^{-1}}$ (empirically determined threshold; Chen et al., 2019, 2020), (2) nighttime (incoming shortwave radiation $<10\,\mathrm{W\,m^{-2}}$; Morin et al., 2014) friction velocity (u^*) $< 0.1\,\mathrm{m\,s^{-1}}$ (Chen et al., 2019, 2020), and (3) single extreme positive FCH_4 spikes occurred beyond the monthly 99.5th FCH_4 percentile where nighttime air temperature was within 1 °C of its dew point (calculated with Magnus formula and Alduchov & Eskridge constants; Alduchov and Eskridge, 1996; Lawrence, 2005) and the open-path gas analyzer may have had condensation (Heusinkveld et al., 2008). Additional extreme FCH_4 ($FCH_4 = 862\,\mathrm{nmol\,m^{-2}\,s^{-1}}$) associated with friction velocity $= 0.93\,\mathrm{m\,s^{-1}}$ and wind speed $= 0.05\,\mathrm{m\,s^{-1}}$ was removed as an outlier. After filtering, the CN-Hgu dataset was 70 % of the original.

For US-StJ, we obtained EC FCH_4 data from the data providers (Hill and Vargas, 2022b; Vázquez-Lule and Vargas, 2021). As ANN-gap-filled EC FCH_4 values were not available at US-StJ, we used only non-gap-filled EC FCH_4. EC FCH_4 were processed by the data providers following AmeriFlux protocols (Chu et al., 2023; Hill and Vargas, 2022b; Vázquez-Lule and Vargas, 2021).

2.2.2 Environmental data

For all sites (except US-StJ), environmental data were obtained from the FLUXNET-CH_4 EC data product, including ANN-gap-filled net ecosystem CO_2 exchange (NEE), friction velocity (u^*), wind direction (WD), gap-filled wind speed, gap-filled vapor pressure deficit (VPD), and gap-filled air pressure (PA) (Delwiche et al., 2021; Knox et al., 2019). Soil temperature (TS; topmost 2–10 cm depth) data was obtained from FLUXNET-CH_4 and site-specific chamber datasets when available. If a site had TS observations from both chamber and FLUXNET-CH_4 datasets, a mean of both was taken to obtain a site-level TS. Similarly, site-level water table level (WTL) was obtained by utilizing ei-

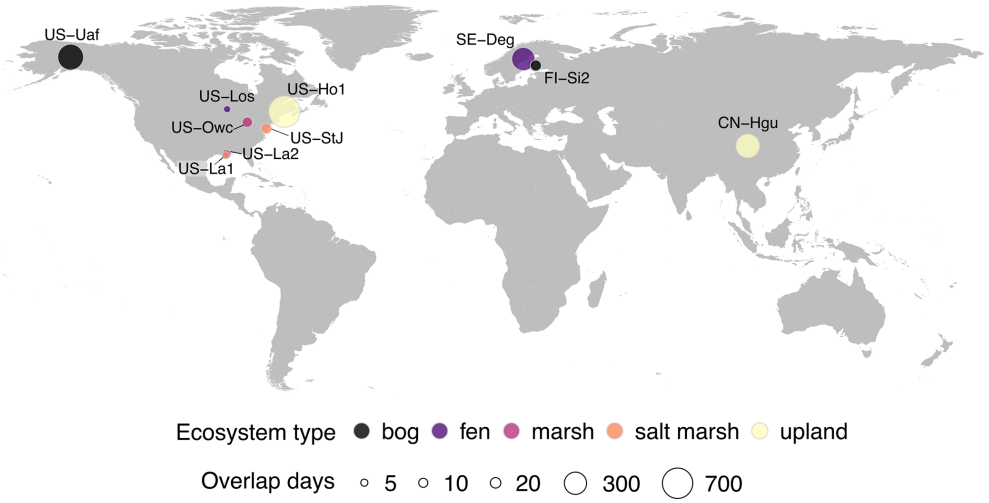

Figure 1. Map of study sites. Point colors indicate ecosystem type and point size reflects the number of overlap days between eddy covariance and chamber measurements (details in Table C1). Ecosystem type follows the site classification in the FLUXNET-CH_4 database (Delwiche et al., 2021; Knox et al., 2019). Base map: Natural Earth (1 : 50 m Cultural Vectors; https://naturalearthdata.com, last access: 1 September 2025), created with R package *maps* (Becker et al., 2023). Country abbreviations: CN = China, FI = Finland, SE = Sweden, US = The United States of America.

ther FLUXNET-CH_4 or chamber-associated WTL measurements, or by taking their mean.

Environmental data for US-StJ were obtained from the data providers (Hill and Vargas, 2022b; Vázquez-Lule and Vargas, 2021). PA, VPD, wind speed, WD, and u^* were not gap-filled, while TS and WTL were gap-filled based on their linear relationships with water temperature and water table level, respectively (Hill and Vargas, 2022b). NEE was gap-filled using marginal distribution sampling moving look-up tables (Hill and Vargas, 2022b).

See a summary of environmental data in Table C3.

2.3 Data processing and harmonization

The chamber datasets were harmonized to a similar structure, and FCH_4 units were standardized to nmol m^{-2} s^{-1}, matching the units used in the FLUXNET-CH_4 EC FCH_4 data. Then, EC and chamber datasets were combined using common timestamps (Fig. 2). To evaluate differences across temporal aggregations, we aggregated data at six temporal scales: (1) half-hourly (automated chamber data only; CN-Hgu, SE-Deg, US-Ho1, US-Uaf; $n = 4$ sites), (2) hourly (CN-Hgu, SE-Deg, US-Ho1, US-Uaf; $n = 4$ sites), (3) daily (all sites, $n = 10$ sites), (4) weekly ($n = 10$ sites), (5) monthly ($n = 10$ sites), and (6) annual ($n = 10$ sites) (Fig. 2). Note that most sites did not include snow-covered periods, and the datasets primarily represent the snow-free season.

The data were aggregated from the timestamp-aligned data by taking the median of FCH_4 measurements (non-normally distributed), mean of NEE (normally distributed) and wind u and v components (see Sect. 2.4.2), and median of the rest of the environment and meteorological variables (non-normally distributed). Half-hourly aggregation was created by taking the median of chamber measurements for each EC timestamp. To check for robustness of our results from the median-based temporal aggregations, we also created temporal aggregations based on FCH_4 means. In addition, we calculated cumulative sums (mg CH_4 m^{-2}) of chamber and EC FCH_4 at daily, weekly, monthly, and annual scales to see how EC-chamber differences scale up to ecosystem CH_4 budgets. As the chamber FCH_4 data from FI-Si2, US-La1, and US-La2 lacked hourly timestamps, we estimated daily cumulative FCH_4 for these sites by using the daily median or mean chamber FCH_4 and multiplied it by 48 while EC cumulative FCH_4 was calculated based on half-hourly EC FCH_4 from FLUXNET-CH_4. As this is not an accurate estimate of daily cumulative chamber FCH_4 for EC-chamber FCH_4 comparisons, we included these sites only in site-specific analyses and excluded them from cross-site analyses.

The difference between ecosystem and plot-scale FCH_4 was calculated as the row-wise difference between instantaneous EC FCH_4 and chamber FCH_4 (ΔFCH_4) in each aggregated dataset by subtracting chamber FCH_4 from the corresponding EC FCH_4 on the same timestamp. For supplementary analyses, we calculated the difference between cumulative EC FCH_4 and chamber FCH_4 at daily, weekly, monthly, and annual scales.

Table 1. Environmental characteristics of the study sites during the FCH_4 observation periods. Site classification, dominant vegetation, air temperature, precipitation, and water table level data were obtained from half-hourly FLUXNET-CH_4 and chamber datasets (Delwiche et al., 2021; Knox et al., 2019). Mean air temperature, total precipitation, and mean water table level were calculated over the EC-chamber overlap periods used in the analyses. Negative water table level indicates that water table level was below the soil surface. Köppen climate abbreviations: Cwc = cold subtropical highland, Dfc = subarctic, Dfb = warm-summer humid continental, Cfa = humid subtropical, Dwc = monsoon-influenced subarctic climate. Column abbreviations: TA = air temperature, P = total precipitation, WTL = water table level, Vegetation = site dominant vegetation type, Overlap days = number of days with both EC and chamber FCH_4 observations. In Overlap days, values marked with and without asterisk (*) represent automated and manual chambers, respectively. Country abbreviations: CN = China, FI = Finland, SE = Sweden, US = The United States of America.

FLUXNET-CH_4ID	Site name	Climate (Köppen)	Site classification	TA (°C)	P (mm)	WTL (min, max; cm)	Vegetation	Overlap days	Month coverage	Chamber FCH_4 data ref.	EC FCH_4 data ref.
CN-Hgu	Hongyuan	Cwc	upland (alpine meadow)	2.6	386	–	Aerenchymatous	363*	February–November	Wang et al. (2021)	Niu and Chen (2020)
FI-Si2	Siikaneva-2 Bog	Dfc	bog	14.6	14	−11.6 (−39, 15.2)	*Sphagnum* moss	26	May–October	Korrensalo et al. (2018)	Alekseychik et al. (2021); Vesala et al. (2020)
SE-Deg	Degerö	Dfc	fen	4.7	394	−1.35 (−10.2, 0.8)	*Sphagnum* moss	338*	May–October	Bond-Lamberty et al. (2020); Järveoja et al. (2018)	Nilsson and Peichl (2020)
US-Ho1	Howland Forest	Dfb	upland (needleleaf forest)	6.9	838	−53.6 (−112, 8.19)	Tree	759*	April–November	Richardson et al. (2019)	Richardson and Hollinger (2020)
US-La1	Pointe-aux-Chenes Brackish Marsh	Cfa	salt marsh	24.7	9	−0.99 (−13.3, 3.13)	Aerenchymatous	5	March–May, September–October	Krauss et al. (2016)	Holm et al. (2020a)
US-La2	Salvador WMA Freshwater Marsh	Cfa	marsh	26	15	1.33 (−8.79, 24.1)	Aerenchymatous	10	January, March–October	Krauss et al. (2016)	Holm et al. (2020b)
US-Los	Lost Creek	Dfb	fen	18.4	92	−11.2 (−16.1, −4.89)	Ericaceous shrub	5	June–August	Desai (2025b)	Desai (2025a); Desai and Thom (2020)
US-Owc	Old Woman Creek	Dfb	marsh	15.2	468	73.9 (35, 120)	Aerenchymatous	18	June–October	Bohrer et al. (2019)	Bohrer et al. (2020)
US-StJ	St Jones Reserve	Cfa	salt marsh	20	520	30.1 (−39, 102)	Aerenchymatous	16	May–December	Hill and Vargas (2022a)	Hill and Vargas (2022b); Vázquez-Lule and Vargas (2021)
US-Uaf	University of Alaska, Fairbanks	Dwc	bog	−0.2	262	−12.5 (−37.8, 12.9)	*Sphagnum* moss	458*	May–October	Ueyama et al. (2022)	Iwata et al. (2020)

2.4 Statistical analyses

2.4.1 Differences between ecosystem and plot-scale FCH_4 observations

We used non-parametric statistics to analyze the FCH_4 data (EC, chamber and ΔFCH_4), because the data were skewed and non-normal. To test the statistical significance ($\alpha = 0.05$) of ΔFCH_4 and to assess ΔFCH_4 differences between chamber types at different temporal scales, we used Wilcoxon-Mann-Whitney tests (*wilcox.test* from *stats*; R Core Team, 2024). Since the mean-based temporal aggregations were used as a sensitivity check, only descriptive statistics and Wilcoxon-Mann-Whitney tests were conducted for the mean-based aggregations (results in Table C4). Similarly, cumulative FCH_4 were analyzed with descriptive statistics and Wilcoxon-Mann-Whitney tests (results in Table C5). The rest of the methods described here were conducted on the median-based temporal aggregations of instantaneous FCH_4.

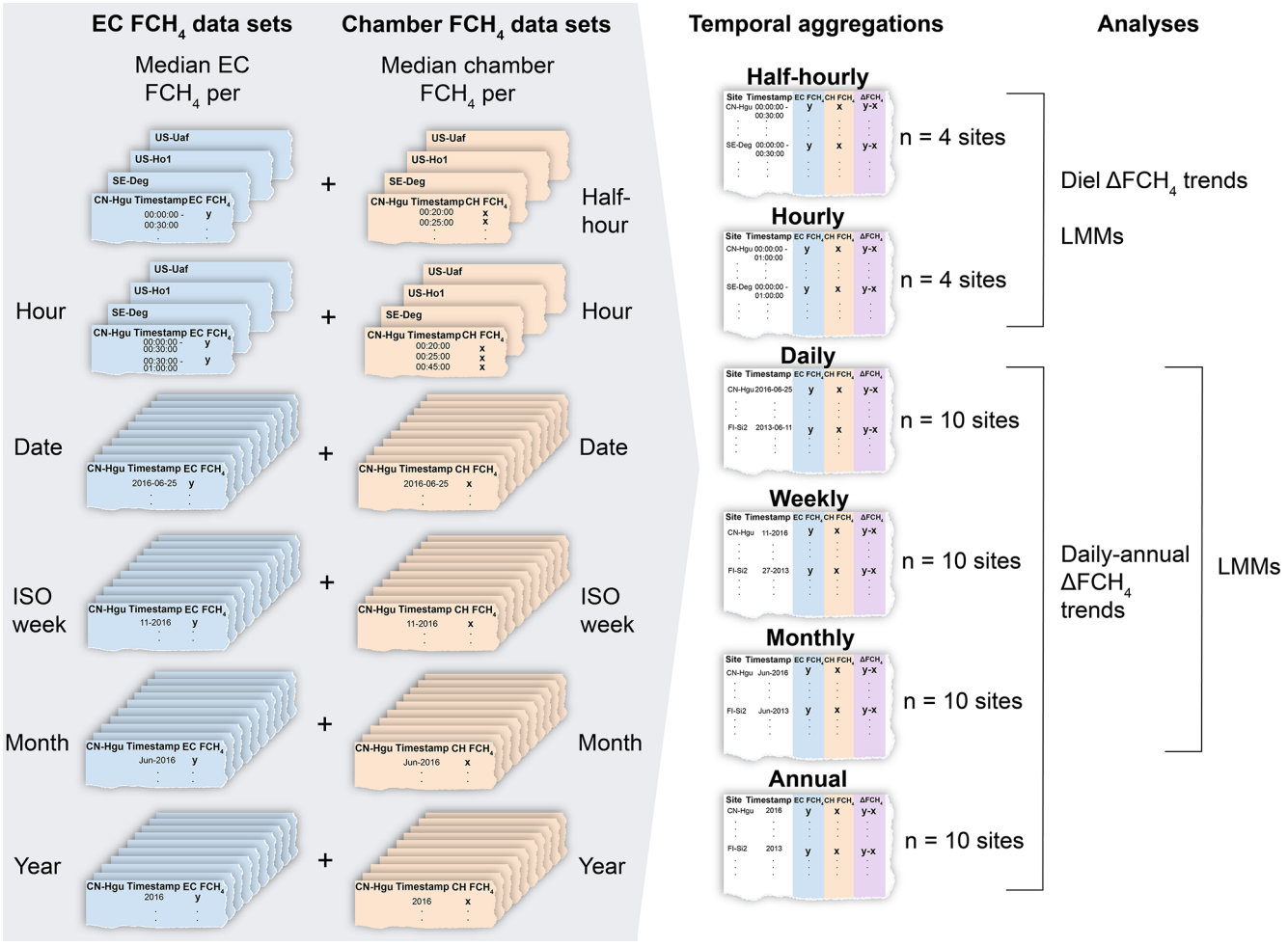

Figure 2. Overview of the main data aggregation workflow. Site-specific eddy covariance (EC) methane (CH_4) flux (FCH_4; blue) and chamber FCH_4 (orange) datasets were combined by taking the median FCH_4 per timestamp (half-hour to annual scale). ISO week is the week number according to the ISO-8601 standard. Then, site-level datasets were combined into multi-site datasets at six temporal scales: half-hourly, hourly, daily, weekly, monthly, and annual. Half-hourly EC FCH_4 data was not aggregated as it was already in half-hourly scale. ΔFCH_4 (purple) was calculated by subtracting median chamber instantaneous FCH_4 from median EC instantaneous FCH_4 per timestamp per site, and this measure was used in all analyses and linear mixed effects models (LMMs). Note that we also created temporal aggregations by taking the mean of EC and chamber FCH_4, and these data sets were used as a sensitivity check with descriptive statistics and pairwise comparisons.

To estimate the slopes of the EC FCH_4–chamber FCH_4 relationship, we built simple linear mixed effects models with site as the random effect using function *lme* from package *nlme* (Pinheiro and Bates, 2000; Pinheiro et al., 2023). For better interpretability of model slopes (in contrast to Yeo-Johnson-transformed values, see Sect. 2.4.2) and to meet the residual normality assumptions of linear mixed modeling, we transformed EC FCH_4 with inverse hyperbolic sine (Table C6). Due to non-convergence and residual non-normality, half-hourly and hourly scales were not assessed for EC-chamber FCH_4 slopes. As the data were non-normally distributed and did not meet the assumptions of linear regression, we used Spearman correlations together with normalized root mean square error (using the standard deviation of pooled EC and chamber FCH_4 as the denominator at each temporal scale) to assess the direction and strength of the relationship between EC FCH_4 and chamber FCH_4, manual and automated chamber FCH_4, as well as FCH_4 magnitude (row-wise mean of EC and chamber FCH_4) and absolute ΔFCH_4.

We used Kruskal-Wallis tests (*kruskal.test* from *stats*; R Core Team, 2024) to test for differences in ΔFCH_4 across hours and months (treated as categorical variables) within each temporal aggregation (half-hourly, hourly, daily, weekly, monthly, and annual). Then, we identified the significantly differing groups using the Conover-Iman post hoc test (function *conover.test* from package *conover.test*; Dinno, 2024).

2.4.2 Predictors of FCH_4 differences between ecosystem and plot scales

We built linear mixed models to estimate the predictors of ΔFCH_4. The aim was to explore how the predictors influence the direction of ΔFCH_4 (i.e., more positive or negative ΔFCH_4 or, in other words, increase ecosystem-scale FCH_4 in relation to plot-scale FCH_4 or vice versa) at the ten sites. To meet the assumptions of linear mixed modeling and to improve residual diagnostics (normality and homoscedasticity of residuals) for model inference, we applied Yeo-Johnson power transformation (Yeo and Johnson, 2000) to absolute ΔFCH_4 values using the function *yeojohnson* from *bestNormalize* (Peterson, 2021). This transformation can be applied to zero values, and it improved our residual diagnostics, which were important for model inference. Acknowledging the difficulty to interpret the precise effect sizes after this transformation, we used this model only to investigate the directionality of ΔFCH_4. All models were built with the function *lme* from *nlme* (Pinheiro and Bates, 2000; Pinheiro et al., 2023).

To evaluate potential predictors of ΔFCH_4, we included environmental and temporal variables available in the FLUXNET-CH_4 and chamber datasets in the models. The predictor selection was based on literature. They included: TS (°C), WTL (cm), PA (kPa), u^* ($m\,s^{-1}$), WD (degrees), VPD (hPa), NEE ($\mu mol\,CO_2\,m^{-2}\,s^{-1}$), month (categorical), site dominant vegetation (VEG; categorical; "tree", "ericaceous shrub", "aerenchymatous", "brown moss", and "*Sphagnum* moss"; taken from Delwiche et al., 2021), and hour (categorical; only with half-hourly and hourly datasets). We included EC-specific variables, such as u^* and WD, as proxies for EC footprint to assess how variables contributing to the EC footprint may affect ΔFCH_4. While two of the VEG classes (tree and ericaceous shrub) were only represented in one site, preliminary linear regression model comparisons showed that VEG explained a large proportion of the ΔFCH_4 variance ($R^2 = 0.4$–0.7), and its inclusion in linear mixed models substantially improved model fit. Therefore, we included VEG as a fixed effect, while acknowledging that for tree and ericaceous shrub classes, the estimated effect may be related to the site rather than vegetation.

For all models, the reference level in VEG was *Sphagnum* moss, 0 in Hour, and May in Month. As WD is a circular variable ($0° = 360°$), we represented WD as a continuous function of wind direction and speed by separating WD into orthogonal u and v wind components (uWD and vWD, respectively), which were averaged from the half-hourly EC datasets in hourly, daily, weekly, monthly, and annual aggregations (Appendix A1). As a result, uWD represents the strength of west-east wind while vWD represents the strength of north-south wind. This representation avoided discontinuity at $360° = 0°$ and potential multicollinearity between model predictors.

For improved model convergence and β-coefficient calculations, Yeo-Johnson-transformed absolute ΔFCH_4 and all predictors were centered and scaled, except hour, month and VEG, which were categorical variables and were included without centering and scaling. To account for multicollinearity, we chose predictors based on Pearson correlation matrices (threshold $|r| < 0.7$) and checked variance inflation factors (VIF; threshold ≤ 3) using the function *vif* from *car* (Fox and Weisberg, 2018). Due to multicollinearity ($VIF > 3$), we built two separate half-hourly models containing either month or TS, two weekly models without NEE or VPD, and a monthly model without VPD and TS. WTL data was not available for CN-Hgu, and thus, this site was excluded from the models.

After accounting for temporal autocorrelation and residual variance (Appendix A2), we used backward variable selection based on likelihood ratio tests (AIC and p-values) together with type I ANOVA tests to determine significant predictors of Yeo-Johnson-transformed absolute ΔFCH_4. During variable selection, the models were fitted with maximum likelihood, and the final models were refitted with restricted maximum likelihood for statistical inference. Model marginal and conditional R^2 were calculated with the function *r.squaredGLMM* from package *MuMIn* (Bartoń, 2024). To test how well the models generalize to other sites, we validated the models with leave-one-site-out cross validation and evaluated model performance with R^2, mean absolute error (MAE) and root mean square error (RMSE) between observed and predicted values. To allow for predictions to new sites with the training data, the fixed effect VEG had to be removed from the models, as some of the VEG classes (tree and ericaceous shrub) were represented only by a single site and the effect of these classes cannot be estimated when they are withheld in the test data. Similarly, due to uneven temporal coverage across sites, observations (e.g., date or year-month) included in the test data but not present in the training data were excluded from evaluation.

We built linear mixed effects models to investigate the effect of spatiotemporal FCH_4 variation on ΔFCH_4. To represent the FCH_4 variation between individual chambers within each site, we calculated the interquartile range (IQR) of chamber FCH_4 from an unaggregated dataset per each site and temporal scale unit (i.e., per day, week, month, or year). To see whether temporal variation within each temporal scale unit in EC FCH_4 may affect absolute ΔFCH_4, we also calculated EC FCH_4 IQR per each site and temporal scale unit. In the models, log-transformed absolute ΔFCH_4 was the response variable, and either log (+0.01)-transformed chamber IQR or log (+0.01)-transformed EC IQR was the explanatory variable, or both were included as explanatory variables to assess their relative effects on absolute ΔFCH_4.

All data processing and statistical analyses were carried out using R v4.3.3 (R Core Team, 2024).

3 Results

3.1 Ecosystem and plot-scale FCH_4 differ most at finer temporal scales

Ecosystem- (EC) and plot-scale (chamber) FCH_4 differed significantly at half-hourly to weekly scales (Table 2). Median ecosystem FCH_4 was higher than plot-scale FCH_4 at all temporal aggregations (half-hourly to annual: 102 %, 109 %, 104 %, 90 %, 58 %, and 87 % higher, respectively). However, the coefficient of variation (CV, %) for ΔFCH_4 was large, particularly in daily (674 %) and weekly (467 %) aggregations (Table 2). Across temporal aggregations and site-years, CH_4 emissions ($FCH_4 > 0$) above the 90th percentile contributed a larger share of total (sum) plot-scale FCH_4 than ecosystem-scale FCH_4 (mean-based aggregations; Table 2, Fig. B2), possibly indicating more CH_4 emission hot spots and hot moments at the plot scale. Our observed trend persisted when we aggregated chamber and EC FCH_4 data with means instead of medians (Tables C4 and C5). In the mean-based aggregations, median ΔFCH_4 ranged between 0.28 nmol m^{-2} s^{-1} (annual) and 1.23 nmol m^{-2} s^{-1} (half-hourly) but mean ΔFCH_4 turned increasingly negative from daily (-1.16 nmol m^{-2} s^{-1}) to annual (-70.94 nmol m^{-2} s^{-1}) scales, highlighting plot-scale CH_4 emission hotspots and hot moments as possible ΔFCH_4 drivers. Ecosystem- and plot-scale FCH_4 were positively correlated across temporal aggregations, with annual aggregation having the best agreement, while the worst agreements were in half-hourly and hourly aggregations (Fig. 3). Using linear mixed models, we showed that an increase of 1 nmol m^{-2} s^{-1} in plot-scale FCH_4 was associated with an ecosystem-scale FCH_4 increase of 0.007 nmol m^{-2} s^{-1} ($p = 0.03$) at daily plot-scale FCH_4 median (0.06 nmol m^{-2} s^{-1}), 0.01 nmol m^{-2} s^{-1} ($p = 0.066$) at weekly plot-scale FCH_4 median (0.51 nmol m^{-2} s^{-1}), 0.009 nmol m^{-2} s^{-1} ($p = 0.183$) at monthly plot-scale FCH_4 median (4.07 nmol m^{-2} s^{-1}), and 0.019 ($p = 0.044$) at annual plot-scale FCH_4 median (6.55 nmol m^{-2} s^{-1}; see Table C6 for details).

Ecosystem- and plot-scale FCH_4 differed between hours, months, and sites. In support of our hypotheses, the highest ΔFCH_4 occurred between 5 AM and 3 PM ($p<0.001$; Figs. B4–B7), with maximum median ΔFCH_4 at 9 AM (2.01 nmol m^{-2} s^{-1}, IQR: 6.16; half-hourly scale) and minimum at 8 PM (0.9 nmol m^{-2} s^{-1}, IQR: 4.16; half-hourly scale). However, the diel ΔFCH_4 trends varied between sites and months ($p<0.001$; Figs. B8–B12). The highest absolute ΔFCH_4 (with observations from all sites) was in August, September, and October (half-hourly to daily $p<0.001$; Fig. B13). In addition, ΔFCH_4 varied in both magnitude and direction within and between sites (Kruskal-Wallis $p<0.001$; half-hourly to monthly scale), with most medians being positive (Tables C6–C11 and Figs. B14–B15). The difference between cumulative sums of ecosystem- and plot-scale FCH_4 increased from daily to annual scales but the seasonal and inter-annual trends varied between sites (Table B4, Fig. B16). The largest absolute ΔFCH_4 medians and CVs were consistently found in US-Owc (median: -108.22 nmol m^{-2} s^{-1}, CV: 169 %; daily scale), while the lowest absolute ΔFCH_4 and FCH_4 were consistently found in US-Ho1 (median $\Delta FCH_4 < 1$ nmol m^{-2} s^{-1}; Tables C6–C11).

Flux magnitude, measured as the mean between EC and chamber FCH_4 (FCH_{4_mean}), was generally positively related to ΔFCH_4 but negative relationships existed when $FCH_{4\_mean} < 0$ (i.e., net uptake). The positive FCH_4 magnitude and absolute ΔFCH_4 relationship became stronger at coarser temporal resolutions (Spearman $p<0.001$; Fig. 4). In all aggregations, the higher ΔFCH_4 came from a higher ecosystem-scale FCH_4 than from a higher plot-scale FCH_4 (≥ 70 % of all observations when $FCH_{4\_mean} > 0$; result not shown). In half-hourly and hourly aggregations, ΔFCH_4 and FCH_{4_mean} were negatively or positively related when FCH_{4_mean} suggested net uptake or emission, respectively (Fig. 4a and b). When $FCH_{4\_mean} < 0$, ecosystem-scale FCH_4 was generally higher than plot-scale FCH_4 (57 % and 58 % of all observations when $FCH_{4\_mean} < 0$ in half-hourly and hourly aggregations, respectively; result not shown). However, most of the highest observations originate from CN-Hgu. Sites also differed in whether the trends in negative FCH_4 came from higher plot or ecosystem-scale FCH_4: for example, at US-Uaf and CN-Hgu, 100 % and 91 % of ΔFCH_4 observations at $FCH_{4\_mean} < 0$, respectively, consisted of higher plot-scale FCH_4 while ca. 66 % of hourly and half-hourly observations ($FCH_{4\_mean} < 0$) in US-Ho1 came from higher ecosystem-scale FCH_4.

3.2 Predictors of ecosystem and plot-scale FCH_4 differences

3.2.1 Atmospheric pressure, friction velocity and wind direction drive daily-to-monthly FCH_4 differences between ecosystem and plot scales

The significance and effect size of ΔFCH_4 predictors varied across temporal aggregations, with site dominant vegetation type having the highest effect sizes at the daily-to-monthly scale (Table 3). Dominance of aerenchymatous vegetation had relatively high effect sizes ($|\beta$-coefficient$| > 0.68$). However, only one site was classified as tree-dominated (US-Ho1) and ericaceous shrub-dominated (US-Los), while three were aerenchymatous and two were *Sphagnum*-moss dominated. Thus, we were unable to separate true vegetation-related effects from site effects.

PA and u^* were significant ΔFCH_4 predictors at the daily and monthly scales (but weekly PA $p = 0.057$), while VPD was significant only at the daily scale. However, the effect sizes were relatively low (β-coefficient ≤ 0.25; Table 3). Wind direction (uWD) was a significant ΔFCH_4 predictor only in the monthly scale. Month was a significant predic-

https://doi.org/10.5194/bg-23-4379-2026

Table 2. Ecosystem- (eddy covariance; EC) and plot-scale (chamber) methane (CH_4) flux (FCH_4) difference (ΔFCH_4) at different temporal aggregations. A positive ΔFCH_4 indicates a higher ecosystem- than plot-scale FCH_4 and vice versa. The EC and chamber data sample sizes in Wilcoxon-Mann-Whitney tests are reported as n_{EC} and n_{CH}, respectively. The 90th percentiles (p90, without parentheses) and proportion (%, in parentheses) of chamber and EC CH_4 emission observations (where $FCH_4 >$ p90 and $FCH_4 > 0$) of the total chamber or EC FCH_4 sum show the contribution of high CH_4 emissions to total CH_4 emissions (see site-specific trends in the unaggregated dataset in Fig. B2). Abbreviations: IQR = interquartile range, SD = standard deviation, CV = coefficient of variation.

Aggregation	ΔFCH_4 median (IQR), nmol m^{-2} s^{-1}	ΔFCH_4 mean (SD), nmol m^{-2} s^{-1}	ΔFCH_4 CV (%)	Chamber FCH_4 median (IQR), nmol m^{-2} s^{-1}	EC FCH_4 median (IQR), nmol m^{-2} s^{-1}	Chamber FCH_4 mean (SD), nmol m^{-2} s^{-1}	EC FCH_4 mean (SD), nmol m^{-2} s^{-1}	Chamber FCH_4 p90, nmol m^2 s^{-1} (% of total FCH_4)	EC FCH_4 p90, nmol m^2 s^{-1} (% of total FCH_4)	Wilcoxon-Mann-Whitney test
Half-hourly	1.4 (5.67)	5.61 (17.71)	196	0.27 (5.79)	1.55 (6.97)	5.88 (14.07)	11.49 (24.25)	33.44 (46)	64.31 (44)	$p<0.001$ ($n_{EC} = 74\,482$, $n_{CH} = 74\,482$)
Hourly	1.41 (5.28)	6.08 (15.34)	191	0.15 (4.07)	1.39 (6.68)	4.98 (12.36)	11.05 (23.59)	45.76 (47)	63.92 (44)	$p<0.001$ ($n_{EC} = 40\,072$, $n_{CH} = 40\,072$)
Daily	1.36 (4.27)	4.01 (81.49)	674	0.06 (4.79)	1.53 (6.27)	13.98 (106.34)	18.0 (69.09)	43.18 (75)	68.5 (60)	$p<0.001$ ($n_{EC} = 1879$, $n_{CH} = 1879$)
Weekly	1.44 (5.29)	−0.62 (105.8)	467	0.51 (11.9)	3.0 (31.19)	34.28 (155.8)	33.66 (103.49)	112.64 (76)	78.08 (63)	$p<0.001$ ($n_{EC} = 349$, $n_{CH} = 349$)
Monthly	1.46 (14.82)	−8.14 (151.18)	350	4.07 (46.41)	5.88 (60.3)	75.55 (223.01)	67.42 (161.75)	247.77 (69)	219.98 (64)	$p = 0.082$ ($n_{EC} = 121$, $n_{CH} = 121$)
Annual	2.58 (24.59)	−1.37 (63.6)	194	6.55 (67.22)	25.91 (53.29)	76.84 (185.83)	75.47 (145.95)	220.35 (64)	250.78 (57)	$p = 0.507$ ($n_{EC} = 22$, $n_{CH} = 22$)

Table 3. Linear mixed effects model results identifying environmental predictors of ecosystem- and plot-scale methane (CH_4) flux (FCH_4) difference (ΔFCH_4) at different temporal scales. Fixed effects are listed in decreasing order based on their β-coefficients. Significant predictors are highlighted in bold. Half-hourly and hourly models had very low marginal R^2 (<0.05) and were excluded from this table. See half-hourly and hourly models in Table C14 and full models in Table C15. Abbreviations: SE = standard error, Df = degrees of freedom, LOOCV = leave-one-out cross validation, MAE = mean absolute error, RMSE = root mean square error, VEG = site dominant vegetation, PA = air pressure (kPa), u^* = friction velocity ($m\,s^{-1}$), WTL = water table level (cm), TS = soil temperature (°C), NEE = net ecosystem CO_2 exchange ($\mu mol\,CO_2\,m^{-2}\,s^{-1}$), VPD = vapor pressure deficit (hPa), vWD = v wind component ($m\,s^{-1}$), uWD = u wind component ($m\,s^{-1}$).

Dataset	Predictors	β-coefficient	SE	p-value (t-test)	Marginal R^2	Conditional R^2	Df	Random effect variation explained, %	LOOCV		
									R^2	MAE	RMSE
Daily	Intercept	0.4867	0.361	0.1779	0.5346	0.9265	1363		−1.65	1.48	1.76
($n = 9$	Fixed effects										
sites)	VEG										
	– Tree	−1.4718	0.6767	0.0816			5				
	– Aerenchymatous	1.0111	0.4723	0.0852			5				
	Month										
	– **Jul**	0.4939	0.1685	**0.0043**			87				
	– **Aug**	0.4577	0.1696	**0.0084**			87				
	VEG										
	– Ericaceous shrub	0.4333	0.7104	0.5686			5				
	Month										
	– Sep	0.2851	0.1656	0.0886			87				
	– Apr	0.234	0.3683	0.5269			87				
	– Dec	0.2281	0.5059	0.6533			87				
	– Oct	0.1884	0.1689	0.2677			87				
	– Jun	0.1595	0.1658	0.3389			87				
	– Nov	0.1118	0.2356	0.6363			87				
	– Mar	−0.0735	0.5003	0.8835			87				
	TS	−0.0525	0.0269	0.051			1371				
	VPD	−0.0457	0.0109	**0**			1371				
	u*	0.0342	0.0076	**0**			1371				
	PA	−0.0259	0.0072	**0**			1371				
	uWD	0.0052	0.0066	0.4305			1371				
	vWD	0.0043	0.007	0.5423			1371				
	NEE	0.0017	0.0104	0.8679			1371				
	WTL	0.0012	0.0376	0.9745			1371				
	Random effects										
	Site							59.59			
	Year–month							24.62			

Table 3. Continued.

Dataset	Predictors	β-coefficient	SE	p-value (t-test)	Marginal R^2	Conditional R^2	Df	Random effect variation explained, %	LOOCV		
									R^2	MAE	RMSE
Weekly	Intercept	0.5066	0.3402	0.1381	0.5554	0.8351	178		−0.82	1.25	1.46
($n = 9$	Fixed effects										
sites)	VEG										
	– Tree	−1.3455	0.6772	0.1036			3				
	– Aerenchymatous	0.8552	0.4642	0.1248			3				
	– Ericaceous shrub	0.5256	0.6837	0.4767			3				
	PA	−0.0716	0.0374	0.0572			178				
	Random effects										
	Site							62.91			
	Year-month							$1.03e^{-05}$			
Monthly	Intercept	−0.2243	0.3145	0.4778	0.6599	0.8788	80		−0.57	1.04	1.25
($n = 9$	Fixed effects										
sites)	Month										
	– Mar	1.4967	1.4236	0.2962			80				
	VEG										
	– **Aerenchymatous**	1.2901	0.4307	**0.0303**			5				
	– Ericaceous shrub	0.7673	0.6684	0.3029			5				
	Month										
	– **Apr**	0.6774	0.2947	**0.0241**			80				
	VEG										
	– Tree	−0.5482	0.5955	0.3995			5				
	PA	−0.2535	0.1046	**0.0177**			80				
	uWD	0.2322	0.0666	**0.0008**			80				
	$\boldsymbol{u^*}$	−0.1875	0.0774	**0.0176**			80				
	Month										
	– Oct	−0.1805	0.1432	0.2111			80				
	WTL	0.1375	0.0809	0.0931			80				

Table 3. Continued.

Dataset	Predictors	β-coefficient	SE	p-value (t-test)	Marginal R^2	Conditional R^2	Df	Random effect variation explained, %	LOOCV		
									R^2	MAE	RMSE
	Month										
	– Dec	0.1258	0.3948	0.7509			80				
	NEE	0.1069	0.0664	0.1114			80				
	Month										
	– Sep	0.0963	0.1475	0.5158			80				
	vWD	0.0686	0.0501	0.1747			80				
	Month										
	– Jul	0.0608	0.1465	0.6789			80				
	– Jun	0.0461	0.1408	0.7442			80				
	– Nov	−0.0404	0.2062	0.8453			80				
	– Aug	0.021	0.1456	0.8857			80				
	Random effects										
	Site							64.35			

tor only in the final half-hourly-daily models, where August and July had the highest effect sizes (β-coefficient > 0.41). Morning hours, particularly 5 AM, were most important in the half-hourly-hourly models (5 AM β-coefficient > 0.08). However, the fixed effects in the final half-hourly and hourly models explained a very small proportion of the total variation (marginal R^2 <0.05, Tables C14–C15). In addition, the high conditional R^2 and high negative LOOCV R^2, high MAE and RMSE showed that the ΔFCH_4 predictors are specific to the sites included in this study (Table 3).

3.2.2 Spatial FCH_4 variation increases ecosystem and plot-scale FCH_4 difference

Spatial variation between FCH_4 measurements by individual chambers increased absolute ΔFCH_4 (Fig. 5). The increasing trend between chamber IQR (log + 0.01) and absolute ΔFCH_4 (log) became clearer in coarser temporal scales, where a unit (e-fold; ca. 2.7×) increase in monthly and annual chamber FCH_4 variation (IQR + 0.01) was associated with ca. 51 % and 63 % increase in absolute ΔFCH_4, respectively (marginal $R^2 \geq 0.31$, $p \leq 0.01$). Temporal EC FCH_4 variation (e.g., within date at the daily scale) did not lead to strong increases in absolute ΔFCH_4 at daily-to-monthly aggregations (marginal $R^2 < 0.01$), but the annual mixed effects model showed a ca. 198 % increase in absolute ΔFCH_4 with a unit increase in EC FCH_4 IQR (+0.01; marginal $R^2 = 0.82$). Models with both chamber and EC IQR (log + 0.01) as explanatory variables showed significant chamber IQR at daily-to-monthly aggregations (p<0.001, marginal $R^2 = 0.06$–0.31) and significant EC IQR at daily scale ($p = 0.005$). In contrast, the annual model had a non-significant chamber IQR and significant EC IQR ($p = 0.001$, marginal $R^2 = 0.81$). The sites also differed in the strength and direction of the relationship between chamber and EC FCH_4 variation and ΔFCH_4 (Fig. 5).

3.2.3 Ecosystem and plot-scale FCH_4 difference does not significantly vary among chamber types

We did not find significant differences in ΔFCH_4 between automated and manual chambers at all aggregations (Wilcoxon-Mann-Whitney; daily $p = 0.948$, weekly $p = 0.361$, monthly $p = 0.565$, annual $p = 0.722$). However, ΔFCH_4 in manual chambers had higher variation than automated chambers at the daily (CV_{manual} = 284 %, $CV_{automated}$ = 181 %), weekly (CV_{manual} = 262 %, $CV_{automated}$ = 181 %), and monthly (CV_{manual} = 240 %, $CV_{automated}$ = 182 %) scales. The correlations between chamber FCH_4 and EC FCH_4 for both automated and manual chambers were strong at the daily-to-annual scales (ρ>0.7, Fig. B19).

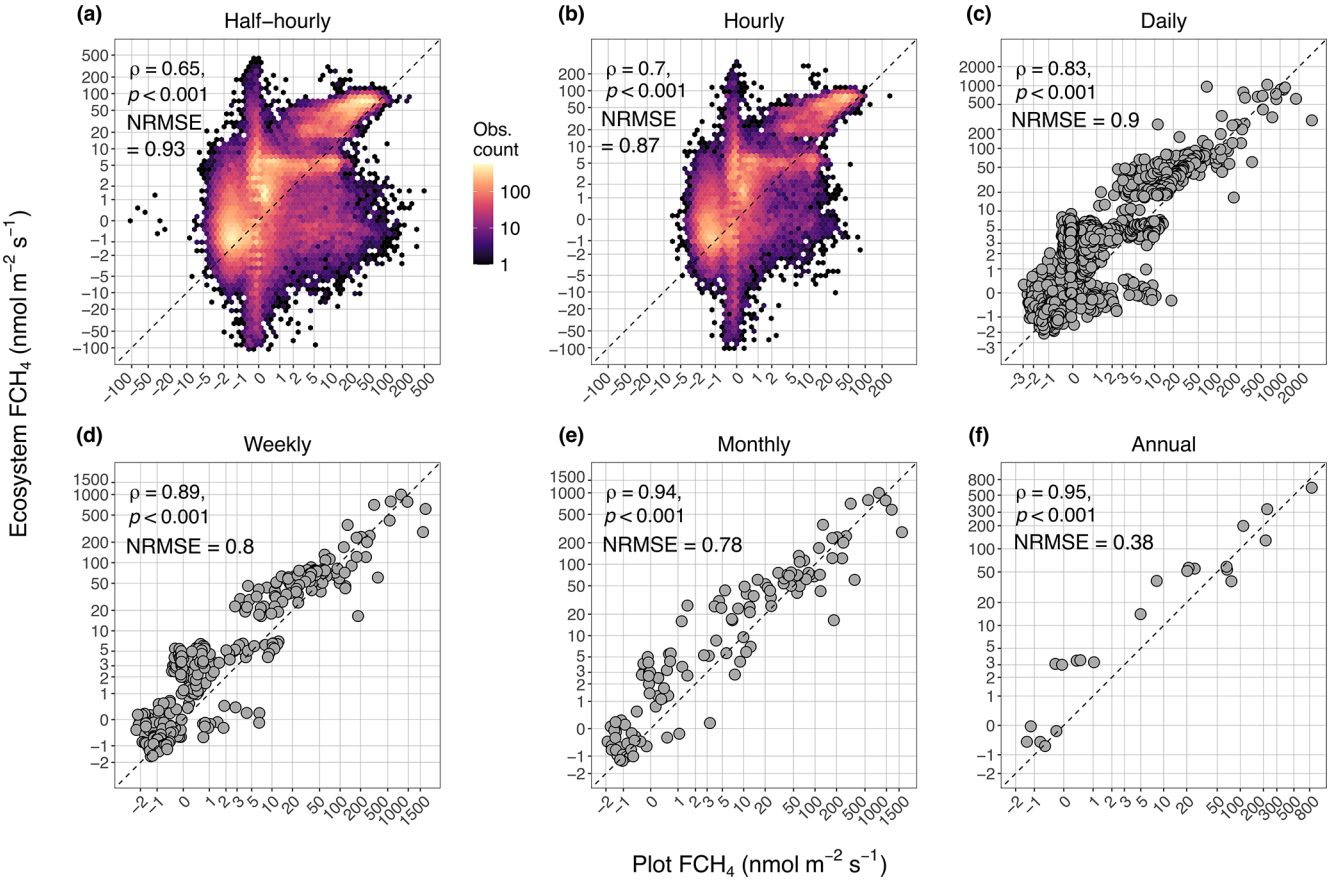

Figure 3. Results of correlation test (Spearman rank correlation coefficient, ρ, its significance level, p, and the normalized root mean square error, NRMSE) between plot-scale (chamber) methane (CH_4) flux (FCH_4) and ecosystem-scale (eddy covariance; EC) FCH_4 at half hourly **(a)**, hourly **(b)**, daily **(c)**, weekly **(d)**, monthly **(e)**, and annual scales **(f)**. For visualization, the plot axes **(a–f)** were transformed with inverse hyperbolic sine to spread out points in the low FCH_4 range and retain negative values (see untransformed plots in Fig. B3). Spearman ρ was calculated with untransformed data. NRMSE was calculated by dividing RMSE by the standard deviation of untransformed ecosystem- and plot-scale FCH_4 at each temporal aggregation. In **(a)** and **(b)** the points for half-hourly ($n = 74\,482$) and hourly ($n = 40\,072$) aggregations are shown in hexagonal density clouds with log10-transformed color range to highlight trends in high point density areas (colors represent number of observations per hexagon). Agreement between chamber and EC FCH_4 improves from finer to coarser temporal aggregations **(a–f)**, as indicated by ρ. The high observation densities in**(a)** and **(b)** reveal site-specific trends in the discrepancy between ecosystem and plot scales (e.g., at $x = 0$ and $y = 5$). For daily **(c)**, weekly **(d)**, monthly **(e)**, and annual **(f)** aggregations, sample sizes were $n = 1879$, 349, 121, and 22, respectively. The dashed line represents 1 : 1 line.

4 Discussion

4.1 Ecosystem-scale FCH_4 is higher than plot-scale FCH_4 at all temporal scales

As a first step to reconcile the discrepancies in FCH_4 data obtained from ecosystem-scale EC and plot-scale chamber measurements, we explored the cross-scale differences across ten sites and six temporal aggregations. Across all temporal scales, ecosystem-scale (EC) FCH_4 was higher than at the plot scale (chamber). Supporting these results, higher EC FCH_4 than chamber FCH_4 have been observed in an arctic peatland with area-weighted chamber FCH_4 (Budishchev et al., 2014), a managed peat meadow with upscaled chamber FCH_4 (Schrier-Uijl et al., 2010), a peatland with downscaled EC FCH_4 (Forbrich et al., 2011), a temperate forest with spatial chamber FCH_4 averages (Wang et al., 2013), and a temperate salt marsh with spatio-temporal chamber and EC FCH_4 averages (Hill and Vargas, 2022b). Other studies at individual sites have observed higher chamber FCH_4 (upscaled to ecosystem-level with different methods) than EC FCH_4 (Chaichana et al., 2018; Clement et al., 1995; Davidson et al., 2017; Krauss et al., 2016; Marushchak et al., 2016; Meijide et al., 2011; Morin et al., 2017; Riutta et al., 2007). Nonetheless, the median difference was relatively low across sites and temporal aggregations (min 1.36 daily, max 2.58 nmol m^{-2} s^{-1} annual), with CV ranging from a minimum of 191 % (hourly) to a maximum of 674 % (daily; Table 2), indicating relatively good agreement between ecosys-

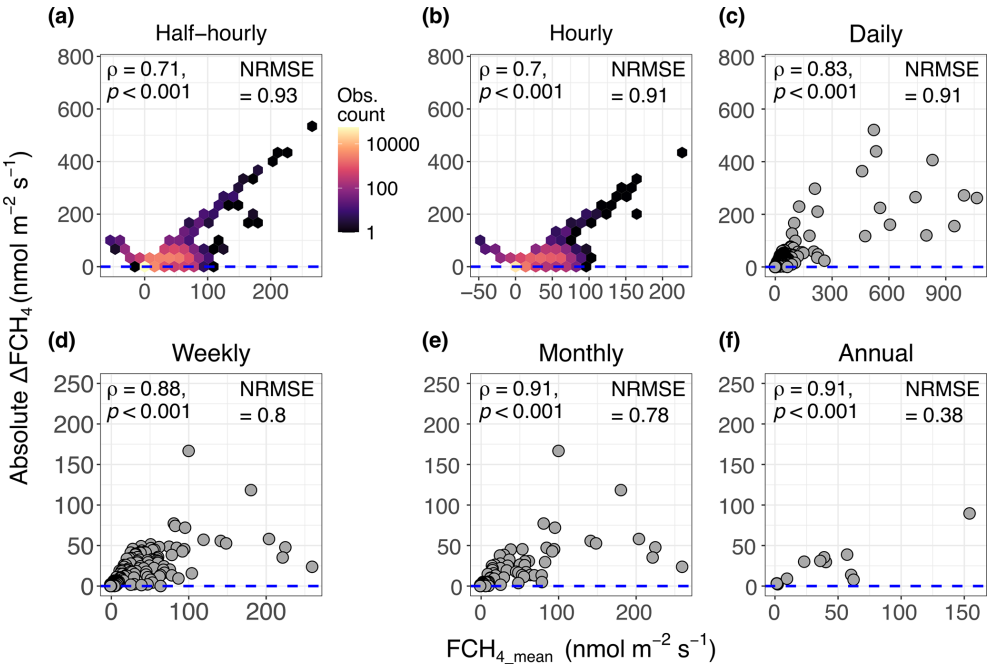

Figure 4. The relationship between methane (CH_4) flux (FCH_4) magnitude (FCH_{4_mean}) and absolute difference between ecosystem-scale (eddy covariance; EC) and plot-scale FCH_4 (ΔFCH_4) from half-hourly **(a)** to annual **(f)** scales, represented by Spearman correlation coefficient, (ρ), its significance, (p), and normalized root mean square error of ΔFCH_4 (NRMSE). FCH_{4_mean} is the row-wise mean of EC FCH_4 and chamber FCH_4. In**(a)** and **(b)** half-hourly and hourly points are shown in hexagonal density clouds with a log-transformed color range to highlight trends in high point density areas (colors represent number of observations per hexagon). Plots **(c)**–**(f)** show daily, weekly, monthly and annual aggregations, respectively. The blue dashed line represents $\Delta FCH_4 = 0$ meaning complete agreement between ecosystem and plot-scale FCH_4. Higher Spearman correlation coefficient ($\alpha = 0.05$) represents stronger deviation from $\Delta FCH_4 = 0$. NRMSE was calculated by dividing RMSE (of ΔFCH_4) by the standard deviation of ecosystem- and plot-scale FCH_4 at each temporal aggregation. For visualization, outliers were removed from daily ($n = 3$), weekly ($n = 10$), monthly ($n = 8$) and annual ($n = 1$) plots but the Spearman correlations and NRMSE are based on original data. See plots with outliers in Fig. B17 and a figure showing how high CH_4 emissions from ecosystem and plot scales contribute to annual CH_4 emissions per site in Fig. B2.

tem and plot-scale FCH_4 across sites despite high variability. While our higher ecosystem- than plot-scale FCH_4 trend was robust across temporal scales, due to the limited data availability ($n = 10$ sites), our results reflect site differences and generalizations should be tested when more data become available.

We found the best general agreement between instantaneous ecosystem- and plot-scale FCH_4 at the monthly and annual aggregations, with the agreement improving from fine to coarse temporal resolutions. The improved agreement is likely a result of the data aggregation, which reduces the influence of inter-daily FCH_4 variability and inflates correlation coefficients (e.g., Clark and Avery, 1976; Pollet et al., 2015). In addition, mean ΔFCH_4 at the weekly, monthly, and annual scales was negative (i.e., higher plot-scale than ecosystem-scale FCH_4; Table 2), and the CV for the weekly aggregation in particular was large (467 %) (Table 2). These results indicate that high CH_4 emissions and FCH_4 variability in plot-scale measurements are associated with more negative ΔFCH_4, particularly at time scales longer than daily (Table 2 and Fig. B2). This suggests that combining plot- and ecosystem-scale bulk FCH_4 at heterogeneous sites is particularly problematic at coarse temporal scales. However, footprint-aware comparisons between upscaled chamber or downscaled EC FCH_4 could show better agreement between ecosystem and plot scales (e.g., Schrier-Uijl et al., 2010) (see Sect. 4.6). Nonetheless, these results highlight the practice of selective chamber placement on high-emitting locations and time periods (Hill and Vargas 2022b; Vargas and Le, 2023). However, our results based on cumulative FCH_4 (Table C5) also show that ecosystem-scale cumulative FCH_4 are generally higher than at plot scale. Therefore, site-level CH_4 budgets calculated with ecosystem-scale FCH_4 data can exceed plot-scale estimates despite localized plot-scale CH_4 emission peaks (with site-specific variation; Fig. B16).

Mismatches in capturing site FCH_4 heterogeneity, and chamber measurement artifacts may have contributed to the higher ecosystem-scale FCH_4 and ΔFCH_4 variation. Chamber measurements are challenged by tall vegetation and ebullition events are often discarded, which could artificially bias chamber FCH_4 estimates. The EC footprints may have covered high-CH_4-emitting areas (i.e., CH_4 emission hot spots)

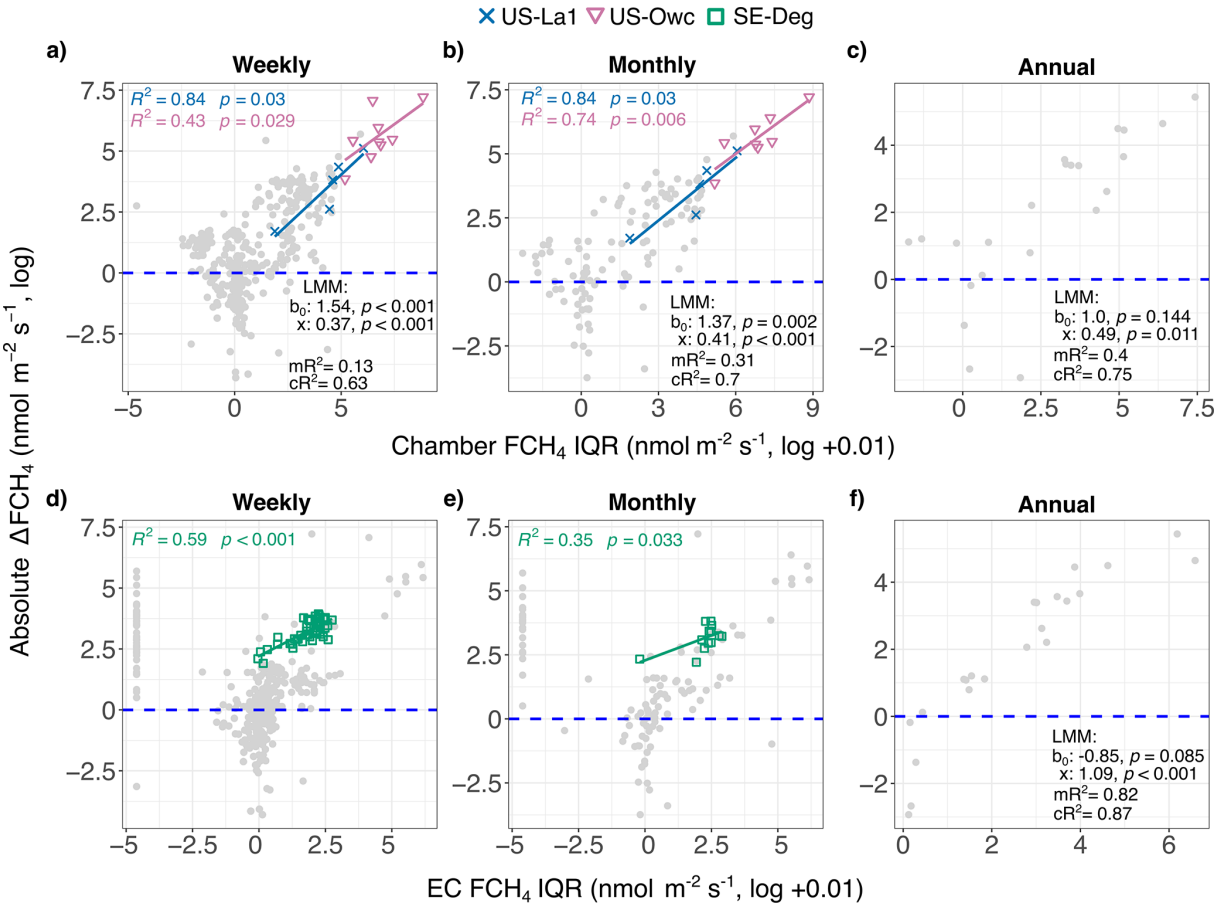

Figure 5. Variation in methane (CH_4) flux (FCH_4) between individual chambers and eddy covariance (EC) timestamps increases absolute ΔFCH_4. **(a–c)** Relationship between chamber FCH_4 variation (variation between individual chambers per aggregation timestamp, represented by interquartile range; IQR) and absolute ΔFCH_4 at weekly **(a)**, monthly **(b)** and annual **(c)** scales. **(d–f)** Relationship between EC timestamp FCH_4 variation (represented by IQR) and absolute ΔFCH_4 at weekly **(d)**, monthly **(e)** and annual **(f)** scales. Linear mixed effects model (LMM) results: b_0 = model intercept, x = predictor (chamber or EC FCH_4 log IQR + 0.01) of log absolute ΔFCH_4, p = predictor significance (preceded by model coefficient estimates), mR^2 and cR^2 = marginal and conditional R^2, respectively. In **(d)** and **(e)** LMM results are not shown due to low marginal R^2 ($mR^2 \leq 0.06$). In **(e)** linear regression results for SE-Deg without data point where $x < 0$: $R^2 = 0.62$ $p = 0.002$. Daily scale is not shown due to the low number ($n = 1$) of sites with significant relationships and low marginal R^2 ($mR^2 \leq 0.06$). Linear regressions, R^2s and p-values are only shown for sites with significant IQR predictor and $R^2 > 0.2$ and are shown in different colors and shapes (gray points: nonsignificant and $R^2 \leq 0.2$ sites). The dashed blue line indicates $\Delta FCH_4 = 0$. See version with untransformed data in Fig. B18.

and ebullition events (i.e., CH_4 emission hot moments) more often than chambers, increasing ΔFCH_4. Although ebullition can also be triggered by chamber placement onto waterlogged soil surface (e.g., Jentzsch et al., 2025), ebullition events were removed from some of the chamber FCH_4 data (see Sect. 2.2.1 and Table C2), so this was unlikely to contribute to the general ΔFCH_4 trends. Indeed, in spatially heterogeneous areas, CH_4 emission hot spots within EC footprints can be important ΔFCH_4 drivers (Desai et al., 2015; Rey-Sanchez et al., 2025; Xu et al., 2018), and at some sites, the majority of FCH_4 is contributed through ebullition (Männistö et al., 2019; Ueyama et al., 2023b; Villa et al., 2021). FCH_4 hot spots and hot moments can also vary in space and time, which manual chamber FCH_4 measurements ($n = 6$ sites) may not capture due to sporadic daytime measurements in weekly or monthly intervals (Anthony and Silver, 2021, 2023; Vargas and Le, 2023). This may result in uncertainties in spatio-temporal FCH_4 and ΔFCH_4 variation across temporal scales (Anthony and Silver, 2021, 2023; Vargas and Le, 2023). The EC footprint effects could be further highlighted by the increasing ΔFCH_4 with greater FCH_4 (Fig. 4), and similar trends were observed in a rice paddy where plot-scale FCH_4 was higher than at ecosystem scale (Meijide et al., 2011). In addition, high CH_4 uptake at the plot scale increased ΔFCH_4 particularly at CN-Hgu (see Sect. 3.1), highlighting selective chamber placement on CH_4-consuming ar-

eas (Table C2). However, ΔFCH_4 in low FCH_4 is uncertain due to EC and chamber detection limits, the reported ranges of which cover the minimum absolute ΔFCH_4 of 0–0.05 nmol m^{-2} s^{-1} (Desai et al., 2015; Erkkilä et al., 2018; Kroon et al., 2007, 2010; Richardson et al., 2019; Smeets et al., 2009). Altogether, the mismatch in EC and chamber footprint coverages, as well as chamber CH_4 ebullition removal, could be important ΔFCH_4 drivers. This highlights the importance of accounting for EC and chamber footprint representativeness as well as chamber data quality control when combining plot- and ecosystem-scale FCH_4 data, particularly at high-FCH_4 sites and time periods (Fig. 4).

4.2 Atmospheric pressure, friction velocity and vapor pressure deficit predict daily and weekly FCH_4 difference between ecosystem and plot scales

PA, u^* and VPD were important daily and weekly-scale ΔFCH_4 predictors. PA is a strong predictor of daily and multiday (ca. 3–21 d) FCH_4 (Knox et al., 2021), and ΔFCH_4 decreased with higher PA (Table 3). Drops in PA have been associated with ebullitive FCH_4 in wetlands (Knox et al., 2021; Nadeau et al., 2013; Sachs et al., 2008; Tokida et al., 2007) and unvented closed chambers can alter chamber air pressure (Jentzsch et al., 2025). Together with chamber CH_4 ebullition filtering (Sect. 2.2.1), this may have led to EC capturing FCH_4 pulses that chamber data did not include. As ebullition events are often removed from chamber FCH_4 data, these results suggest that the large variation in chamber FCH_4 data processing protocols could increase ΔFCH_4 and uncertainty in multi-site syntheses utilizing cross-scale FCH_4 data (e.g., Jentzsch et al., 2025; Levy et al., 2011). Friction velocity likely increased ΔFCH_4 mainly via effects on CH_4 ebullition in open water (Wille et al., 2008), which EC detected but chambers excluded. EC FCH_4 can be underestimated in low u^*, decreasing ΔFCH_4. However, EC FCH_4 under low u^* were filtered out by the FLUXNET-CH_4 team, so low u^* was unlikely to influence the observed ΔFCH_4 trends (Aubinet, 2008; Baldocchi, 2003; Knox et al., 2019; Delwiche et al., 2021). The strong effect size of site dominant vegetation and the negative VPD effect can reflect species- and site-specific stomatal conductance and CH_4 transport (Cernusak et al., 2018; Grossiord et al., 2020). For example, at US-Owc (dominated by aerenchymatous vegetation), plant CH_4 conductance varies spatially and temporally between *Nelumbo lutea*, *Nymphaeae odorata*, and *Typha angustifolia*, which may have been covered differently by chamber and EC FCH_4 footprints (Villa et al., 2020). The importance of plant activity is further supported by the marginally-significant TS (Table 3), a possible proxy for increased plant activity in the peak growing season months in the northern hemisphere (July and August; Table 3). Chamber artifacts could have also contributed to the u^* and VPD effects: short chamber deployments in high u^* and low WTL can underestimate chamber FCH_4 (Lai et al., 2012), while longer measurements (e.g., FI-Si2, US-La1 and US-La2: >30 min) in high WTL can keep stomata open and increase CH_4 transport and chamber FCH_4 (Knapp and Yavitt, 1992; Langensiepen et al., 2012). However, given the limited sample size in the models ($n = 9$ sites) and the low model performance based on leave-one-site-out analyses (Table 3), these results are influenced by site selection and generalizations to other sites are not possible.

As hypothesized, greater variation in FCH_4 between chambers led to higher ΔFCH_4 especially at the weekly to annual scales. Chamber FCH_4 can vary strongly between individual chambers (Davidson et al., 2002) but FCH_4 variation can be even stronger between chamber patches (due to differences in vegetation and microtopography) than within them (Stewart et al., 2024), a factor which was not included in our analyses. Similar to CH_4, spatial variation in soil CO_2 respiration measurements has been an important driver of the discrepancies between ecosystem and soil CO_2 respiration observations, indicating that chambers may weigh soil respiration hot spots and moments more heavily than the larger EC footprints where CO_2 fluxes are averaged out (Phillips et al., 2017). While CH_4 cycling is driven by different controls than CO_2, chambers capturing CH_4 emission hot spots and hot moments may have similarly led to the large ΔFCH_4 CVs and negative mean ΔFCH_4, particularly at the daily and weekly scales in both median and mean-based temporal aggregations (Tables 2 and C4). The spatial variation between chambers could have also contributed to chamber FCH_4 random errors and ΔFCH_4 patterns in Fig. 4 (Levy et al., 2011). Nevertheless, despite the possible importance of chamber CH_4 emission hot spots and moments in driving ΔFCH_4, cumulative plot-scale FCH_4 is increasingly exceeded by higher ecosystem-scale FCH_4 at coarser temporal scales (albeit with site-specific trends; Table C5, Fig. B16).

The FCH_4 variation between chambers and its influence on ΔFCH_4 differed between sites. Between-chamber variation explained ΔFCH_4 best at US-La1 (but $n = 5$) and US-Owc where plot-scale FCH_4 were also higher (Tables C9–C12). At US-Owc, these trends are likely related to spatial FCH_4 heterogeneity: the daily mean FCH_4 range from 500 nmol m^{-2} s^{-1} in open water areas to 21 000 nmol m^{-2} s^{-1} in mud flats, and CH_4 ebullition, diffusion, and plant-mediated CH_4 transport rates are highest at and differ between the *Nelumbo lutea* and *Typha angustifolia*-dominated vegetation patches (Rey-Sanchez et al., 2018; Villa et al., 2020, 2021). In contrast, SE-Deg has a relatively homogeneous vegetation composition dominated by *Sphagnum* spp. mosses, *Eriophorum vaginatum*, and *Andromeda polifolia* (Järveoja et al., 2018), which may explain why EC FCH_4 variation had a better fit than between-chamber FCH_4 variation (Fig. 5). Across sites, the increasing absolute ΔFCH_4 with between-chamber FCH_4 variation may result from the EC footprint capturing patches that only a portion of the chamber measurements may represent. This may be highlighted in sites with manual chamber measurements which were conducted 1–3 times a month and dur-

ing daytime when FCH_4 are often higher than at nighttime (Koebsch et al., 2015; Long et al., 2010; Parmentier et al., 2011) (e.g., US-La1; Fig. 5). However, at some sites median plot-scale FCH_4 was higher than at the ecosystem scale and very high plot-scale FCH_4 contributed more to annual FCH_4 than ecosystem-scale FCH_4, (e.g., US-Owc), highlighting the ability of chambers to capture fine-scale spatial FCH_4 heterogeneity as a ΔFCH_4 driver (Tables C9–C12). Therefore, using representative chamber patches and measurement times to upscale chamber FCH_4 to the EC footprint could potentially decrease ΔFCH_4 (Schrier-Uijl et al., 2010; Vargas and Le, 2023). This could be achieved for example by utilizing statistical optimization for temporal sampling (Vargas and Le, 2023) and matching the chamber, EC and site spatial heterogeneity by surveying the vegetation, hydrological and edaphic properties of the study site, EC footprint, and the surrounding area/region that the footprint represents (e.g., Chu et al., 2021; Schrier-Uijl et al., 2010; Riutta et al., 2007) (see also Sect. 4.6).

4.3 Wind direction, atmospheric pressure and friction velocity drive monthly ecosystem- and plot-scale FCH_4 differences

At the monthly scale ΔFCH_4 was best explained by wind direction (uWD), PA and u^*. Wind direction has been an important EC FCH_4 predictor in wetlands similar to the sites of this study in multiday (ca. 3–21 d) and seasonal (ca. 43–341 d) scales (Knox et al., 2021). The significant effect of uWD may indicate monthly-scale variation in EC footprint and the possibly systematically different land cover coverage than that of chambers, but footprint-aware analyses with a larger sample size are required to confirm these hypotheses. PA and u^* are also considered to be more influential FCH_4 drivers at the diel to multiday scales, which potentially represent ΔFCH_4 seasonality, driven by continental-scale air pressure systems or regional land-sea winds (Griebel et al., 2016; Montaldo and Oren, 2016; Rebmann et al., 2005). The significant and positive effect of aerenchymatous vegetation may further suggest a role of seasonal plant activity with higher CH_4-emitting or -consuming aerenchymatous plant biomass in growing season months (Knox et al., 2021; Niu et al., 2011). The significant effect of April in the monthly model (Table 3) was likely influenced by site-specificity, as only three out of ten sites had observations in that month (Fig. B1, Table 1). Thus, more sites with year-round FCH_4 observations should aid in confirming the significance of, and the possible ΔFCH_4 drivers in, April.

Monthly and annual ΔFCH_4 trends may have also reflected seasonal snow and ice thaw dynamics, as well as changes in the chamber measurement system. The higher ecosystem-scale FCH_4 at CN-Hgu in cooler months (February–April, Fig. B15) may have resulted from spring snowmelt releasing stored CH_4 below the ice and snow cover (Hargreaves et al., 2001; Morin et al., 2017; Rinne et al., 2007; Zhang et al., 2012). These fluxes may be captured by EC but not by chambers since chamber placement in frozen conditions tends to be located further from ice cracks and fissures. Furthermore, due to the practical difficulties with sampling in frozen conditions, FCH_4 data from winter months was limited (Fig. B1, Table 1) and full year co-occurring chamber and EC FCH_4 coverage would allow further investigation of seasonal ΔFCH_4 dynamics. Changes in the chamber measurement system also likely contributed to monthly and interannual ΔFCH_4. In US-Ho1 and US-Uaf, the number of chambers per chamber surface cover class varied between years and months: due to instrument malfunction or chamber replacements, in some timestamps spatial chamber medians did not include CH_4-emitting or -consuming patches while EC did, leading to a large monthly- and annual-scale ΔFCH_4 variation (Richardson et al., 2019; Ueyama et al., 2023a). The chamber footprint variations likely influenced ΔFCH_4 particularly at US-Ho1, where the EC footprint often covers both CH_4-consuming upland forest and CH_4-emitting wetland areas. In contrast, chamber FCH_4 measurements did not always include wetland areas, increasing ΔFCH_4 (Richardson et al., 2019). This further highlights the influence of selective site-specific chamber and EC tower placement and the development of methods for plot selection over time on ΔFCH_4.

4.4 FCH_4 difference between ecosystem and plot scales is highest in the morning and at noon

Our diel analyses revealed that ΔFCH_4 and ecosystem-scale FCH_4 are higher from morning to noon (max ΔFCH_4 at 9 AM) and lower in the evening and at night (min ΔFCH_4 at 8 PM). Higher daytime FCH_4 has been observed particularly during growing seasons (Koebsch et al., 2015; Long et al., 2010; Parmentier et al., 2011), and higher daytime EC FCH_4 than chamber FCH_4 also by Yu et al. (2013). Ecosystem-scale FCH_4 seemed to be driving the monthly diel ΔFCH_4 particularly in July with noon and August with morning FCH_4 peaks, while plot-scale FCH_4 showed less diel variation (Figs. B8–B12). The lack of diel variation in plot-scale FCH_4 possibly resulted from the spatial aggregation of chamber measurements across ecohydrological patches that differ in FCH_4 (e.g., from wet *Carex* sp. to dry lichen in US-Uaf; Ueyama et al., 2023a). Our findings of increasing absolute ΔFCH_4 with FCH_4 (Fig. 4) may reflect these differences, as EC and chamber FCH_4 random error can increase with flux magnitude (Hollinger and Richardson, 2005; Knox et al., 2019; Richardson et al., 2006, 2008), and may also be associated with diel variation in turbulence, EC footprint, and spatial FCH_4 heterogeneity (Hollinger and Richardson, 2005; Knox et al., 2021; Levy et al., 2011), and vary between sites (Delwiche et al., 2021; Richardson et al., 2006). The diel-scale mixed models also had very low explanatory power and high site-specificity (conditional $R^2 > 0.79$), making it difficult to identify drivers for the observed ΔFCH_4

trends. Thus, more sites with hourly chamber FCH_4 measurements could help disentangle the diel ΔFCH_4 predictors.

The high daytime ΔFCH_4 (CN-Hgu, SE-Deg, US-Ho1) could have resulted from diel variation in u^* and VPD. High daytime u^* can enhance ebullition, CH_4 volatilization and release of stored CH_4 from nocturnal boundary layer (Baldocchi, 2003; Long et al., 2010; Morin et al., 2014; Sachs et al., 2008; Wille et al., 2008). Related to VPD, pressurized plant-mediated CH_4 transport peaks from late morning to afternoon, as temperature and humidity gradients between cooler belowground tissues and warmer, drier aboveground air enhance pressure differences that drive gas flow through aerenchyma (van den Berg et al., 2020; Knox et al., 2021; Morin et al., 2014; Vroom et al., 2022; Whiting and Chanton, 1996). However, very high VPD can induce stomatal closure, thereby reducing CH_4 transport (Grossiord et al., 2020). Enhanced stomatal conductance under high solar radiation may have also increased diffusive plant-mediated CH_4 transport (van der Nat et al., 1998), leading to higher daytime ecosystem-scale FCH_4 than plot-scale FCH_4 as dark chambers possibly closed the stomata. However, longer chamber deployment can decrease VPD within the chamber, and reopen the stomata (Knapp and Yavitt, 1992; Langensiepen et al., 2012). In addition, the lower plot- than ecosystem-scale diel FCH_4 at CN-Hgu (e.g., Fig. B9) likely reflected the selective chamber placement at CH_4-consuming areas whereas the EC footprint captured CH_4 emission events more often (Table C2). The high nighttime ΔFCH_4 (US-Uaf) could have been driven by u^*: the nighttime EC footprint may have covered high-CH_4-emitting areas when u^* was low and EC footprint larger (Baldocchi et al., 2012; Chu et al., 2021; Vesala et al., 2008). Deeply-rooted aerenchymatous vegetation (e.g., *Carex* sp.) may have also decreased daytime ecosystem-scale FCH_4 by increasing rhizospheric oxidation and CH_4 consumption under high solar radiation, VPD, and soil temperature (Cho et al., 2012; Zhao et al., 2021, Ueyama et al., 2023a). However, these hypotheses and diel ΔFCH_4 patterns should be explored further with footprint-aware methods (see Sect. 4.6).

4.5 Plot-scale FCH_4 may have been underestimated

EC and chamber techniques fundamentally differ in how ecosystem FCH_4 is measured, which could influence ΔFCH_4. Gas analyzers used for EC can be either open- or closed-path analyzers, the former of which is more sensitive to weather conditions, while the latter is influenced by the choice of the air pump and time lags between sonic anemometer and the gas analyzer (Baldocchi, 2003; Detto et al., 2011). The specific EC CH_4 analyzers can also differ in signal noise (Peltola et al., 2014). However, the random and systematic errors associated with open- and closed-path EC gas analyzers do not contribute significantly to the total EC FCH_4 random error, which may be more affected by the movement of EC footprint and turbulence (Deventer et al., 2019; Knox et al., 2019; Peltola et al., 2014). Thus, the two analyzers agree relatively well in practice and they can be combined in multi-site syntheses (Detto et al., 2011; Deventer et al., 2019; Peltola et al., 2014). However, detecting upland CH_4 uptake rates accurately with open-path analyzers is challenging due to uptake rates often falling within the instrument's detection limits (Chamberlain et al., 2017; Iwata et al., 2014). Of the two upland sites included in this study, these artifacts may have affected the results from CN-Hgu where EC FCH_4 were measured with an open-path gas analyzer.

As manual and automated chambers differ in temporal representation, the similarity in ΔFCH_4 between automated and manual chambers was surprising. The similarity was also reflected in the strong correlations between automated and manual chamber FCH_4 and EC FCH_4 (Fig. B19), which have been observed previously in a Tibetan wetland (Yu et al., 2013). While manual chambers allow researchers to capture higher spatial FCH_4 variation than automated chambers (e.g., Vargas and Le, 2023), the use of spatial medians for chamber FCH_4 may have reduced manual chamber FCH_4 variation so that the resulting median FCH_4 was similar to the FCH_4 measured by automated chambers. However, the higher ΔFCH_4 variation of manual chambers could have also resulted from chamber measurements being conducted 1–3 times a month leading to data gaps (Morin et al., 2014, 2017). Thus, care should be taken when combining manual chamber FCH_4 data with EC FCH_4 data in multi-site syntheses.

Chamber FCH_4 measurement and calculation methodology may have contributed to the generally lower plot-scale FCH_4. As previously discussed (see Sect. 4.1 and 4.2), plot-scale FCH_4 could have been generally underestimated due to the removal of ebullition events from some of the chamber FCH_4 data (Table C2), calling for standardization of chamber-based ebullition measurements and data processing (Jentzsch et al., 2025). In addition, all chamber FCH_4 data was calculated using linear regression which may underestimate FCH_4 (Forbrich et al., 2010; Korkiakoski et al., 2017; Levy et al., 2011; Nakano, 2004; Pihlatie et al., 2013). High-precision CH_4 analyzers, such as cavity ring-down spectrometers and near-infrared laser gas analyzers, could capture nonlinear CH_4 concentration gradients which linear regression fails to do (Forbrich et al., 2010). With gas chromatography, the underestimation and related uncertainties may become even greater due to smaller sample sizes and difficulty in detecting low-quality FCH_4 measurements during chamber measurements (Christiansen et al., 2015; Levy et al., 2011). In sites which used gas chromatography, the number of samples was 4–7 per chamber deployment (e.g., FI-Si2, US-Owc), while sites that used high-precision CH_4 analyzers (CN-Hgu, SE-Deg, US-Ho1, US-Uaf) had ca. 1 Hz sampling interval, resulting in vastly different sample sizes per chamber deployment between sites, and thus higher uncertainties in chamber FCH_4. However, linear regression can be statistically more robust for comparing chamber FCH_4

from different sites with varying soil properties (Venterea et al., 2009). Depending on chamber design, chambers can alter soil conditions (e.g., soil moisture) which may also contribute to ΔFCH_4 (Bansal et al., 2023b; Subke et al., 2021). It may be valuable to compare chamber and EC FCH_4 using both linear and exponential fits for chamber FCH_4 (from both high-precision CH_4 analyzers and gas chromatography) to better understand ΔFCH_4 trends across sites.

4.6 Limitations and uncertainties

As we were able to include only ten sites in the analyses, our results are limited by the site-specific climate, vegetation, and methodology. Thus, in order to produce results that would be better generalizable to other sites and regions (e.g., tropics), future studies could include more sites from a variety of climates, ecosystem types, dominant vegetation types, and chamber measurement systems (i.e., automated and manual, gas chromatography and high-precision CH_4 analyzers) ($n>3$ sites per group to allow statistical inference). In addition, year-round FCH_4 observations were lacking, which introduced uncertainty, particularly into the annual ΔFCH_4 trends. While challenging to measure, nongrowing season FCH_4 can be significant (Treat et al., 2018). Thus, future syntheses could include nongrowing season FCH_4 observations to improve annual ΔFCH_4 estimates and investigate the possible effects of ice thaw and snowmelt on ΔFCH_4.

Another source of uncertainty in our study arose from the EC and chamber FCH_4 footprints. Since we used spatial medians of chamber FCH_4 measurements instead of upscaled chamber FCH_4 in the analyses to investigate cross-scale FCH_4 differences, the results should not be taken as indication of systematic methodological differences between EC and chamber FCH_4. Thus, the next steps could include comparing EC and chamber methods by upscaling chamber FCH_4 to the EC footprint level, or downscaling EC FCH_4 to chamber level, using footprint models and indices of footprint spatial heterogeneity based on fine-scale land cover classification (Hartley et al., 2015; Metzger, 2018; Räsänen et al., 2021; Tuovinen et al., 2019; Xu et al., 2018). Future studies could apply high-resolution (e.g., 1–2 m) remotely-sensed data together with field surveys to determine chamber patch classes which could be used in upscaling chamber FCH_4 to the EC footprint level (Davidson et al., 2017; Forbrich et al., 2011; Morin et al., 2017; Rey-Sanchez et al., 2018; Schrier-Uijl et al., 2010; Stewart et al., 2024; Tuovinen et al., 2019), or downscaling EC FCH_4 to land cover classes (Forbrich et al., 2011; Rößger et al., 2019). By comparing footprint- and patch-weighted chamber FCH_4 to EC FCH_4, we would expect ΔFCH_4 to decrease or chamber FCH_4 exceed EC FCH_4 due to the incorporation of footprint FCH_4 heterogeneity (Budishchev et al., 2014; Schrier-Uijl et al., 2010). As our results may indicate FCH_4 hot spots and moments within the study sites as a possible ΔFCH_4 driver, identifying FCH_4 hot spots within the EC footprint with the aid of footprint-weighted FCH_4 maps (Rey-Sanchez et al., 2022) could also assist in finding representative chamber FCH_4 locations to reconcile the ecosystem and plot-scale FCH_4 differences.

In addition, our cross-scale FCH_4 comparisons contain uncertainties due to differences in chamber FCH_4 outlier removal (Table C2), design and the gas analyzer used (Table C1) (Jentzsch et al., 2025; Levy et al., 2011; Pihlatie et al., 2013; Pumpanen et al., 2004). To minimize these uncertainties in future comparison studies, it is therefore recommended to use chamber FCH_4 data that has been processed in as standardized a way as possible. Given that our results indicated ebullition removal from some of the chamber FCH_4 data as one potential driver of ΔFCH_4, future studies could also conduct cross-scale FCH_4 comparisons based on chamber FCH_4 data with ebullition events both included and excluded from a variety of wetland types. Similar comparisons could be done for the EC FCH_4 data where ebullition events are sometimes also removed following standard data quality protocols.

5 Conclusions

We explored the differences between ecosystem-scale (eddy covariance, EC) and plot-scale (chamber, spatially-aggregated median) instantaneous CH_4 flux (FCH_4) across ten sites and in different temporal aggregations. Contrary to our expectations, we observed significantly higher median ecosystem-scale FCH_4 than plot-scale FCH_4 across all temporal scales. However, the median FCH_4 difference between ecosystem- and plot-scales (ΔFCH_4) remained relatively low. Ecosystem- and plot-scale FCH_4 correlated strongly from daily to annual scales, which indicates that ecosystem- and plot-scale FCH_4 observations could be combined in multi-site analyses at coarse temporal scales. However, care must be taken when combining cross-scale FCH_4 data, as variation in (based on instantaneous FCH_4) and magnitude of ΔFCH_4 (based on cumulative FCH_4) was large at daily to annual scales, and the agreement was worst at the half-hourly to hourly scales. In addition, ΔFCH_4 increased with FCH_4 magnitude at all temporal scales, suggesting that combining ecosystem- and plot-scale FCH_4 in high CH_4-emission ecosystems, such as wetlands, could lead to large FCH_4 uncertainties.

We attribute the higher ecosystem-scale FCH_4 than plot-scale FCH_4 mainly to the combination of selective chamber placement, ebullition removal from chamber FCH_4 data, and the spatiotemporal dynamics of the EC footprint which may have captured CH_4 emission events that were not detected by chambers. Our results highlight the importance of monthly and seasonal variation in variables related to plant activity, atmospheric pressure, wind direction, and friction velocity as drivers of ΔFCH_4 at the ten sites. Between-chamber

FCH_4 variation also led to higher ΔFCH_4, which highlights the mismatch of chamber and EC footprint coverage of the study sites as a ΔFCH_4 driver. Nevertheless, ΔFCH_4 varied strongly between sites and the models' ability to predict to other sites was limited by the low sample size, warranting further research on ΔFCH_4 controls within and across ecosystem types. Based on our findings, we recommend the following:

- Cross-site efforts to upscale chamber FCH_4 to EC footprint level, or conversely, to downscale EC FCH_4 to chamber scale, using chamber measurements stratified by surface cover classes which take into account for vegetation and soil characteristics
- Further investigation of diel ΔFCH_4 dynamics from a higher number of sites with automated chamber measurements, particularly related to the spatial representativeness of the chamber measurements in relation to the EC footprint and chamber artifacts on the observed FCH_4
- Standardized protocols for chamber FCH_4 data quality control, especially related to ebullition removal (see Jentzsch et al., 2025 for recent recommendations for chamber FCH_4 data processing), and accounting for these differences when combining chamber and EC FCH_4 data
- More widely adopted, standardized methods for examining heterogeneity of FCH_4 in EC footprints, which can inform representative chamber and EC tower placement within study sites (e.g., EC footprint modeling and targeted manual chamber sampling; Rey-Sanchez et al., 2022, Barba et al., 2018)
- Systematic bias and uncertainty of chamber and EC FCH_4 observations are recommended to be incorporated into model evaluation and parameterization studies

As syntheses and databases are increasingly utilizing both plot- and ecosystem-scale FCH_4 measurements, it is important to understand their differences across multiple sites. Taking these differences into account in future studies could improve ecosystem CH_4 budget estimates.

Appendix A: Supplementary methods (Supplementary Methods A1–A2)

A1 Supplementary Methods A1

Wind u and v component calculation.

Wind direction was separated into u (calculated with sine; Eq. 1) and v (calculated with cosine; Eq. 2) component vectors which combine both wind speed and direction for each half-hour measurement period.

$$u = -\mathrm{WS} \cdot \sin\left[\frac{2\pi \cdot \mathrm{WD}}{360}\right] \quad \text{(A1)}$$

$$v = -\mathrm{WS} \cdot \cos\left[\frac{2\pi \cdot \mathrm{WD}}{360}\right], \quad \text{(A2)}$$

where WS is wind speed ($\mathrm{m\,s^{-1}}$) and WD is wind direction in decimal degrees.

The u and v component averages were then calculated by taking the mean over the temporal unit in each aggregation (e.g., hour or day), resulting in temporally-aggregated u and v components in $\mathrm{m\,s^{-1}}$.

A2 Supplementary Methods A2

Details of linear mixed effects models.

Temporal autocorrelation and residual variance structures were examined and chosen based on Akaike Information Criteria (AIC) and residual diagnostics, with more emphasis on the latter. Temporal autocorrelation was modeled using an autoregressive structure of order 1 (AR1) in the daily, weekly, and monthly models. To meet the requirements of the corAR1 argument in R, random effects in these models were nested to account for site-specific sampling times (e.g., daily model: random = $\sim 1 \mid$ Site/YearMonth, correlation = corAR1(form = $\sim$ Day $\mid$ Site/YearMonth)). The nesting allowed for the inclusion of temporal autocorrelation within each temporal scale, for example "YearMonth", at the site level, reducing residual temporal autocorrelation compared to models with un-nested random effects. However, incorporating AR1 in the half-hourly model did not improve model fit or reduce residual variance and was therefore excluded. In addition, despite improvements in AIC in the hourly model, inclusion of AR1 led to model non-convergence and it had to be excluded from the model, leading to higher AIC but temporal autocorrelation and residual normality and variance heterogeneity were still acceptable when the random effect was nested (Site/Date).

Heterogeneous residual variance caused by some of the predictors was modeled in some of the models using an exponential variance structure (varExp; half-hourly and hourly: VPD, u^*, PA; daily: PA and TS; weekly: PA; monthly: uWD, u^*), as well as variance per stratum (varIdent; weekly: Year). We also tested other variance structures but, according to AIC and residual diagnostics, exponential variance structure led to best model fit and some of the other structures led to model non-convergence. Despite our efforts to account for the residual variance heterogeneity, some heterogeneity remained in the models while AIC and general model residual heterogeneity improved.

Appendix B: Supplementary figures (Figs. B1–B19)

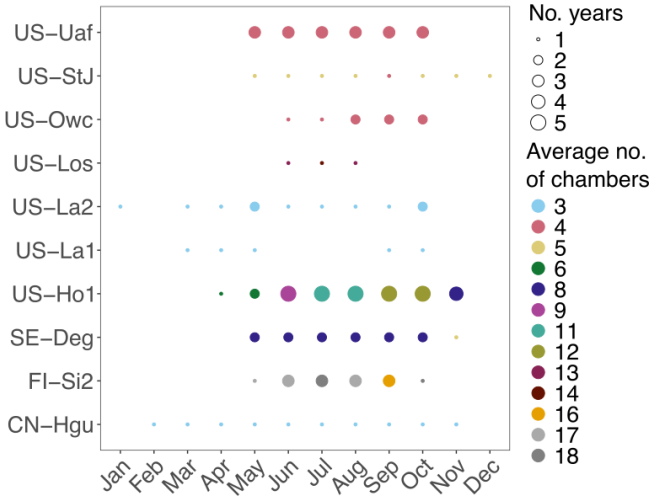

Figure B1. Number of individual chambers and years per month per site. The size of the point describes the number of years and color the average number of individual chambers used within each month across years.

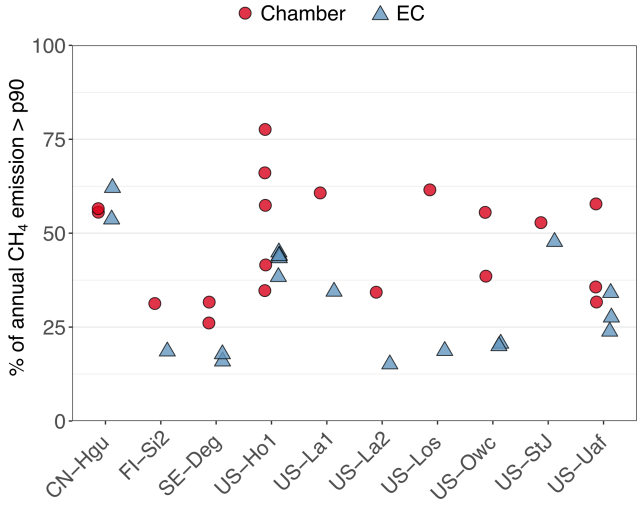

Figure B2. Contribution of high methane (CH_4) emissions to annual CH_4 emissions per site in the unaggregated data set. For each site and year, high CH_4 emissions were estimated as CH_4 flux (FCH_4) above the 90th percentile (p90) and their proportion (%) of the total annual CH_4 emission was calculated separately for chamber (red circle) and EC (blue triangle). In the unaggregated data set, all eddy covariance (EC) FCH_4 data is in the half-hourly scale, but the chamber data measurement frequency varies across sites (see Table S1).

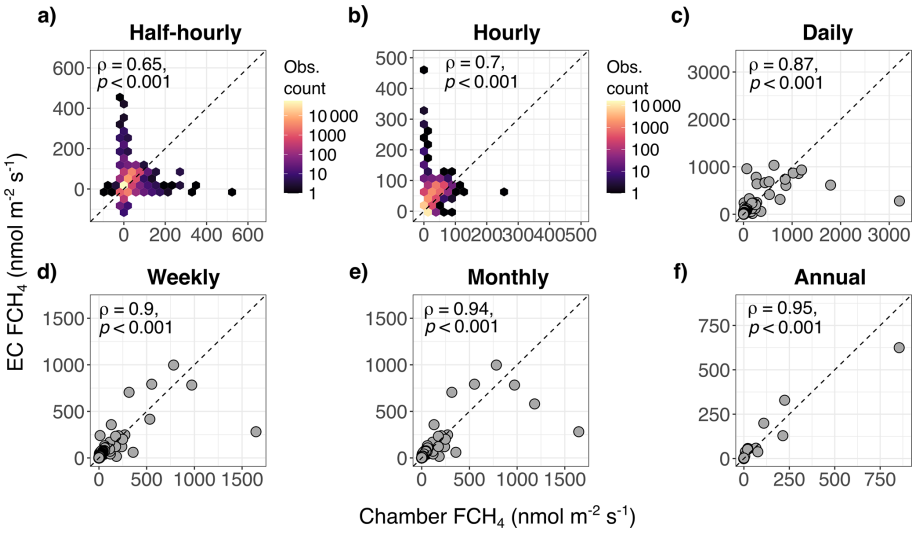

Figure B3. Relationship between eddy covariance (EC; ecosystem scale) methane (CH_4) flux (FCH_4) and chamber FCH_4 (plot scale) with untransformed plot axes. Higher Spearman correlation coefficients (ρ) indicate stronger agreement between EC FCH_4 and chamber FCH_4. In **(a)** and **(b)** the points for half-hourly ($n = 74\,482$) and hourly ($n = 40\,072$) aggregations are shown in hexagonal density clouds with a log-transformed color range to highlight trends in high point density areas (colors represent number of observations per hexagon). For daily **(c)**, weekly **(d)**, monthly **(e)**, and annual **(f)** aggregations, sample sizes were $n = 1879$, 349, 121, and 22, respectively. The dashed line represents 1 : 1 line.

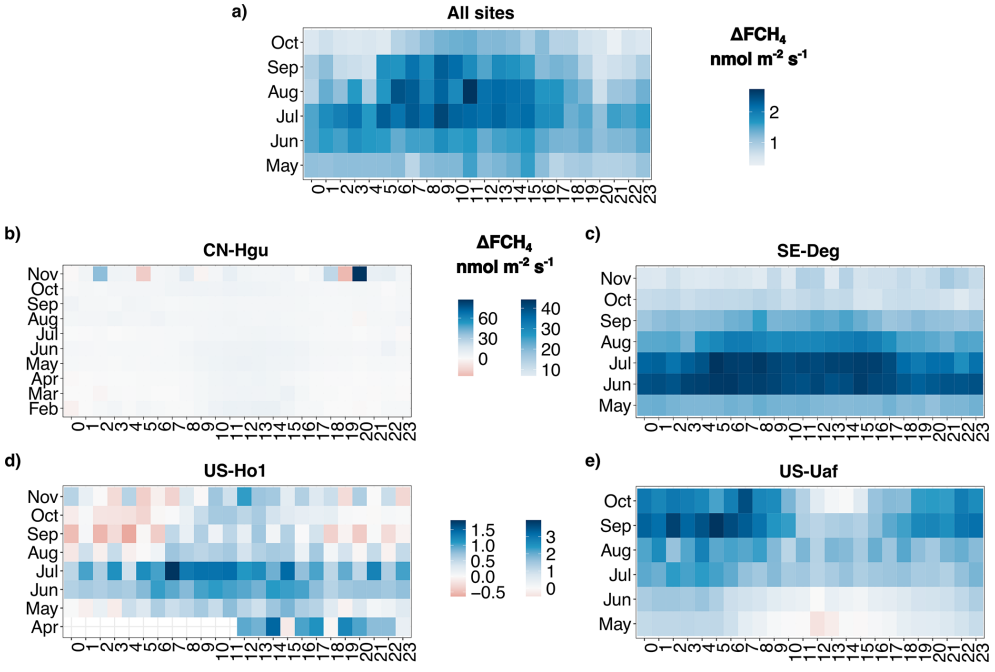

Figure B4. Heatmaps of hourly median methane (CH_4) flux (FCH_4) difference between ecosystem- and plot-scale FCH_4 (ΔFCH_4) across months in the half-hourly aggregation. Positive ΔFCH_4 (blue) represents higher eddy covariance (EC) FCH_4 than chamber FCH_4, and negative (red) higher chamber FCH_4 than EC FCH_4. x axis represents hours of day (24 h) and y axis months. **(a)** Data set containing all sites ($n = 4$ sites). Only months which were included in all sites are shown (May–October). **(b)** CN-Hgu (all months), **(c)** SE-Deg (all months), **(d)** US-Ho1 (all months), **(e)** US-Uaf (all months).

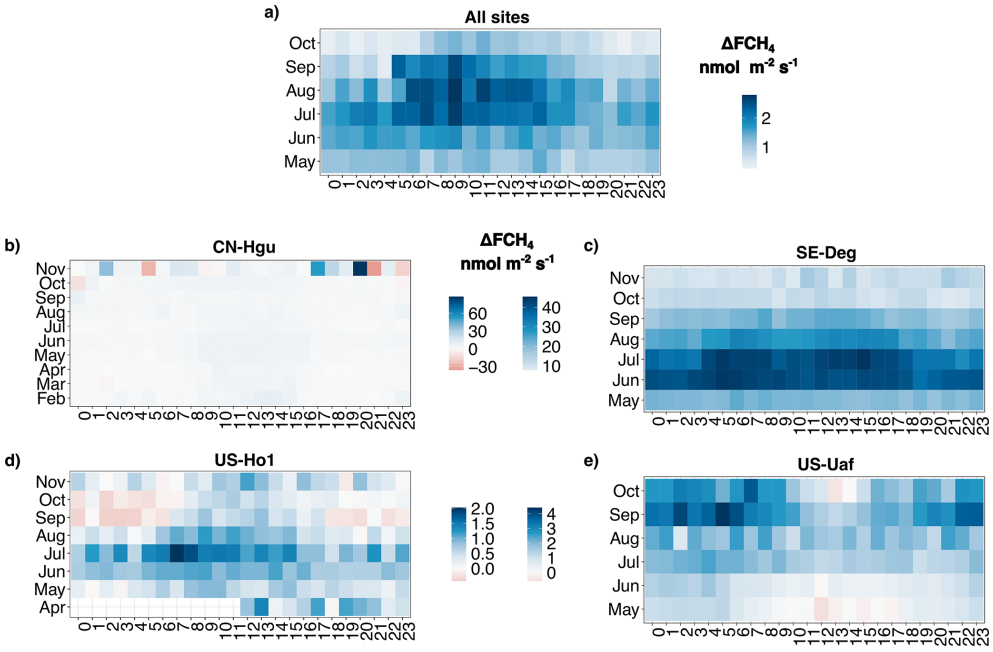

Figure B5. Heatmaps of hourly median methane (CH_4) flux (FCH_4) difference between ecosystem- and plot-scale FCH_4 (ΔFCH_4) across months in the hourly aggregation. Positive ΔFCH_4 (blue) represents higher ecosystem-scale (eddy covariance; EC) FCH_4 than plot-scale (chamber) FCH_4, and negative (red) higher plot-scale FCH_4 than ecosystem-scale FCH_4. x axis represents hours of day (24 h) and y axis months. **(a)** Data set containing all sites ($n = 4$ sites). Only months which were included in all sites are shown (May–October). **(b)** CN-Hgu (all months), **(c)** SE-Deg (all months), **(d)** US-Ho1 (all months), **(e)** US-Uaf (all months).

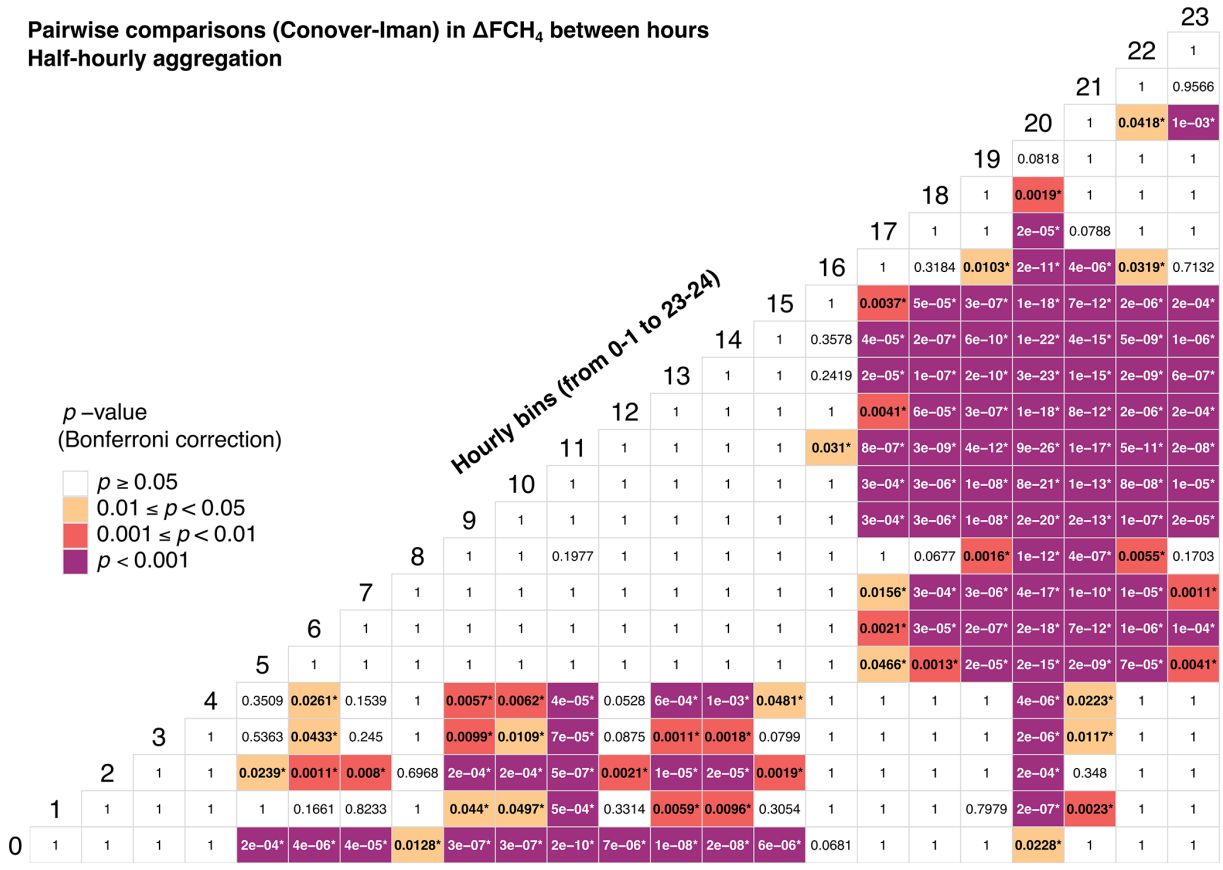

Figure B6. Significance levels (Bonferroni-adjusted p-values) of Conover-Iman multiple pairwise comparisons in methane (CH_4) flux (FCH_4) difference (ΔFCH_4) in the half-hourly aggregation containing sites with automated chamber measurements ($n = 4$ sites). Numbers on the diagonal line are labels for the hourly bins, starting from 0–1 and ending in 23–24. Different colors represent the Bonferroni-adjusted p-values, with reference to an overall significance threshold of $\alpha = 0.05$. Numbers inside the tiles are Bonferroni-adjusted p-values of the pairwise comparisons at four decimal places. Values in bold and asterisk (*) represent p-values that remain significant after Bonferroni correction.

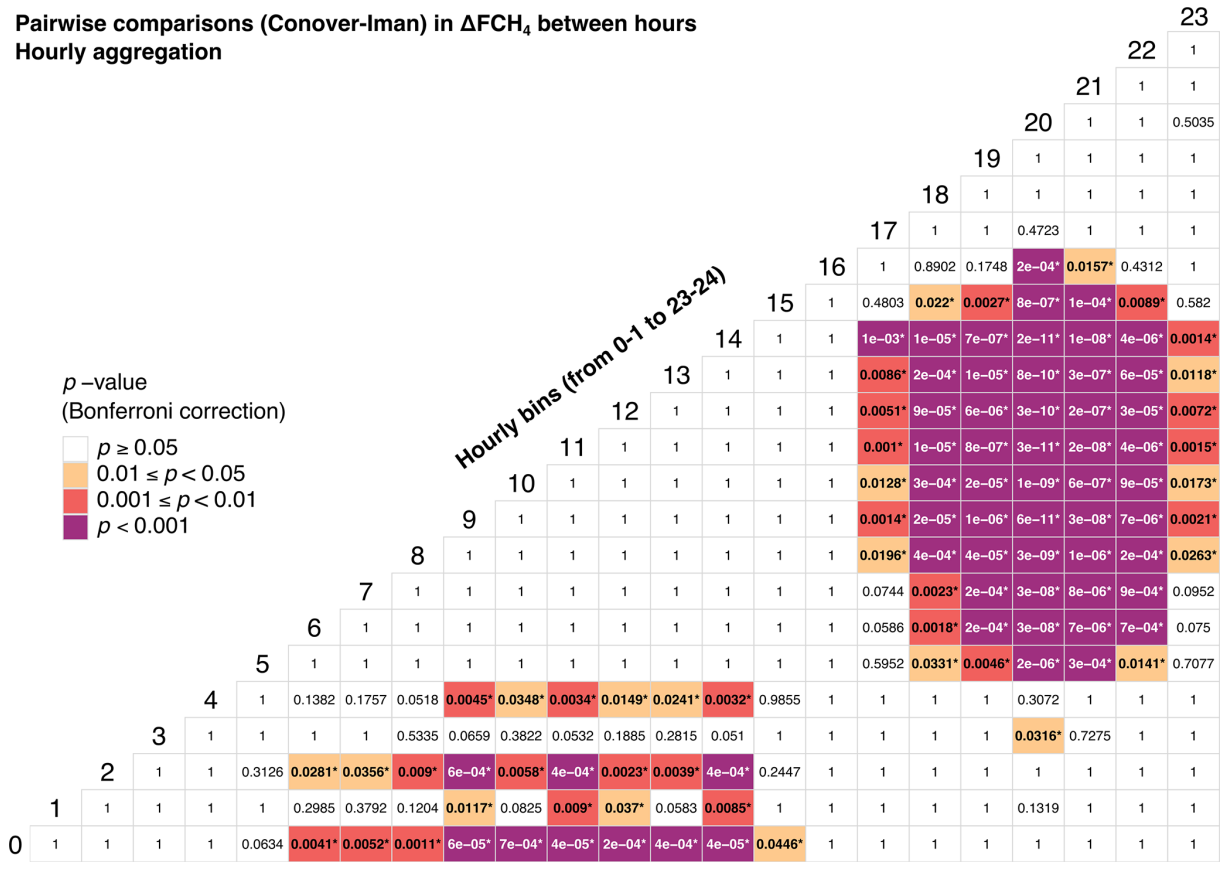

Figure B7. Significance levels (Bonferroni-adjusted p-values) of Conover-Iman multiple pairwise comparisons in methane (CH_4) flux (FCH_4) difference (ΔFCH_4) in the hourly aggregation containing sites with automated chamber measurements ($n = 4$ sites). Numbers on the diagonal line are labels for the hourly bins, starting from 0–1 and ending in 23–24. Different colors represent the Bonferroni-adjusted p-values, with reference to an overall significance threshold of $\alpha = 0.05$. Numbers inside the tiles are Bonferroni-adjusted p-values of the pairwise comparisons at four decimal places. Values in bold and asterisk (*) represent p-values that remain significant after Bonferroni correction.

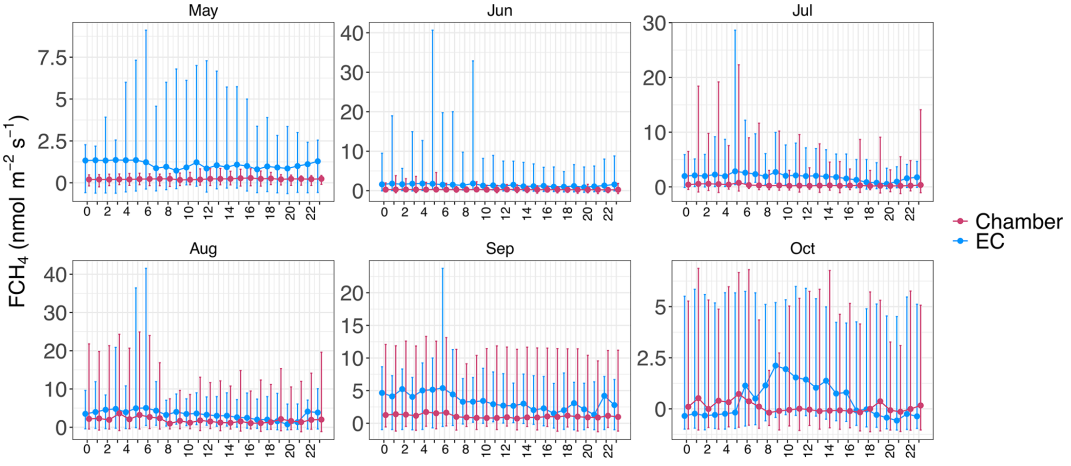

Figure B8. Hourly median chamber (red; plot scale) and eddy covariance (EC; ecosystem scale) methane (CH_4) flux (FCH_4; blue) per month in the half-hourly data set. Variation around the median is represented by the interquartile range (between 25 % and 75 %). Only months containing all sites ($n = 4$) with automated chamber measurements are shown.

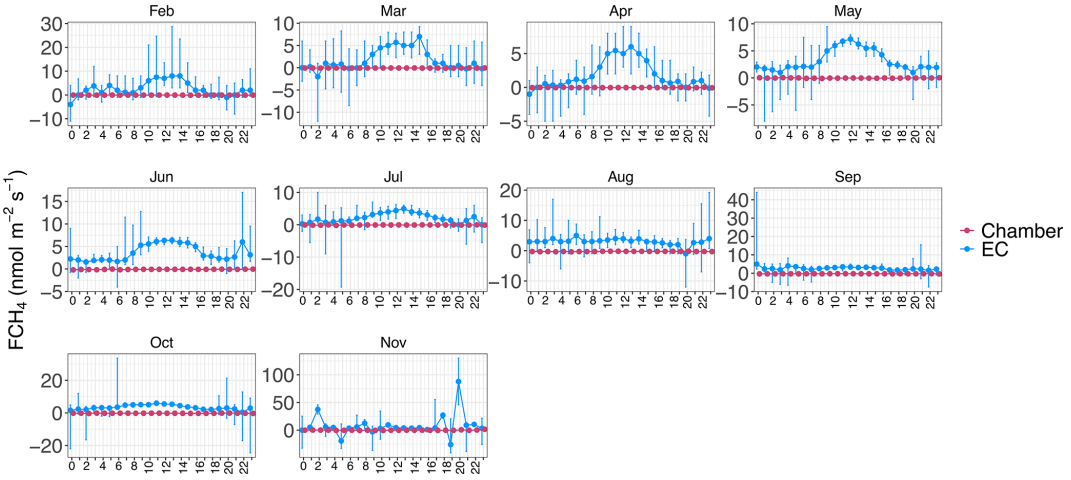

Figure B9. Hourly median chamber (red; plot scale) and eddy covariance (EC; ecosystem scale) methane (CH_4) flux (FCH_4; blue) per month at CN-Hgu in the half-hourly dataset. Variation around the median is represented by the interquartile range (between 25 % and 75 %).

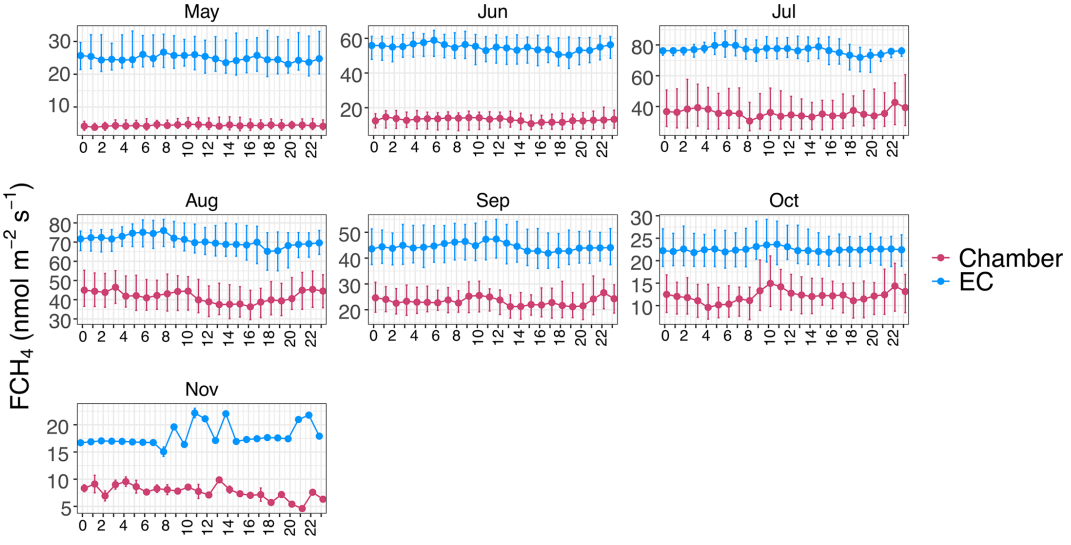

Figure B10. Hourly median chamber (red; plot scale) and eddy covariance (EC; ecosystem scale) methane (CH_4) flux (FCH_4; blue) per month at SE-Deg in the half-hourly dataset. Variation around the median is represented by the interquartile range (between 25 % and 75 %).

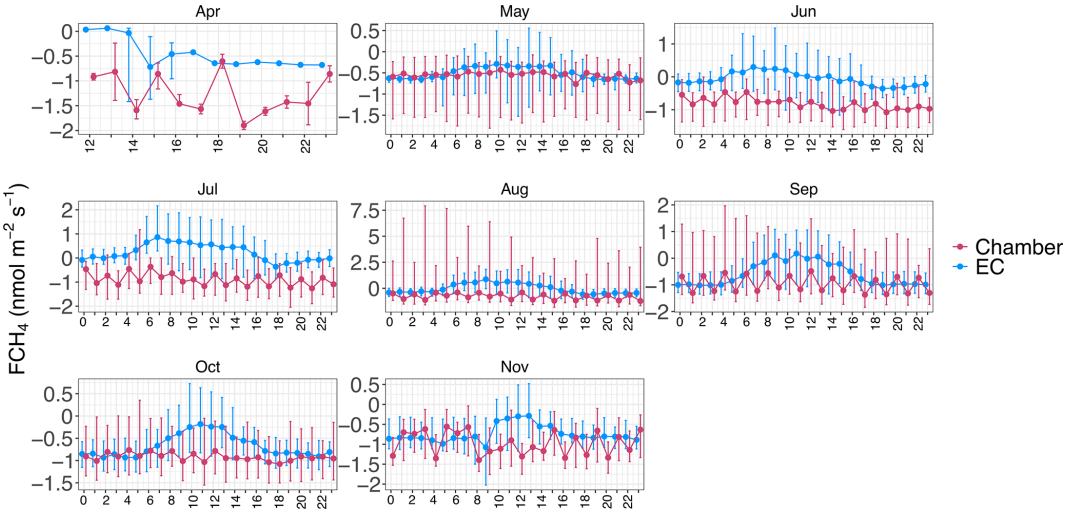

Figure B11. Hourly median chamber (red; plot scale) and eddy covariance (EC; ecosystem scale) methane (CH_4) flux (FCH_4; blue) per month at US-Ho1 in the half-hourly dataset. Variation around the median is represented by the interquartile range (between 25 % and 75 %).

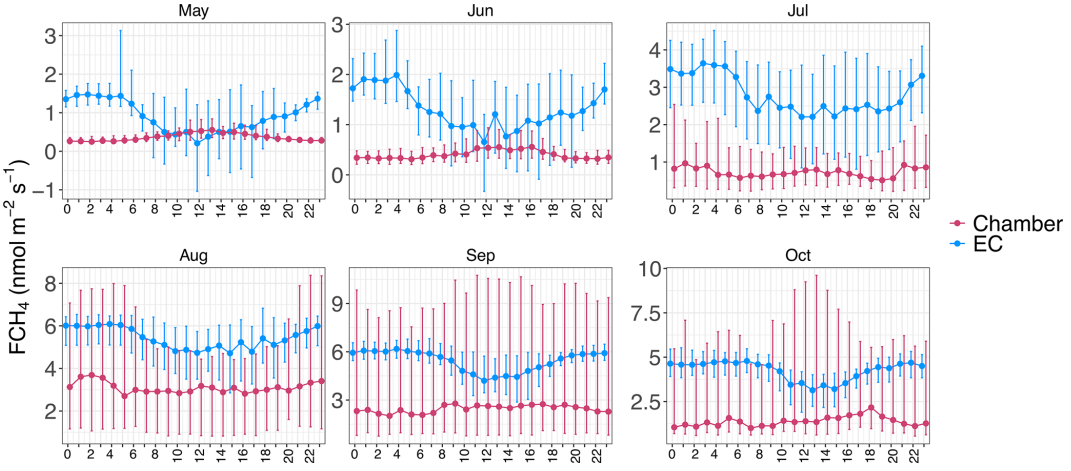

Figure B12. Hourly median chamber (red; plot scale) and eddy covariance (EC; ecosystem scale) methane (CH_4) flux (FCH_4; blue) per month at US-Uaf in the half-hourly dataset. Variation around the median is represented by the interquartile range (between 25 % and 75 %).

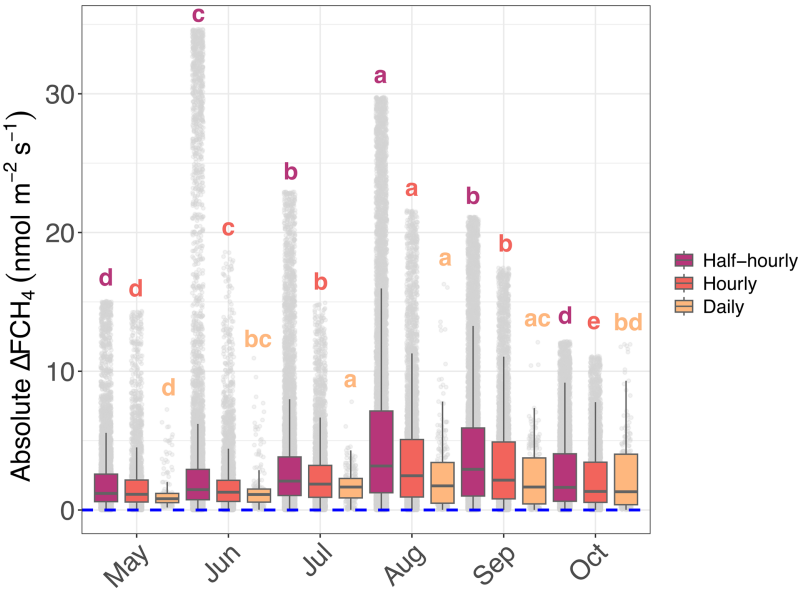

Figure B13. Absolute difference between ecosystem-scale (eddy covariance; EC) and plot-scale (chamber) methane (CH_4) flux (FCH_4) differences (ΔFCH_4) between months in half-hourly, hourly and daily aggregations. Different colors represent different temporal aggregations and gray points show the underlying data. For visualization, we filtered out data points 1.5 × IQR below the first quartile and 1.5 × IQR above the third quartile but statistics were based on the original data. The letters indicate whether ΔFCH_4 differs significantly between months: months that share at least one shared letter are not significantly different ($p>0.05$) while months with different letters differ significantly ($p \leq 0.05$). Pairwise comparisons were conducted with the Conover-Iman post hoc test. While there was data in other months, the May–October period was chosen for this figure due to these months including either all ($n = 4$; half-hourly and hourly aggregations) or almost all sites ($n = 7$ or 8 sites; daily aggregation). Weekly and monthly aggregations did not have significant ΔFCH_4 differences between months (Kruskal-Wallis $p>0.05$) and are not shown in this figure.

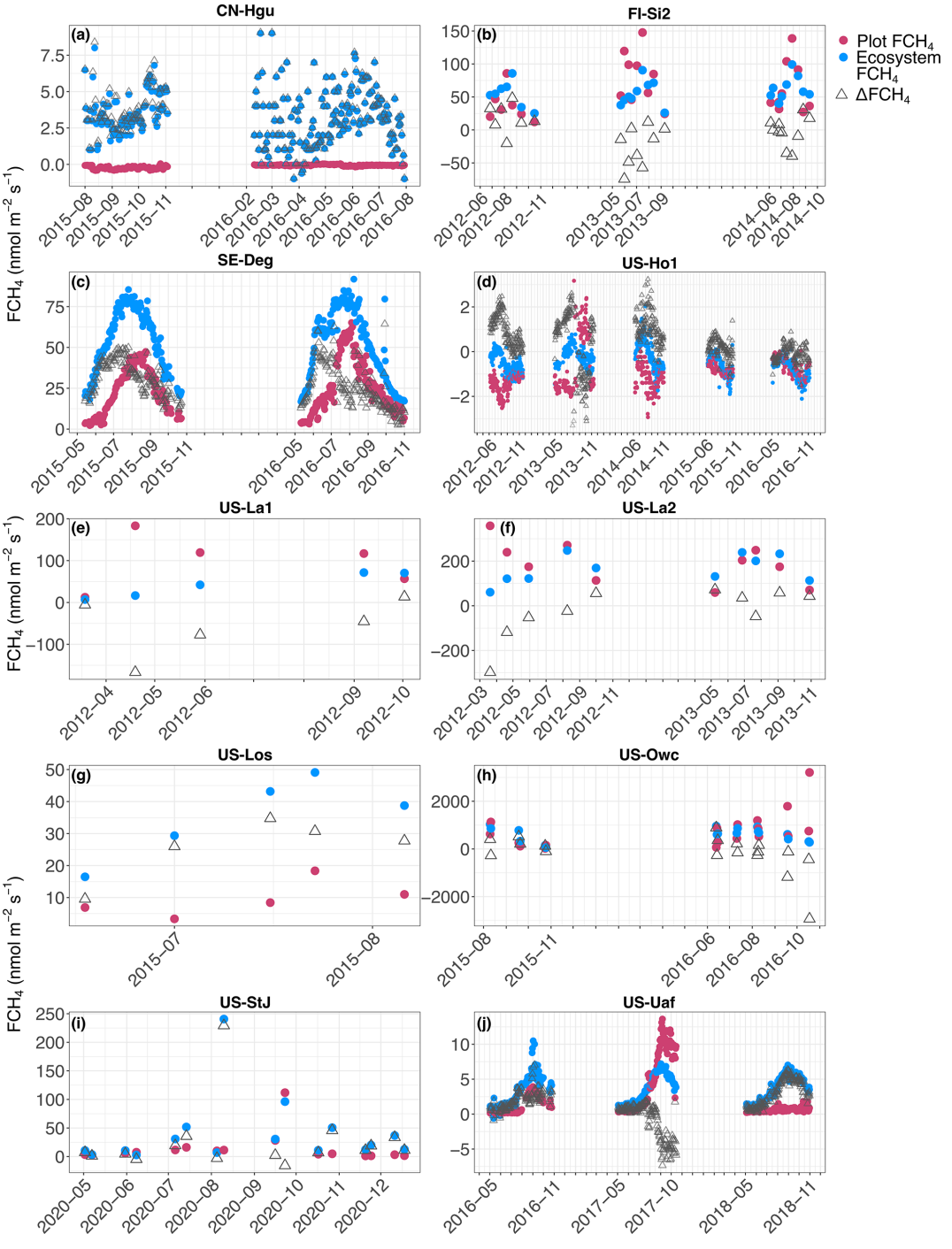

Figure B14. Site-specific trends in daily ecosystem- (eddy covariance; EC) and plot-scale (chamber) methane (CH_4) flux (FCH_4), and FCH_4 difference between ecosystem and plot scales (ΔFCH_4) (**a** to **j**). Red circles represent plot- and blue ecosystem-scale FCH_4 measurements. Hollow gray triangles are ΔFCH_4. In **(d)** 46 outlier points from 2013 were removed to improve visualization. Negative ΔFCH_4 indicates higher plot-scale FCH_4 than ecosystem-scale FCH_4, and positive higher ecosystem-scale FCH_4 than plot-scale FCH_4.

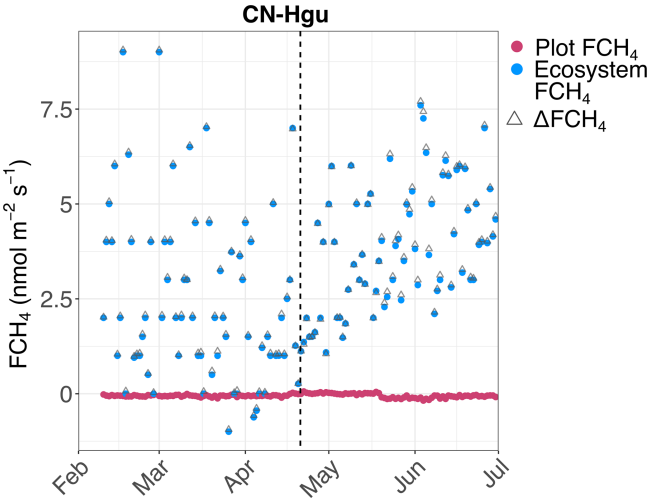

Figure B15. Daily-aggregated methane (CH_4) flux (FCH_4) at CN-Hgu between February and July highlighting the higher ecosystem- than plot-scale FCH_4 during the ice thawing period (February–end of April). Red circles represent plot- and blue ecosystem-scale FCH_4 measurements. Hollow gray triangles are the difference between ecosystem- and plot-scale FCH_4 (ΔFCH_4). Negative ΔFCH_4 indicates higher plot-scale FCH_4 than ecosystem-scale FCH_4, and positive higher ecosystem-scale FCH_4 than plot-scale FCH_4. The dashed vertical black line represents the mean end period of frozen-thawing period at a nearby peatland (between 2015 and 2016), calculated by Liu et al. (2021).

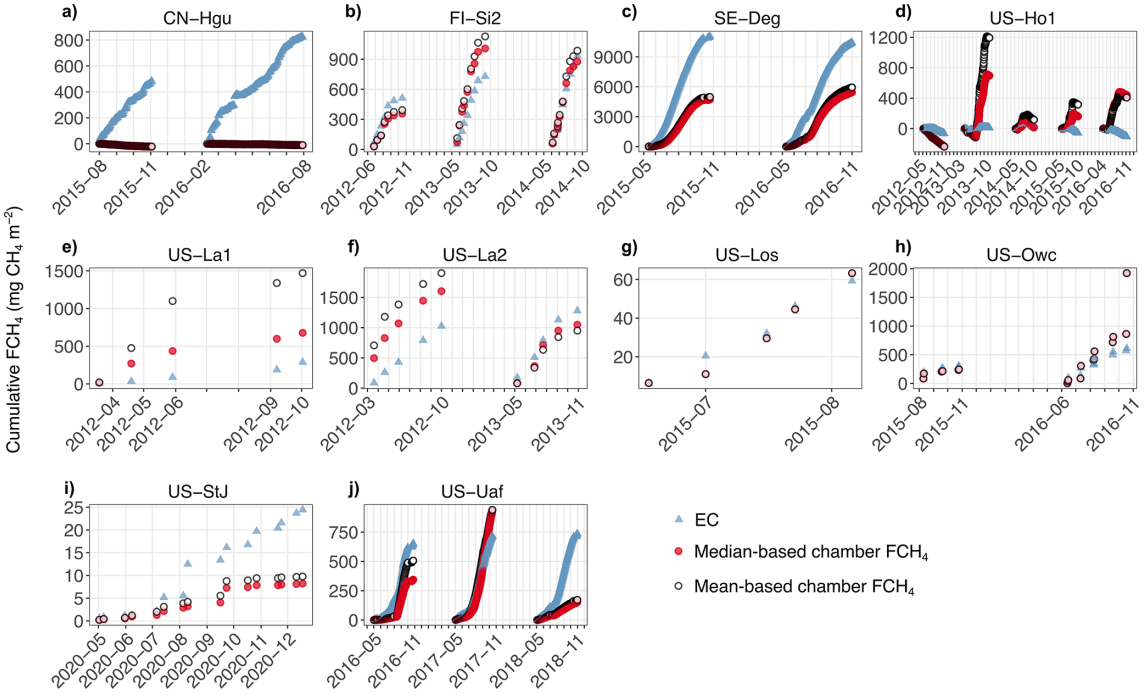

Figure B16. Cumulative sums of ecosystem-scale (eddy covariance; EC) and plot-scale (chamber) methane (CH_4) flux (FCH_4) at the daily scale across sites **(a–j)**. Blue triangles represent EC, red points chamber FCH_4 calculated from the median-based aggregation, and white points chamber FCH_4 calculated from the mean-based aggregation. Note that since the chamber FCH_4 data at FI-Si2, US-La1, and US-La2 lacked hourly timestamps, we roughly estimated daily cumulative FCH_4 by using the daily chamber FCH_4 median or mean for all 24 h of the measurement date (EC cumulative FCH_4 was calculated based on daily half-hourly FCH_4 from FLUXNET-CH_4), and these estimates should thus be interpreted with caution.

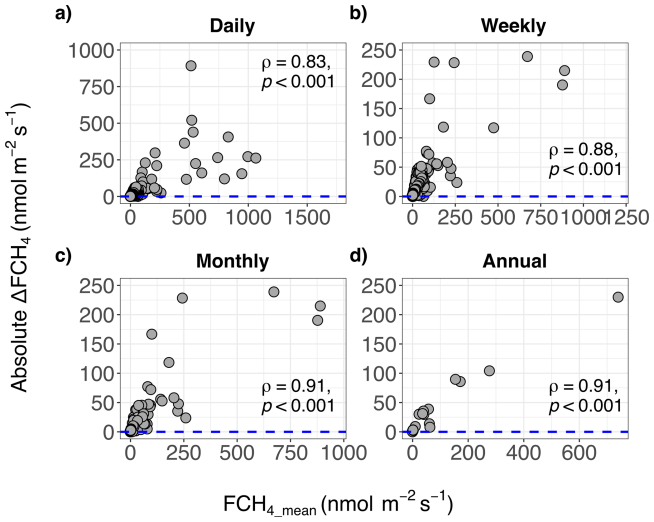

Figure B17. The relationship between methane (CH_4) flux (FCH_4) magnitude and absolute difference between ecosystem- and plot-scale FCH_4 (ΔFCH_4) with outliers in daily **(a)**, weekly **(b)**, monthly **(c)** and annual **(d)** scales. FCH_{4_mean} is the row-wise mean of eddy covariance (EC) FCH_4 and chamber FCH_4, and EC-chamber FCH_4 difference (ΔFCH_4) was calculated by subtracting chamber FCH_4 from EC FCH_4. Positive ΔFCH_4 indicates higher EC FCH_4 than chamber FCH_4 and negative values higher chamber FCH_4 than EC FCH_4. The blue dashed line represents the line of equality where EC FCH_4 and chamber FCH_4 are equal. ρ represents Spearman correlation coefficient, followed by its statistical significance ($\alpha = 0.05$). Higher ρ represents stronger deviation from the line of equality, i.e., $\Delta FCH_4 = 0$ while perfect agreement between chamber and EC FCH_4 would result in $\rho = 0$.

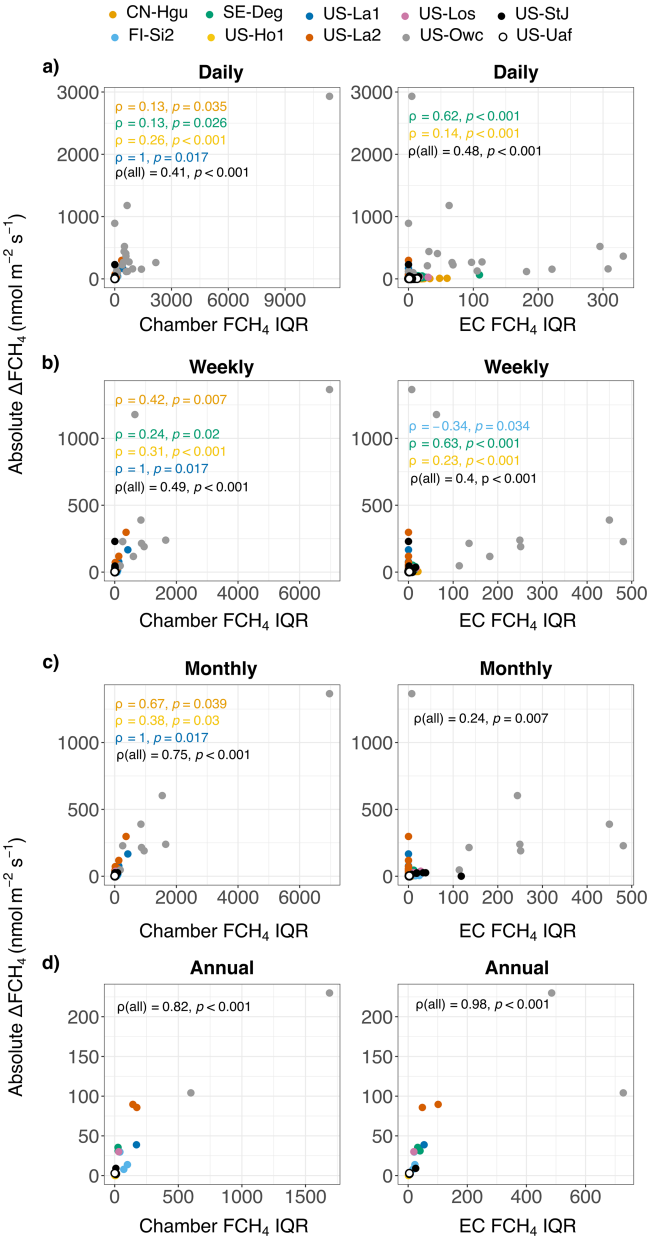

Figure B18. Untransformed absolute difference between ecosystem (eddy covariance; EC)- and plot-scale (chamber) methane (CH_4) flux (FCH_4) (ΔFCH_4), chamber and EC FCH_4 IQR in daily **(a)**, weekly **(b)**, monthly **(c)**, and annual **(d)** aggregations. Different colors represent individual sites. Plots in the left panel show the relationship between daily variation in FCH_4 between individual chambers within each site and site-level absolute ΔFCH_4. The right side panel shows the same but with daily variation in EC FCH_4. The strength and general direction of the relationship was measured with Spearman correlation coefficient (ρ). "ρ(all)" refers to the Spearman correlation for the whole dataset.

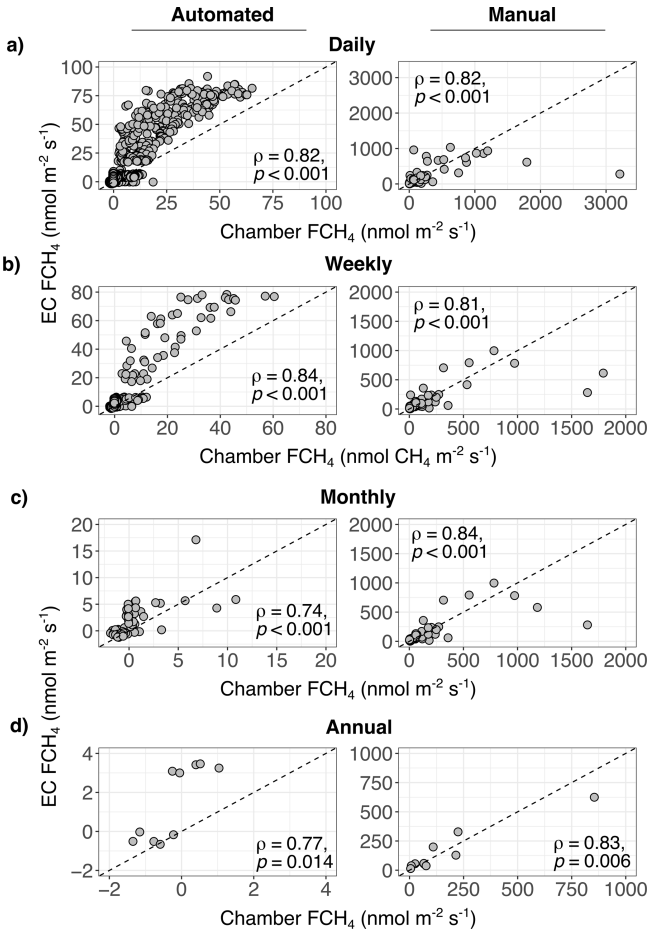

Figure B19. Automated (left panel) and manual (right panel) chamber methane (CH_4) flux (FCH_4) had strong positive relationships with EC FCH_4 across sites and temporal scales (**a** to **d**). The dashed line represents the 1 : 1 line, and ρ Spearman correlation coefficient of the relationship. Automated chambers were included in four sites (CN-Hgu, SE-Deg, US-Ho1, and US-Uaf) and manual chambers in six sites (FI-Si2, US-La1, US-La2, US-Los, US-Owc, and US-StJ). Half-hourly and hourly plots are in Fig. 3. Note different x and y axis scales.

Appendix C: Supplementary tables (Tables C1–C14)

Table C1. Methodological and data details of the site chamber (CH) and eddy covariance (EC) measurement systems. "CH method" refers to whether the chambers are manual or automated, and whether chambers were dark or transparent to sunlight. CH meas. frequency = chamber measurement frequency. CH-EC overlap is the total duration of overlap between chamber and EC measurements in days (note: the measurements are spread out over different seasons and years; see Fig. B1 and Table 1). Gap-filled EC is the percentage of ANN-gap-filled EC methane (CH_4) flux (FCH_4) values of all EC FCH_4 values per site (in the unaggregated data set). Further details of the CH and EC measurement systems can be found in the corresponding references. Abbreviations in "CH analyzer": LI-COR = LI-COR Biosciences, Nebraska, USA; Picarro = Picarro Inc., Santa Clara, CA, USA; Los Gatos = Los Gatos Research Inc., San Jose, CA, USA; Aerodyne = TILDAS CS, Aerodyne Research Inc., Billerica, MA, USA; Varian = Varian, Inc., Palo Alto, CA, USA; Shimadzu = Shimadzu Scientific Instruments, Kyoto, Japan.

FLUXNET-CH_4 ID	Location (lat, lon)	CH method	CH analyzer	EC analyzer	EC tower height (m)	No. of CH	CH meas. frequency	EC-CH start, end year	EC-CH overlap days	Gap-filled EC (%)	CH data ref.	EC data ref.
CN-Hgu	32.845278, 102.59	automated, dark	near infrared laser gas analyzer (model 915-0011, Los Gatos)	open-path infrared gas analyzer (LI-7700; LI-COR)	3	3	56 min	2015, 2016	363	44	Wang et al. (2021)	Niu and Chen (2020)
FI-Si2	61.8372, 24.1967	manual, dark	gas chromatograph (Agilent Technologies 7890A) and liquid handler (Gilson GX-271)	open- path gas analyzer (LI-7700, LI-COR)	2.4	18	1–3× month	2012, 2014	26	5	Korrensalo et al. (2018)	Alekseychik et al. (2021), Vesala et al. (2020)
SE-Deg	64.182029, 19.556539	automated, dark and transparent	cavity ring-down spectrometer (model GGA-24EP, Los Gatos)	Closed-path gas analyzer (Model 911-0011-0004, Los Gatos)	3	4	1 h	2015, 2016	338	31	Bond-Lamberty et al. (2020), Järveoja et al. (2018)	Nilsson and Peichl (2020)
US-Ho1	45.2041, −68.7402	automated, dark	cavity ring-down spectrometer (model G2121-i; Picarro) & Aerodyne Quantum Cascade Laser (Aerodyne)	Closed-path gas analyzer (model G2311-f, Picarro cavity ring-down spectrometer)	31	20	ca. 1 h (varied between years and chambers)	2012, 2016	759	52	Richardson et al. (2019)	Richardson and Hollinger (2020)
US-La1	29.5013, −90.4449	manual, dark	gas chromatograph (model CP-3800, Varian)	open-path gas analyzer (LI-7700, LI-COR)	3.4	3	1× month	2012, 2012	5	0	Krauss et al. (2016)	Holm et al. (2020a)
US-La2	29.8587, −90.2869	manual, dark	gas chromatograph (model CP-3800, Varian)	open-path gas analyzer (LI-7700, LI-COR)	3.6	3	1× month	2012, 2013	10	10	Krauss et al. (2016)	Holm et al. (2020b)

Table C1. Continued.

FLUXNET-CH_4 ID	Location (lat, lon)	CH method	CH analyzer	EC analyzer	EC tower height (m)	No. of CH	CH meas. frequency	EC-CH start, end year	EC-CH overlap days	Gap-filled EC (%)	CH data ref.	EC data ref.
US-Los	46.0827, −89.9792	manual, dark	near-infrared laser gas analyzer (Los Gatos UGGA)	open-path gas analyzer (LI-7700, LI-COR)	10.2	14	1–3× month	2015, 2015	5	31	Desai (2025b)	Desai (2025a), Desai and Thom (2020)
US-Owc	41.37951667, −82.5124667	manual, dark	gas chromatograph (GC-2014, Shimadzu)	open-path gas analyzer (LI-7700, LI-COR)	2.7	4	1× month	2015, 2016	18	50	Bohrer et al. (2019)	Bohrer et al. (2020)
US-StJ	39.08821106, −75.43722534	manual, dark	near-infrared laser gas analyzer (Los Gatos)	open-path gas analyzer (LI-7700, LI-COR)	3.5	5	1–2× month	2020	16	0	Hill and Vargas (2022a)	Vargas (2018)
US-Uaf	64.86627, −147.85553	automated, dark	near-infrared laser gas analyzer (Los Gatos)	closed-path gas analyzer (RMT200 Fast Methane Analyzer or Greenhouse Gas Analyzer, Los Gatos)	6	5	30 min	2016, 2018	458	59	Ueyama et al. (2022)	Iwata et al. (2020)

Table C2. Details of chamber methane (CH_4) flux (FCH_4) data quality control and chamber placement rationale in the study sites. Data quality control was done by data providers prior to sharing chamber FCH_4 data, and a summary of the methods are listed here. For more details, please see the site-specific references. EC = eddy covariance.

Site	FCH_4 corrections	Low-quality FCH_4data filtering	Ebullition removal	Chamber placement rationale	Reference
CN-Hgu	Air temperature and H_2O dilution	R^2 <0.9	No (ebullition assumed negligible)	To investigate the effect of experimental warming on CH4 uptake. Both the warming treatment and the control each included three chambers. The chambers were located approx. 500 m from the EC tower and covered spatial variation in environmental conditions	Wang et al. (2021)
FI-Si2	Air temperature	Nonlinear changes in CH_4 concentrations removed (altogether 10.4 % of measurements removed)	Yes	To cover spatial variation in vegetation and environmental conditions (three chambers per plant community/bog micrtopography type: high hummock, hummock, high lawn, lawn, hollow, and bare peat). Chamber placement was based on a systematic survey of surface cover within a 200 m radius the EC tower	Korrensalo et al. (2018)
SE-Deg	Air temperature and H2O dilution	R^2 <0.95 and RMSE > 0.02	Yes	To understand how different microtopographic forms (water table level and vegetation composition) explain EC flux patterns. In addition, cross-checking the information from EC at the diel scale, especially during calm night-time conditions	Bond-Lamberty et al. (2020), Järveoja et al. (2018)
US-Ho1	Air temperature, air pressure and H_2O dilution	R^2 <0.9	No	To sample representative land cover classes covered by the EC footprint for measuring CO_2, CH_4 and N_2O (3-5 chambers per upland control, upland trenched, transitional and wetland class)	Richardson et al. (2019)
US-La1	Air temperature	None (few data points discarded based on very low R^2 and standard deviation > 3 from the mean)	No	To sample representative areas (chambers installed around vegetation clusters to avoid cutting roots. Open water not included) within the EC footprint.	Krauss et al. (2016)
US-La2	Air temperature	None (few data points discarded based on very low R^2 and standard deviation > 3 from the mean)	No	To sample representative areas within the EC footprint (chambers installed around boardwalks)	Krauss et al. (2016)
US-Los	Air temperature, air pressure and H_2O dilution	None (but most mean R^2 >0.9 across replicates; ca. 15 % $R^2 < 0.66$)	No	To sample representative landscapes (hummocks, hollows, shrubs, open water) within the EC footprint to evaluate drivers, spatial variation, and hotspots/moments of FCH_4 and ways to scale fluxes from chambers to EC to landscape	Desai (2025b)
US-Owc	Air temperature and air pressure	$R^2 \leq 0.85$ (whole chamber measurement discarded if in n>3 observations within measurement)	Yes	To sample random locations with equal sample size per patch type (open water, *Typha* sp., floating vegetation). Chambers were placed floating on the water, excluding plants	Bohrer et al. (2019)

Table C2. Continued.

Site	FCH_4 corrections	Low-quality FCH_4data filtering	Ebullition removal	Chamber placement rationale	Reference
US-StJ	Air temperature, air pressure and H_2O dilution	R^2 <0.9 (based on CO_2 flux measured simultaneously)	Yes	To sample representative (based on marsh vegetation) areas within the EC footprint that were safely accessible. The main goal was to investigate when to measure CH_4 fluxes with manual chambers in a spatiotemporally heterogeneous wetland and using this information, to see how and when to combine both EC and manual chamber measurements for analyses.	Hill and Vargas (2022a, 2022b)
US-Uaf	Air temperature, air pressure and H_2O dilution	RMSE > 0.3 ppb or $R^2 < 0.1$	No (ebullition assumed negligible)	To cover spatial variation in forest floor microtopography and vegetation in 2016–2018 (one chamber per wet *Sphagnum*, wet *Carex* spp., dry lichen, and dry *Carex* spp.)	Ueyama et al. (2022)

Table C3. Details of the used environmental data. FLUXNET-CH_4 soil temperature data was from the topmost soil depths (2-10 cm below soil surface). Abbreviations: NEE = net ecosystem exchange, u^* = friction velocity, WD = wind direction, WS = wind speed, VPD = vapor pressure deficit, PA = air pressure, WTL = water table level, TS = soil temperature, ANN = artificial neural network, MDS = marginal distribution sampling.

Site	Environmental variable	Data	Data reference
CN-Hgu	NEE	Half-hourly FLUXNET-CH_4: ANN-gap-filled	Delwiche et al. (2021); Knox et al. (2019)
	u^*	Half-hourly FLUXNET-CH_4: ANN-gap-filled	
	WD	Half-hourly FLUXNET-CH_4: ANN-gap-filled	
	WS	Half-hourly FLUXNET-CH_4: gap-filled	
	VPD	Half-hourly FLUXNET-CH_4: gap-filled	
	PA	Half-hourly FLUXNET-CH_4: gap-filled	
	WTL	–	–
	TS	Half-hourly FLUXNET-CH_4	Delwiche et al. (2021); Knox et al. (2019)
FI-Si2	NEE	Half-hourly FLUXNET-CH_4: ANN-gap-filled	Delwiche et al. (2021); Knox et al. (2019)
	u^*	Half-hourly FLUXNET-CH_4: ANN-gap-filled	
	WD	Half-hourly FLUXNET-CH_4: ANN-gap-filled	
	WS	Half-hourly FLUXNET-CH_4: gap-filled	
	VPD	Half-hourly FLUXNET-CH_4: gap-filled	
	PA	Half-hourly FLUXNET-CH_4: gap-filled	
	WTL	Mean of daily gap-filled FLUXNET-CH_4 WTL and chamber-associated WTL	Delwiche et al. (2021); Knox et al. (2019), Korrensalo et al. (2018)
	TS	Chamber-associated TS	Korrensalo et al. (2018)
SE-Deg	NEE	Half-hourly FLUXNET-CH_4: ANN-gap-filled	Delwiche et al. (2021); Knox et al. (2019)
	u^*	Half-hourly FLUXNET-CH_4: ANN-gap-filled	
	WD	Half-hourly FLUXNET-CH_4: ANN-gap-filled	
	WS	Half-hourly FLUXNET-CH_4: gap-filled	
	VPD	Half-hourly FLUXNET-CH_4: gap-filled	
	PA	Half-hourly FLUXNET-CH_4: gap-filled	
	WTL	Mean of half-hourly gap-filled FLUXNET-CH_4 WTL and chamber-associated WTL	Delwiche et al. (2021); Knox et al. (2019); Järveoja et al. (2018); Bond-Lamberty et al. (2020)
	TS	Mean of half-hourly FLUXNET-CH_4 TS and chamber-associated TS	
US-Ho1	NEE	Half-hourly FLUXNET-CH_4: ANN-gap-filled	Delwiche et al. (2021); Knox et al. (2019)
	u^*	Half-hourly FLUXNET-CH_4: ANN-gap-filled	
	WD	Half-hourly FLUXNET-CH_4: ANN-gap-filled	
	WS	Half-hourly FLUXNET-CH_4: gap-filled	
	VPD	Half-hourly FLUXNET-CH_4: gap-filled	
	PA	Half-hourly FLUXNET-CH_4: gap-filled	
	WTL	Half-hourly FLUXNET-CH_4: gap-filled	
	TS	Chamber-associated TS	Richardson et al. (2019)
US-La1 & US-La2	NEE	Half-hourly FLUXNET-CH_4: ANN-gap-filled	Delwiche et al. (2021); Knox et al. (2019)
	u^*	Half-hourly FLUXNET-CH_4: ANN-gap-filled	
	WD	Half-hourly FLUXNET-CH_4: ANN-gap-filled	
	WS	Half-hourly FLUXNET-CH_4: gap-filled	
	VPD	Half-hourly FLUXNET-CH_4: gap-filled	
	PA	Half-hourly FLUXNET-CH_4: gap-filled	
	WTL	Mean of daily FLUXNET-CH_4 WTL and chamber-associated WTL	Delwiche et al. (2021); Knox et al. (2019); Krauss et al. (2016)
	TS	Mean of daily gap-filled FLUXNET-CH_4 TS and chamber-associated TS	

Table C3. Continued.

Site	Environmental variable	Data	Data reference
US-Los	NEE	Half-hourly FLUXNET-CH_4: ANN-gap-filled	Delwiche et al. (2021); Knox et al. (2019)
	u^*	Half-hourly FLUXNET-CH_4: ANN-gap-filled	
	WD	Half-hourly FLUXNET-CH_4: ANN-gap-filled	
	WS	Half-hourly FLUXNET-CH_4: gap-filled	
	VPD	Half-hourly FLUXNET-CH_4: gap-filled	
	PA	Half-hourly FLUXNET-CH_4: gap-filled	
	WTL	Mean of half-hourly gap-filled FLUXNET-CH_4 WTL and chamber-associated WTL	Delwiche et al. (2021); Knox et al. (2019); Pugh et al. (2018)
	TS	Mean of half-hourly FLUXNET-CH_4 TS and chamber-associated TS	
US-Owc	NEE	Half-hourly FLUXNET-CH_4: ANN-gap-filled	Delwiche et al. (2021); Knox et al. (2019)
	u^*	Half-hourly FLUXNET-CH_4: ANN-gap-filled	
	WD	Half-hourly FLUXNET-CH_4: ANN-gap-filled	
	WS	Half-hourly FLUXNET-CH_4: gap-filled	
	VPD	Half-hourly FLUXNET-CH_4: gap-filled	
	PA	Half-hourly FLUXNET-CH_4: gap-filled	
	WTL	Mean of half-hourly gap-filled FLUXNET-CH_4 WTL and chamber-associated WTL	Delwiche et al. (2021); Knox et al. (2019); Bohrer et al. (2019)
	TS	Half-hourly FLUXNET-CH_4 TS	Delwiche et al. (2021); Knox et al. (2019)
US-StJ	NEE	Half-hourly: MDS-gap-filled	Hill and Vargas (2022a, b); Vargas (2018)
	u^*	Half-hourly: not gap-filled	
	WD	Half-hourly: not gap-filled	
	WS	Half-hourly: not gap-filled	
	VPD	Half-hourly: not gap-filled	
	PA	Half-hourly: not gap-filled	
	WTL	Half-hourly: gap-filled with a linear relationship with NOAA water table level	
	TS	Half-hourly: gap-filled with a linear relationship with water temperature	
US-Uaf	NEE	Half-hourly FLUXNET-CH_4: ANN-gap-filled	Delwiche et al. (2021); Knox et al. (2019)
	u^*	Half-hourly FLUXNET-CH_4: ANN-gap-filled	
	WD	Half-hourly FLUXNET-CH_4: ANN-gap-filled	
	WS	Half-hourly FLUXNET-CH_4: gap-filled	
	VPD	Half-hourly FLUXNET-CH_4: gap-filled	
	PA	Half-hourly FLUXNET-CH_4: gap-filled	
	WTL	Mean of half-hourly gap-filled FLUXNET-CH_4 WTL and chamber-associated WTL	Delwiche et al. (2021); Knox et al. (2019); Ueyama et al. (2023a, b)
	TS	Mean of half-hourly FLUXNET-CH_4 TS and chamber-associated TS	

Table C4. Descriptive statistics and Wilcoxon-Mann-Whitney test results based on temporal aggregations from chamber and eddy covariance (EC) methane (CH_4) flux (FCH_4) means instead of medians. Proportions of annual chamber and EC CH_4 emission (i.e., $FCH_4 \leq 0$ excluded) above the 90th percentile (p90) are reported to highlight the contribution of high CH_4 emission values to FCH_4. Abbreviations: IQR = interquartile range, SD = standard deviation, CV = coefficient of variation (%), EC = eddy covariance.

Data set	ΔFCH_4 median (IQR), nmol m^{-2} s^{-1}	ΔFCH_4 mean (SD), nmol m^{-2} s^{-1}	ΔFCH_4 CV (%)	Wilcoxon-Mann-Whitney test	Chamber FCH_4 p90 (% of total FCH_4)	EC FCH_4 p90 (% of total FCH_4)
Half-hourly	1.23 (5.74)	4.84 (18.56)	206	$p<0.001$ ($n_{EC} = 74\,482$, $n_{CH} = 74\,482$)	36.42 (46)	64.31 (44)
Hourly	1.19 (5.42)	4.76 (16.28)	198	$p<0.001$ ($n_{EC} = 40\,072$, $n_{CH} = 40\,072$)	36.62 (46)	75.81 (24)
Daily	1.11 (4.77)	-1.16 (170.67)	1106	$p<0.001$ ($n_{EC} = 1879$, $n_{CH} = 1879$)	43.47 (78)	66.67 (60)
Weekly	1.03 (6.73)	−19.55 (284.31)	770	$p = 0.015$ ($n_{EC} = 349$, $n_{CH} = 349$)	98.12 (82)	77.82 (64)
Monthly	1.05 (13.15)	−58.55 (472.15)	566	$p = 0.511$ ($n_{EC} = 121$, $n_{CH} = 121$)	315.38 (78)	218.47 (63)
Annual	0.28 (16.93)	−70.94 (311.86)	333	$p = 0.972$ ($n_{EC} = 22$, $n_{CH} = 22$)	307.19 (72)	251.67 (60)

Table C5. Descriptive statistics and Wilcoxon-Mann-Whitney test results for the difference between ecosystem- and plot-scale methane (CH_4) flux (FCH_4) (ΔFCH_4) based on cumulative eddy covariance (EC) and chamber FCH_4 (mg CH_4 m^{-2}) at daily to annual aggregations (note: cumulative FCH_4 were calculated only for exact EC-chamber FCH_4 timestamps and do not represent cumulative sums for ecosystem CH_4 budget calculations). Due to a lack of hourly timestamps in the chamber FCH_4 data at FI-Si2, US-La1 and US-La2, these three sites were excluded from this table, resulting in $n = 7$ sites. Results are given separately for data sets based on median (left) and mean (right) aggregations of chamber and EC FCH_4 at each temporal scale. The EC and chamber data sample sizes in Wilcoxon-Mann-Whitney tests are reported as n_{EC} and n_{CH}, respectively. Abbreviations: IQR = interquartile range, SD = standard deviation, CV = coefficient of variation (%).

Data set	Median-based aggregation				Mean-based aggregation			
	ΔFCH_4 median (IQR), mg CH_4 m^{-2}	ΔFCH_4 mean (SD), mg CH_4 m^{-2}	ΔFCH_4 CV (%)	Wilcoxon-Mann-Whitney test	ΔFCH_4 median (IQR), mg CH_4 m^{-2}	ΔFCH_4 mean (SD), mg CH_4 m^{-2}	ΔFCH_4 CV (%)	Wilcoxon-Mann-Whitney test
Daily	1.29 (5.5)	5.88 (29.22)	303	$p<0.001$ ($n_{EC} = 1838$, $n_{CH} = 1838$)	1.15 (5.47)	4.99 (29.1)	305	$p<0.001$ ($n_{EC} = 1838$, $n_{CH} = 1838$)
Weekly	6.39 (32.68)	34.65 (117.8)	212	$p = 0.006$ ($n_{EC} = 312$, $n_{CH} = 312$)	5.53 (32.52)	29.37 (116.05)	211	$p = 0.028$ ($n_{EC} = 312$, $n_{CH} = 312$)
Monthly	13.4 (93.83)	117.5 (385.22)	213	$p = 0.314$ ($n_{EC} = 92$, $n_{CH} = 92$)	8.85 (88.37)	99.62 (385.22)	209	$p = 0.485$ ($n_{EC} = 92$, $n_{CH} = 92$)
Annual	37.1 (742.78)	675.63 (2024.37)	193	$p = 0.897$ ($n_{EC} = 16$, $n_{CH} = 16$)	35.23 (781.38)	572.81 (1945.22)	188	$p = 0.897$ ($n_{EC} = 16$, $n_{CH} = 16$)

Table C6. Linear mixed effects model results for assessing the slopes between ecosystem-scale (eddy covariance; EC) methane (CH_4) flux (FCH_4) and plot-scale (chamber) FCH_4. To meet residual normality assumptions of linear mixed models, EC FCH_4 was transformed with inverse hyperbolic sine (IHS) and the fixed effect estimates, p-values and standard errors (SE) are in transformed scale. Average marginal effects (AME) and their 95 % confidence intervals (CI) are reported in the back-transformed units (nmol m^{-2} s^{-1}) and represent the average change in EC FCH_4 with a 1 nmol m^{-2} s^{-1} increase in chamber FCH_4 across all chamber FCH_4 observations. AME CIs were obtained with parametric simulation from the fixed effect estimate and covariance. Half-hourly and hourly models are not included due to non-convergence and residual non-normality.

Model	Fixed effect	Estimateβ (IHS scale)	p-value	SE	AME (95 % CI)
Daily	Intercept	3.647	<0.001	0.657	0.007
	Chamber FCH_4	0.0004	0.031	0.0002	(0.0006–0.032)
Weekly	Intercept	3.612	<0.001	0.645	0.011
	Chamber FCH_4	0.0006	0.066	0.0003	(−0.0007–0.049)
Monthly	Intercept	3.591	<0.001	0.646	0.009
	Chamber FCH_4	0.0005	0.183	0.0004	(−0.005–0.049)
Annual	Intercept	3.653	<0.001	0.636	0.02
	Chamber FCH_4	0.001	0.044	0.0004	(0.002–0.088)

Table C7. Wilcoxon-Mann-Whitney test results for half-hourly aggregation. The eddy covariance (EC) and chamber data sample sizes in Wilcoxon Mann-Whitney tests are reported as n_{EC} and n_{CH}, respectively. Proportions of annual chamber and EC methane (CH_4) emission (i.e., CH_4 flux (FCH_4) ≤ 0 excluded) above the 90th percentile (p90) are reported as the mean of year-specific 90th percentiles (not in parentheses) and percentages (in parentheses). This data set contains chamber measurements only from automated chambers ($n = 4$ sites). Abbreviations: IQR = interquartile range, CV = coefficient of variation (%).

Site	Mean EC FCH_4 (SD), nmol m^{-2} s^{-1}	Mean chamber FCH_4 (SD), nmol m^{-2} s^{-1}	Median EC FCH_4 (IQR, CV), nmol m^{-2} s^{-1}	Median chamber FCH_4 (IQR, CV), nmol m^{-2} s^{-1}	Median ΔFCH_4 (IQR, CV), nmol m^{-2} s^{-1}	Chamber FCH_4 p90 (% of total FCH_4)	EC FCH_4 p90 (% of total FCH_4)	Wilcoxon-Mann-Whitney test
CN-Hgu	4.73 (25.36)	−0.12 (0.35)	3.0 (6.0, 241)	−0.1 (0.24, 165)	3.12 (6.04, 239)	0.63 (55)	20 (58)	p<0.001 ($n_{EC} = 9571$, $n_{CH} = 9571$)
SE-Deg	53.18 (22.31)	25.19 (18.24)	54.1 (36.28, 42)	21.61 (24.24, 72)	26.94 (23.98, 62)	50.5 (25)	79.85 (17)	p<0.001 ($n_{EC} = 13987$, $n_{CH} = 13987$)
US-Ho1	−0.21 (1.84)	1.21 (10.47)	−0.4 (1.32, 158)	−0.89 (1.44, 334)	0.38 (2.36, 311)	18.06 (49)	3.24 (43)	p<0.001 ($n_{EC} = 30716$, $n_{CH} = 30716$)
US-Uaf	3.61 (4.35)	2.45 (3.58)	3.39 (4.17, 107)	0.78 (2.32, 146)	1.22 (3.76, 146)	5.73 (36)	6.99 (29)	p<0.001 ($n_{EC} = 20208$, $n_{CH} = 20208$)

Table C8. Wilcoxon-Mann-Whitney test results for hourly aggregation. The eddy covariance (EC) and chamber data sample sizes in Wilcoxon Mann-Whitney tests are reported as n_{EC} and n_{CH}, respectively. Proportions of annual chamber and EC methane (CH_4) emission (i.e., CH_4 flux (FCH_4) ≤ 0 excluded) above the 90th percentile (p90) are reported as the mean of year-specific 90th percentiles (not in parentheses) and percentages (in parentheses). This data set contains chamber measurements only from automated chambers ($n = 4$ sites). Abbreviations: IQR = interquartile range, CV = coefficient of variation (%).

Site	Mean EC FCH_4 (SD), nmol CH_4 m^{-2} s^{-1}	Mean chamber FCH_4 (SD), nmol CH_4 m^{-2} s^{-1}	Median EC FCH_4 (IQR, CV), nmol CH_4 m^{-2} s^{-1}	Median chamber FCH_4 (IQR, CV), nmol CH_4 m^{-2} s^{-1}	Median ΔFCH_4 (IQR, CV), nmol CH_4 m^{-2} s^{-1}	Chamber FCH_4 p90 (% of total FCH_4)	EC FCH_4 p90 (% of total FCH_4)	Wilcoxon-Mann-Whitney test
CN-Hgu	4.56 (22.87)	−0.11 (0.26)	3.0 (6.11, 229)	−0.09 (0.2, 145)	3.08 (5.99, 227)	0.6 (54)	19.75 (56)	$p<0.001$ ($n_{EC} = 5305$, $n_{CH} = 5305$)
SE-Deg	53.17 (22.05)	25.11 (17.42)	54.41 (36.28, 41)	21.6 (25.34, 69)	26.9 (23.04, 51)	49.59 (23)	79.67 (17)	$p<0.001$ ($n_{EC} = 7243$, $n_{CH} = 7243$)
US-Ho1	−0.21 (1.53)	−0.37 (3.05)	−0.36 (1.23, 149)	−0.95 (1.27, 192)	0.47 (1.95, 188)	7.43 (53)	2.82 (41)	$p<0.001$ ($n_{EC} = 17215$, $n_{CH} = 17215$)
US-Uaf	3.61 (3.71)	2.37 (3.53)	3.32 (4.04, 96)	0.73 (2.17, 149)	1.28 (3.55, 137)	5.47 (35)	7.02 (27)	$p<0.001$ ($n_{EC} = 10309$, $n_{CH} = 10309$)

Table C9. Wilcoxon-Mann-Whitney test results for daily aggregation. The eddy covariance (EC) and chamber data sample sizes in Wilcoxon-Mann-Whitney tests are reported as n_{EC} and n_{CH}, respectively. Proportions of annual chamber and EC CH_4 emission (i.e., CH_4 flux (FCH_4) ≤ 0 excluded) above the 90th percentile (p90) are reported as the mean of year-specific 90th percentiles (not in parentheses) and percentages (in parentheses). This dataset contains all sites ($n = 10$). Note: due to small sample sizes ($n = 5$) in US-La1 and US-Los, the Wilcoxon-Mann-Whitney test results should be interpreted with caution. Abbreviations: IQR = interquartile range, CV = coefficient of variation (%).

Site	Mean EC FCH_4 (SD), nmol CH_4 m^{-2} s^{-1}	Mean chamber FCH_4 (SD), nmol CH_4 m^{-2} s^{-1}	Median EC FCH_4 (IQR, CV), nmol CH_4 m^{-2} s^{-1}	Median chamber FCH_4 (IQR, CV), nmol CH_4 m^{-2} s^{-1}	Median ΔFCH_4 (IQR, CV), nmol CH_4 m^{-2} s^{-1}	Chamber FCH_4 p90 (% of total FCH_4)	EC FCH_4 p90 (% of total FCH_4)	Wilcoxon-Mann-Whitney test
CN-Hgu	3.22 (1.79)	−0.12 (0.11)	3.0 (2.14, 55)	−0.07 (0.12, 93)	3.2 (2.21, 54)	0.04 (17)	5.69 (20)	$p<0.001$ ($n_{EC} = 265$, $n_{CH} = 265$)
FI-Si2	57.13 (18.74)	62.14 (37.85)	54.37 (21.48, 33)	49.46 (57.04, 61)	0.81 (30.53, 132)	98.37 (25)	77.5 (19)	$p = 0.737$ ($n_{EC} = 26$, $n_{CH} = 26$)
SE-Deg	52.44 (20.75)	24.24 (15.76)	55.88 (39.7, 40)	21.39 (24.96, 65)	0.81 (30.53, 132)	48.56 (21)	78.16 (15)	$p<0.001$ ($n_{EC} = 317$, $n_{CH} = 317$)
US-Ho1	−0.43 (0.54)	−0.68 (1.67)	−0.45 (0.73, 96)	−1.01 (0.9, 130)	0.39 (1.22, 165)	2.04 (52)	0.4 (39)	$p<0.001$ ($n_{EC} = 759$, $n_{CH} = 759$)
US-La1	41.49 (29.79)	97.72 (65.37)	42.12 (53.85, 72)	116.91 (62.59, 67)	−45.43 (71.64, 115)	157.64 (37)	71.03 (34)	$p = 0.222$ ($n_{EC} = 5$, $n_{CH} = 5$)
US-La2	163.74 (63.81)	191.35 (93.46)	150.22 (103.39, 39)	189.16 (117.65, 49)	5.75 (103.92, 141)	276.98 (32)	226.3 (30)	$p = 0.436$ ($n_{EC} = 10$, $n_{CH} = 10$)
US-Los	35.37 (12.78)	9.61 (5.62)	38.75 (13.82, 36)	8.43 (4.09, 58)	27.75 (4.74, 37)	15.42 (38)	46.72 (28)	$p = 0.016$ ($n_{EC} = 5$, $n_{CH} = 5$)
US-Owc	607.26 (289.11)	770.24 (766.66)	652.8 (490.18, 48)	579.95 (721.2, 100)	−108.22 (485.14, 169)	1306.07 (46)	936.62 (28)	$p = 0.988$ ($n_{EC} = 18$, $n_{CH} = 18$)
US-StJ	39.2 (58.96)	13.98 (27.01)	16.4 (29.69, 150)	5.26 (8.31, 193)	9.15 (20.85, 202)	22.15 (63)	73.94 (54)	$p = 0.007$ ($n_{EC} = 16$, $n_{CH} = 16$)
US-Uaf	3.5 (2.09)	2.15 (3.12)	3.49 (3.96, 60)	0.66 (2.0, 145)	1.27 (2.29, 111)	4.97 (25)	6.09 (20)	$p<0.001$ ($n_{EC} = 458$, $n_{CH} = 458$)

Table C10. Wilcoxon-Mann-Whitney test results for weekly aggregation. The eddy covariance (EC) and chamber data sample sizes in Wilcoxon-Mann-Whitney tests are reported as n_{EC} and n_{CH}, respectively. Proportions of annual chamber and EC methane (CH_4) emission (i.e., CH_4 flux (FCH_4) ≤ 0 excluded) above the 90th percentile (p90) are reported as the mean of year-specific 90th percentiles (not in parentheses) and percentages (in parentheses). This dataset contains all sites ($n = 10$). Note: due to small sample sizes ($n = 5$) in US-La1 and US-Los, the Wilcoxon-Mann-Whitney test results should be interpreted with caution. Abbreviations: IQR = interquartile range, CV = coefficient of variation (%).

Site	Mean EC FCH_4 (SD), nmol CH_4 m^{-2} s^{-1}	Mean chamber FCH_4 (SD), nmol CH_4 m^{-2} s^{-1}	Median EC FCH_4 (IQR, CV), nmol CH_4 m^{-2} s^{-1}	Median chamber FCH_4 (IQR, CV), nmol CH_4 m^{-2} s^{-1}	Median ΔFCH_4 (IQR, CV), nmol CH_4 m^{-2} s^{-1}	Chamber FCH_4 p90 (% of total FCH_4)	EC FCH_4 p90 (% of total FCH_4)	Wilcoxon-Mann-Whitney test
CN-Hgu	3.02 (1.18)	−0.12 (0.11)	3.0 (1.98, 39)	−0.07 (0.13, 90)	3.08 (1.98, 39)	0.02 (59)	4.26 (20)	$p<0.001$ ($n_{EC} = 40$, $n_{CH} = 40$)
FI-Si2	55.43 (17.61)	59.55 (35.23)	53.36 (18.93, 32)	49.46 (48.82, 59)	1.45 (24.92, 139)	88.39 (27)	73.87 (22)	$p = 0.789$ ($n_{EC} = 22$, $n_{CH} = 22$)
SE-Deg	50.17 (21.18)	22.73 (15.64)	50.94 (38.12, 42)	18.74 (22.04, 69)	24.83 (19.9, 43)	46.5 (27)	76.31 (19)	$p<0.001$ ($n_{EC} = 50$, $n_{CH} = 50$)
US-Ho1	−0.42 (0.48)	−0.69 (1.34)	−0.42 (0.72, 90)	−0.99 (0.91, 112)	0.32 (1.28, 146)	6.02 (43)	0.41 (27)	$p<0.001$ ($n_{EC} = 119$, $n_{CH} = 119$)
US-La1	41.49 (29.79)	97.72 (65.37)	42.12 (53.85, 72)	116.91 (62.59, 67)	−45.43 (71.64, 115)	157.64 (37)	71.03 (34)	$p = 0.222$ ($n_{EC} = 5$, $n_{CH} = 5$)
US-La2	163.74 (63.81)	191.35 (93.46)	150.22 (103.39, 39)	189.16 (117.65, 49)	5.75 (103.92, 141)	276.98 (32)	226.3 (30)	$p = 0.436$ ($n_{EC} = 10$, $n_{CH} = 10$)
US-Los	35.37 (12.78)	9.61 (5.62)	38.75 (13.82, 36)	8.43 (4.09, 58)	27.75 (4.74, 37)	15.42 (38)	46.72 (28)	$p = 0.016$ ($n_{EC} = 5$, $n_{CH} = 5$)
US-Owc	561.44 (287.63)	753.88 (619.97)	642.45 (446.31, 51)	552.85 (657.0, 82)	47.22 (728.26, 145)	1185.44 (56)	828.1 (45)	$p = 0.796$ ($n_{EC} = 9$, $n_{CH} = 9$)
US-StJ	39.2 (58.96)	13.98 (27.01)	16.4 (29.69, 150)	5.26 (8.31, 193)	9.15 (20.85, 202)	22.12 (63)	73.94 (54)	$p = 0.007$ ($n_{EC} = 16$, $n_{CH} = 16$)
US-Uaf	3.4 (1.97)	2.01 (3.04)	3.46 (3.82, 58)	0.64 (1.87, 151)	1.18 (2.13, 107)	4.76 (29)	5.85 (23)	$p<0.001$ ($n_{EC} = 73$, $n_{CH} = 73$)

Table C11. Wilcoxon-Mann-Whitney test results for monthly aggregation. The eddy covariance (EC) and chamber data sample sizes in Wilcoxon-Mann-Whitney tests are reported as n_{EC} and n_{CH}, respectively. Proportions of annual chamber and EC methane (CH_4) emission (i.e., CH_4 flux (FCH_4) ≤ 0 excluded) above the 90th percentile (p90) are reported as the mean of year-specific 90th percentiles (not in parentheses) and percentages (in parentheses). This dataset contains all sites ($n = 10$). Note: due to small sample sizes ($n = 5$) in US-La1 and US-Los, the Wilcoxon-Mann-Whitney test results should be interpreted with caution. Abbreviations: IQR = interquartile range, CV = coefficient of variation (%). * CN-Hgu had only negative chamber FCH_4 values and chamber p90 was not calculated for this site.

Site	Mean EC FCH_4 (SD), nmol CH_4 m^{-2} s^{-1}	Mean chamber FCH_4 (SD), nmol CH_4 m^{-2} s^{-1}	Median EC FCH_4 (IQR, CV), nmol CH_4 m^{-2} s^{-1}	Median chamber FCH_4 (IQR, CV), nmol CH_4 m^{-2} s^{-1}	Median ΔFCH_4 (IQR, CV), nmol CH_4 m^{-2} s^{-1}	Chamber FCH_4 p90 (% of total FCH_4)	EC FCH_4 p90 (% of total FCH_4)	Wilcoxon-Mann-Whitney test
CN-Hgu	3.1 (1.06)	−0.12 (0.1)	3.0 (1.08, 34)	−0.07 (0.14, 84)	3.05 (1.2, 34)	−*	4.14 (30)	$p<0.001$ ($n_{EC} = 10$, $n_{CH} = 10$)
FI-Si2	52.49 (16.25)	51.0 (26.4)	53.36 (23.22, 31)	47.79 (44.33, 52)	2.68 (26.17, 120)	73.18 (32)	68.51 (29)	$p = 0.635$ ($n_{EC} = 14$, $n_{CH} = 14$)
SE-Deg	46.58 (22.45)	20.66 (15.23)	46.85 (44.64, 48)	15.7 (22.22, 74)	25.1 (11.52, 46)	40.22 (33)	73.06 (25)	$p = 0.002$ ($n_{EC} = 13$, $n_{CH} = 13$)
US-Ho1	−0.44 (0.45)	−0.8 (0.97)	−0.46 (0.6, 86)	−1.05 (0.8, 88)	0.35 (1.12, 124)	2.86 (67)	0.28 (41)	$p<0.001$ ($n_{EC} = 32$, $n_{CH} = 32$)
US-La1	41.49 (29.79)	97.72 (65.37)	42.12 (53.85, 72)	116.91 (62.59, 67)	−45.43 (71.64, 115)	157.64 (37)	71.03 (34)	$p = 0.222$ ($n_{EC} = 5$, $n_{CH} = 5$)
US-La2	163.74 (63.81)	191.35 (93.46)	150.22 (103.39, 39)	189.16 (117.65, 49)	5.75 (103.92, 141)	276.98 (32)	226.3 (30)	$p = 0.436$ ($n_{EC} = 10$, $n_{CH} = 10$)
US-Los	32.8 (14.3)	7.78 (2.88)	38.75 (13.34, 44)	6.91 (2.78, 37)	27.75 (14.07, 57)	10.18 (47)	42.28 (44)	$p = 0.1$ ($n_{EC} = 3$, $n_{CH} = 3$)
US-Owc	575.34 (301.58)	705.33 (549.45)	642.45 (446.31, 52)	667.58 (756.29, 78)	131.03 (524.49, 144)	1056.3 (58)	828.57 (47)	$p = 0.798$ ($n_{EC} = 8$, $n_{CH} = 8$)
US-StJ	24.14 (19.65)	9.92 (11.72)	21.19 (22.71, 81)	6.0 (7.45, 118)	18.45 (22.01, 82)	20.73 (47)	44.15 (33)	$p = 0.105$ ($n_{EC} = 8$, $n_{CH} = 8$)
US-Uaf	3.39 (1.87)	2.17 (3.15)	3.42 (3.87, 55)	0.65 (1.97, 145)	1.24 (1.84, 114)	4.5 (34)	5.52 (28)	$p = 0.006$ ($n_{EC} = 18$, $n_{CH} = 18$)

Table C12. Wilcoxon-Mann-Whitney test results for annual aggregation. The eddy covariance (EC) and chamber data sample sizes in Wilcoxon-Mann-Whitney tests are reported as n_{EC} and n_{CH}, respectively. Annual chamber and EC methane (CH_4) flux (FCH_4) 90th percentiles were not calculated for this aggregation. This dataset contains all sites ($n = 10$). Note: due to small sample sizes ($n = 5$) in US-La1 and US-Los, the Wilcoxon-Mann-Whitney test results should be interpreted with caution. Abbreviations: IQR = interquartile range, CV = coefficient of variation (%).

Site	Mean EC FCH_4 (SD), nmol CH_4 m^{-2} s^{-1}	Mean chamber FCH_4 (SD), nmol CH_4 m^{-2} s^{-1}	Median EC FCH_4 (IQR, CV), nmol CH_4 m^{-2} s^{-1}	Median chamber FCH_4 (IQR, CV), nmol CH_4 m^{-2} s^{-1}	Median ΔFCH_4 (IQR, CV), nmol CH_4 m^{-2} s^{-1}	Wilcoxon-Mann-Whitney test
CN-Hgu	3.04 (0.06)	−0.15 (0.14)	3.04 (0.04, 2)	−0.15 (0.1, 94)	3.2 (0.14, 6)	–
FI-Si2	55.7 (2.45)	53.01 (23.84)	55.19 (2.41, 4)	66.22 (20.91, 45)	−7.85 (21.73, 138)	$p = 0.7$ ($n_{EC} = 3$, $n_{CH} = 3$)
SE-Deg	54.08 (3.69)	20.78 (0.59)	54.08 (2.61, 7)	20.78 (0.42, 3)	33.3 (2.19, 9)	–
US-Ho1	−0.38 (0.27)	−0.82 (0.45)	−0.51 (0.34, 70)	−0.77 (0.57, 55)	0.25 (0.78, 111)	$p = 0.095$ ($n_{EC} = 5$, $n_{CH} = 5$)
US-La1	37.77 (–)	76.56 (–)	37.77 (–,–)	76.56 (–,–)	−38.79 (–,–)	–
US-La2	163.81 (49.76)	161.89 (74.25)	163.81 (35.19, 30)	161.89 (52.5, 46)	1.93 (87.69, 141)	–
US-Los	38.18 (–)	8.12 (–)	38.18 (–,–)	8.12 (–,–)	30.05 (–,–)	–
US-Owc	476.61 (209.52)	539.49 (445.72)	476.61 (148.15, 44)	539.49 (315.17, 83)	−62.88 (167.02, 141)	–
US-StJ	14.06 (–)	4.97 (–)	14.06 (–,–)	4.97 (–,–)	9.09 (–,–)	–
US-Uaf	3.38 (0.11)	0.65 (0.34)	3.42 (0.11, 3)	0.52 (0.32, 52)	2.95 (0.41, 16)	$p = 0.1$ ($n_{EC} = 3$, $n_{CH} = 3$)

Table C13. Final linear mixed effects model results of significant predictors of the difference between ecosystem- and plot-scale methane (CH_4) flux (FCH_4) (ΔFCH_4) for the half-hourly model (site $n = 3$) with soil temperature (TS) instead of Month as one of the predictors. Absolute ΔFCH_4 was Yeo-Johnson-transformed, centered and scaled, while all continuous predictors were only centered and scaled. The predictors are listed in decreasing order based on β-coefficients. The reference level in Hour was 0 and May in Month. Abbreviations: SE = standard error, Df = degrees of freedom of denominator, LOOCV = leave-one-out cross validation, MAE = mean absolute error, RMSE = root mean square error, PA = air pressure (kPa), u^* = friction velocity ($m\,s^{-1}$), WTL = water table level (cm), TS = soil temperature (°C), NEE = net ecosystem exchange ($\mu mol\,CO_2\,m^{-2}\,s^{-1}$), VPD = vapor pressure deficit (hPa), vWD = v wind component ($m\,s^{-1}$), uWD = u wind component ($m\,s^{-1}$). Significant predictors are highlighted in bold.

Predictors	β-coefficient	SE	p-value (t-test)	Marginal R^2	Conditional R^2	Df	Random effect variation explained, %	LOOCV		
								R^2	MAE	RMSE
Intercept	0.0581	0.5465	0.9153	0.0109	0.805	43 522		−0.94	1.36	1.5
Fixed effects										
Hour										
– 5 AM	0.0838	0.0166	**0**			43 522				
u*	0.0836	0.004	**0**			43 522				
Hour	−0.0565	0.01	**0**			43 522				
– 6 AM	0.0727	0.0163	**0**			43 522				
PA	−0.0684	0.0105	**0**			43 522				
Hour										
– 4 AM	0.0567	0.0163	**0.0005**			43 522				
– 7 AM	0.0489	0.0165	**0.003**			43 522				
– 10 AM	−0.0406	0.0169	**0.0161**			43 522				
– 8 AM	0.0392	0.0166	**0.0181**			43 522				
– 3 AM	0.0375	0.0166	**0.0238**			43 522				
– 10 PM	−0.0311	0.0163	0.0559			43 522				
– 5 PM	−0.0294	0.0166	0.0776			43 522				
NEE	−0.0289	0.004	**0**			43 522				
TS	−0.027	0.0068	**0.0001**			43 522				
VPD	−0.0268	0.0054	**0**			43 522				
Hour										
– 3 PM	−0.0248	0.0172	0.1498			43 522				
– 9 PM	−0.0246	0.0168	0.1412			43 522				
– 6 PM	−0.0221	0.0163	0.1741			43 522				
– 8 PM	−0.0201	0.0165	0.2224			43 522				
– 7 PM	−0.018	0.0165	0.2745			43 522				
vWD	−0.018	0.0036	**0**			43 522				

Table C13. Continued.

Predictors	β-coefficient	SE	p-value (t-test)	Marginal R^2	Conditional R^2	Df	Random effect variation explained, %	LOOCV		
								R^2	MAE	RMSE
Hour										
– 2 AM	0.0175	0.0163	0.2827			43 522				
– 1 PM	−0.0148	0.0173	0.394			43 522				
– 12 PM	−0.0094	0.0172	0.5833			43 522				
– 1 AM	0.0072	0.0166	0.6597			43 522				
– 11 PM	−0.0054	0.0165	0.7413			43 522				
– 2 PM	−0.0042	0.0171	0.8068			43 522				
– 11 AM	−0.0028	0.0172	0.8698			43 522				
– 9 AM	−0.0024	0.0171	0.8847			43 522				
– 4 PM	−0.0013	0.0167	0.9376			43 522				
Random effects										
Site							72.29			
Date							8			

Table C14. Half-hourly and hourly linear mixed effects model results after backward variable selection. In the models, absolute the difference between ecosystem- and plot-scale methane (CH_4) flux (FCH_4) (ΔFCH_4) was Yeo-Johnson-transformed, centered and scaled, while all continuous predictors were only centered and scaled. Note that in both models temporal variables were included in nested random effects (see Supplementary Methods A2). In both models, the reference level in dominant vegetation type was *Sphagnum* moss, 0 in Hour and May in Month. Note that we excluded TS from the half-hourly model due to high multicollinearity with Month (VIF > 3; see models with TS instead of Month in S17). The predictors are listed in a decreasing order according to their ??-coefficients. SE = standard error, Df = degrees of freedom of denominator, LOOCV = leave-one-out cross validation, MAE = mean absolute error, RMSE = root mean square error, PA = air pressure (kPa), u^* = friction velocity ($m\,s^{-1}$), WTL = water table level (cm), TS = soil temperature (°C), NEE = net ecosystem exchange ($\mu mol\,CO_2\,m^{-2}\,s^{-1}$), VPD = vapor pressure deficit (hPa), vWD = v wind component ($m\,s^{-1}$), uWD = u wind component ($m\,s^{-1}$). Significant predictors are highlighted in bold.

Data set	Predictors	β-coefficient	SE	p-value (t-test)	Marginal R^2	Conditional R^2	Df	Random effect variation explained, %	LOOCV		
									R^2	MAE	RMSE
Half-hourly ($n = 3$ sites)	Intercept	−0.236	0.5259	0.6537	0.0329	0.7933	43 522		−0.62	1.37	1.22
	Fixed effects										
	Month										
	– **Aug**	0.4626	0.0291	**0**			1408				
	– **Jul**	0.4169	0.029	**0**			1408				
	– **Sep**	0.3972	0.0294	**0**			1408				
	– **Jun**	0.2157	0.0293	**0**			1408				
	– Apr	0.1615	0.0164	0.6751			1408				
	– **Oct**	0.1105	0.0316	**0.0005**			1408				
	u*	0.0876	0.0039	**0**			43 522				
	Hour										
	– **5 AM**	0.0873	0.0166	**0**			43 522				
	– **6 AM**	0.0742	0.0163	**0**			43 522				
	WTL	0.0617	0.0121	**0**			43 522				
	Hour										
	– **4 AM**	0.0593	0.0163	**0.0003**			43 522				
	PA	−0.056	0.0097	**0**			43 522				
	Hour										
	– **7 AM**	0.0486	0.0165	**0.0032**			43 522				
	– **10 AM**	−0.0449	0.0168	**0.0075**			43 522				
	– **3 AM**	0.0409	0.0166	**0.0137**			43 522				
	VPD	−0.0394	0.0049	**0**			43 522				
	Hour										
	– **8 AM**	0.0376	0.0166	**0.0235**			43 522				
	Month										
	– Nov	0.0372	0.0535	0.4865			1408				
	Hour										
	– 10 PM	−0.0323	0.0163	0.0476			43 522				
	– 5 PM	−0.0323	0.0166	0.0515			43 522				
	– 3 PM	−0.0297	0.0171	0.0825			43 522				

Table C14. Continued.

Data set	Predictors	β-coefficient	SE	p-value (t-test)	Marginal R^2	Conditional R^2	Df	Random effect variation explained, %	LOOCV		
									R^2	MAE	RMSE
	NEE	−0.0295	0.0039	**0**			43 522				
	Hour										
	– 9 PM	−0.0259	0.0168	0.1221			43 522				
	– 6 PM	−0.0245	0.0163	0.1319			43 522				
	– 8 PM	−0.0207	0.0164	0.2072			43 522				
	– 1 PM	−0.0206	0.0172	0.2309			43 522				
	– 7 PM	−0.0198	0.0165	0.2293			43 522				
	– 2 AM	0.0194	0.0163	0.2336			43 522				
	vWD	−0.0179	0.0035	**0**			43 522				
	Hour										
	– 12 PM	−0.0155	0.0171	0.363			43 522				
	– 2 PM	−0.0095	0.017	0.5736			43 522				
	– 1 AM	0.0089	0.0166	0.5925			43 522				
	– 11 AM	−0.008	0.0171	0.6385			43 522				
	– 11 PM	−0.0052	0.0165	0.7522			43 522				
	– 4 PM	−0.0049	0.0166	0.7696			43 522				
	– 9 AM	−0.0045	0.0171	0.7928			43 522				
	Random effects										
	Site							72.44			
	Date							6.22			
Hourly	Intercept	−0.2978	0.5368	0.5791	0.0439	0.816	25 231		-0.46	1.22	1.37
($n = 3$	Fixed effects										
sites)	Month										
	– **Aug**	0.6418	0.0359	**0**			1405				
	– **Jul**	0.5815	0.0365	**0**			1405				
	– **Sep**	0.5118	0.035	**0**			1405				
	– Apr	−0.3979	0.4686	0.3959			1405				
	– **Jun**	0.27	0.0354	**0**			1405				
	– **Oct**	0.1829	0.0373	**0**			1405				
	Hour										
	– **5 AM**	0.1371	0.0208	**0**			25 231				
	WTL	0.0936	0.0142	**0**			25 231				
	Hour										
	– **7 AM**	0.0926	0.0207	**0**			25 231				
	– **3 AM**	0.0841	0.0206	**0**			25 231				
	TS	−0.0838	0.0092	**0**			25 231				
	Hour										
	– **6 AM**	0.0831	0.0204	**0**			25 231				
	u*	0.0687	0.0051	**0**			25 231				

Table C14. Continued.

Data set	Predictors	β-coefficient	SE	p-value (t-test)	Marginal R^2	Conditional R^2	Df	Random effect variation explained, %	LOOCV		
									R^2	MAE	RMSE
	Hour										
	– **9 AM**	0.0657	0.0216	**0.0024**			25 231				
	– **8 AM**	0.0656	0.0207	**0.0016**			25 231				
	– **1 AM**	0.0594	0.0206	**0.0039**			25 231				
	– **11 PM**	0.0578	0.0204	**0.0046**			25 231				
	– **1 PM**	0.0488	0.0222	**0.028**			25 231				
	– **7 PM**	0.0479	0.0206	**0.0197**			25 231				
	– **11 AM**	0.0476	0.022	**0.0302**			25 231				
	PA	−0.0458	0.0117	**0.0001**			25 231				
	Hour										
	– **4 AM**	0.0417	0.0201	**0.0383**			25 231				
	– 3 PM	0.0417	0.0218	0.056			25 231				
	– 2 AM	0.0377	0.0201	0.0612			25 231				
	– 12 PM	0.0336	0.0219	0.1259			25 231				
	– 2 PM	0.0272	0.0218	0.2113			25 231				
	– 5 PM	0.0267	0.021	0.2039			25 231				
	NEE	−0.0243	0.0052	**0**			25 231				
	Hour										
	– 10 AM	−0.0183	0.0215	0.3942			25 231				
	VPD	−0.0181	0.0066	**0.0063**			25 231				
	Month										
	– Nov	0.0176	0.0628	0.7792			1405				
	Hour										
	– 6 PM	−0.0167	0.0204	0.4144			25 231				
	– 9 PM	0.0149	0.0207	0.4738			25 231				
	– 4 PM	0.0148	0.0212	0.4851			25 231				
	– 8 PM	−0.0129	0.0202	0.523			25 231				
	– 10 PM	−0.0121	0.0202	0.5514			25 231				
	vWD	−0.0081	0.0045	0.0705			25 231				
	Random effects										
	Site							72.46			
	Date							8.29			

Table C15. Full linear mixed effects model results. In the models, absolute the difference between ecosystem- and plot-scale methane (CH_4) flux (FCH_4) (ΔFCH_4) was Yeo-Johnson-transformed, centered and scaled, while all continuous predictors were only centered and scaled. This table presents the full models with both nonsignificant and significant predictors before backward variable selection. The final daily and monthly models were the full models which are shown in Table 3 of the main text. Note that in all models temporal variables were included in nested random effects (see methods and Supplementary Methods A2). In all models, the reference level in site dominant vegetation (VEG) was *Sphagnum* moss, 0 in Hour and May in Month. Annual models were not included due to an inadequate number of observations. Due to lack of complete case observations, US-Owc was not included in the weekly and monthly models ($n = 7$ sites). We excluded TS from the half-hourly model due to high multicollinearity with Month (VIF > 3). Due to multicollinearity in the weekly model, we built one model without NEE and one without VPD. Fixed effects are listed in decreasing order based on their β-coefficients. SE = standard error, Df = degrees of freedom of denominator, LOOCV = leave-one-out cross validation, MAE = mean absolute error, RMSE = root mean square error, PA = air pressure (kPa), u^* = friction velocity ($m\,s^{-1}$), WTL = water table level (cm), TS = soil temperature (°C), NEE = net ecosystem exchange ($\mu mol\,CO_2\,m^{-2}\,s^{-1}$), VPD = vapor pressure deficit (hPa), vWD = v wind component ($m\,s^{-1}$), uWD = u wind component ($m\,s^{-1}$). Significant predictors are highlighted in bold.

Data set	Predictors	β-coefficient	SE	p-value (t-test)	Marginal R^2	Conditional R^2	Df	Random effect variation explained, %	LOOCV		
									R^2	MAE	RMSE
Half-hourly ($n = 3$ sites)	Intercept	0.0962	0.7069	0.8917	0.2041	0.8518	43 521		−2.27	1.46	1.55
	Fixed effects										
	VEG										
	– Tree	−0.9969	1.2237	0.5648			1				
	Month										
	– **Aug**	0.4629	0.029	**0**			1408				
	– **Jul**	0.4172	0.029	**0**			1408				
	– **Sep**	0.3974	0.0294	**0**			1408				
	– **Jun**	0.2161	0.0294	**0**			1408				
	– Apr	0.1613	0.3852	0.6753			1408				
	– **Oct**	0.1109	0.0316	**0.0005**			1408				
	u*	0.088	0.004	**0**			43 521				
	Hour										
	– **5 AM**	0.0873	0.0166	**0**			43 521				
	– **6 AM**	0.0741	0.0163	**0**			43 521				
	WTL	0.0615	0.0121	**0**			43 521				
	Hour										
	– **4 AM**	0.0592	0.0163	**0.0003**			43 521				
	PA	−0.056	0.0097	**0**			43 521				
	Hour										
	– **7 AM**	0.0484	0.0165	**0.0033**			43 521				
	– **10 AM**	−0.0451	0.0168	**0.0073**			43 521				
	– **3 AM**	0.0409	0.0166	**0.0138**			43 521				
	VPD	−0.0393	0.0049	**0**			43 521				

Table C15. Continued.

Data set	Predictors	β-coefficient	SE	p-value (t-test)	Marginal R^2	Conditional R^2	Df	Random effect variation explained, %	LOOCV		
									R^2	MAE	RMSE
	Month										
	– Nov	0.0376	0.0535	0.4822			1408				
	Hour										
	– **8 AM**	0.0373	0.0166	**0.0244**			43 521				
	– 5 PM	−0.0325	0.0166	0.0502			43 521				
	– 10 PM	−0.0323	0.0163	0.0476			43 521				
	– 3 PM	−0.0299	0.0171	0.0808			43 521				
	NEE	−0.0294	0.0039	**0**			43 521				
	Hour										
	– 9 PM	−0.0259	0.0168	0.1219			43 521				
	– 6 PM	−0.0247	0.0163	0.1296			43 521				
	– 8 PM	−0.0208	0.0164	0.2056			43 521				
	– 1 PM	−0.0207	0.0172	0.2282			43 521				
	– 7 PM	−0.0199	0.0165	0.2267			43 521				
	– 2 AM	0.0194	0.0163	0.234			43 521				
	vWD	−0.0182	0.0036	**0**			43 521				
	Hour										
	– 12 PM	−0.0156	0.0171	0.3593			43 521				
	– 2 PM	−0.0097	0.017	0.5678			43 521				
	– 1 AM	0.0089	0.0166	0.5925			43 521				
	– 11 AM	−0.0082	0.0171	0.6317			43 521				
	– 11 PM	−0.0052	0.0165	0.7538			43 521				
	– 4 PM	−0.0051	0.0166	0.7589			43 521				
	– 9 AM	−0.0047	0.0171	0.7818			43 521				
	uWD	−0.0015	0.0035	0.6716			43 521				
	Random effects										
	Site							75.96			
	Date							5.43			
Hourly	Intercept	0.0199	0.7487	0.9788	0.2116	0.8752	25 230				1.62
($n = 3$	Fixed effects										
sites)	VEG										
	– Tree	−0.9517	1.2957	0.5967			1				

Table C15. Continued.

Data set	Predictors	β-coefficient	SE	p-value (t-test)	Marginal R^2	Conditional R^2	Df	Random effect variation explained, %	LOOCV		
									R^2	MAE	RMSE
	Month										
	– **Aug**	0.6413	0.036	**0**			1405				
	– **Jul**	0.5811	0.0366	**0**			1405				
	– **Sep**	0.5114	0.035	**0**			1405				
	– Apr	−0.3974	0.4686	0.3966			1405				
	– **Jun**	0.2697	0.0355	**0**			1405				
	– **Oct**	0.1826	0.0373	**0**			1405				
	Hour										
	– **5 AM**	0.1371	0.0208	**0**			25 230				
	WTL	0.0933	0.0142	**0**			25 230				
	Hour										
	– **7 AM**	0.0927	0.0207	**0**			25 230				
	– **3 AM**	0.0841	0.0206	**0**			25 230				
	TS	−0.0837	0.0093	**0**			25 230				
	Hour										
	– **6 AM**	0.0831	0.0204	**0**			25 230				
	u*	0.0685	0.0052	**0**			25 230				
	Hour										
	– **9 AM**	0.0658	0.0217	**0.0024**			25 230				
	– **8 AM**	0.0656	0.0207	**0.0015**			25 230				
	– **1 AM**	0.0594	0.0206	**0.0039**			25 230				
	– **11 PM**	0.0578	0.0204	**0.0046**			25 230				
	– **1 PM**	0.0488	0.0222	**0.028**			25 230				
	– **7 PM**	0.048	0.0206	**0.0196**			25 230				
	– **11 AM**	0.0476	0.022	**0.0302**			25 230				
	PA	−0.0455	0.0117	**0.0001**			25 230				
	Hour										
	– 3 PM	0.0417	0.0218	0.0558			25 230				
	– **4 AM**	0.0417	0.0201	**0.0384**			25 230				
	– 2 AM	0.0377	0.0201	0.0611			25 230				
	– 12 PM	0.0336	0.0219	0.126			25 230				
	– 2 PM	0.0272	0.0218	0.2111			25 230				
	– 5 PM	0.0268	0.021	0.2028			25 230				
	NEE	−0.0244	0.0052	**0**			25 230				
	Hour										
	– 10 AM	−0.0183	0.0215	0.3958			25 230				
	VPD	−0.0182	0.0066	**0.0061**			25 230				
	Month										
	– Nov	0.0177	0.0628	0.7786			1405				

Table C15. Continued.

Data set	Predictors	β-coefficient	SE	p-value (t-test)	Marginal R^2	Conditional R^2	Df	Random effect variation explained, %	LOOCV		
									R^2	MAE	RMSE
	Hour										
	– 6 PM	−0.0166	0.0204	0.4159			25 230				
	– 4 PM	0.0149	0.0212	0.4826			25 230				
	– 9 PM	0.0149	0.0207	0.4738			25 230				
	– 8 PM	−0.0129	0.0202	0.5236			25 230				
	– 10 PM	−0.0121	0.0202	0.5505			25 230				
	vWD	−0.0079	0.0045	0.0833			25 230				
	uWD	0.0009	0.0044	0.8346			25 230				
	Random effects										
	Site							77.37			
	Date							6.81			
Weekly	Intercept	0.3046	0.3665	0.407	0.5468	0.8357	180		−1.15	1.34	1.58
(no NEE,	Fixed effects										
$n = 9$	VEG										
sites)	– Tree	−1.4712	0.702	0.0903			5				
	– Aerenchymatous	0.9949	0.5112	0.1092			5				
	– Ericaceous shrub	0.5253	0.7163	0.4962			5				
	Month										
	– Apr	0.3907	0.416	0.3502			86				
	– Nov	0.3193	0.2602	0.2232			86				
	– Dec	0.316	0.6993	0.6524			86				
	– **Jul**	0.3104	0.142	**0.0315**			86				
	– **Aug**	0.3012	0.1442	**0.0396**			86				
	– **Sep**	0.2964	0.14	**0.0371**			86				
	– Jun	0.2082	0.1388	0.1373			86				
	– Oct	0.169	0.1457	0.2492			86				
	WTL	−0.0727	0.0551	0.1887			180				
	PA	−0.0604	0.0407	0.14			180				
	VPD	−0.0352	0.0318	0.2701			180				
	u^*	0.0317	0.0272	0.244			180				
	Month										
	– Mar	−0.0234	0.5319	0.9649			86				
	vWD	−0.0167	0.0175	0.3418			180				
	TS	−0.0104	0.06	0.862			180				
	uWD	−0.0081	0.0198	0.6819			180				

Table C15. Continued.

Data set	Predictors	β-coefficient	SE	p-value (t-test)	Marginal R^2	Conditional R^2	Df	Random effect variation explained, %	LOOCV		
									R^2	MAE	RMSE
	Random effects										
	Site							63.74			
	Year-month							$6.38e^{-07}$			
Weekly	Intercept	0.3008	0.3724	0.4202	0.5423	0.8365	180		−1.03	1.3	1.54
(no VPD,	Fixed effects										
$n = 9$	VEG										
sites)	– Tree	−1.4642	0.713	0.0952			5				
	– Aerenchymatous	0.9763	0.5228	0.1208			5				
	– Ericaceous shrub	0.4435	0.7268	0.5684			5				
	Month										
	– Apr	0.3611	0.4145	0.386			86				
	– Dec	0.3525	0.7059	0.6188			86				
	– Nov	0.3375	0.263	0.2029			86				
	– **Aug**	0.317	0.1484	**0.0355**			86				
	– **Jul**	0.3144	0.1438	**0.0315**			86				
	– **Sep**	0.3086	0.1408	**0.0311**			86				
	– Jun	0.2001	0.141	0.1596			86				
	– Oct	0.1847	0.1473	0.2134			86				
	– Mar	−0.0786	0.5287	0.8822			86				
	PA	−0.0737	0.039	0.0603			180				
	WTL	−0.07	0.0546	0.2046			180				
	u^*	0.032	0.0276	0.2464			180				
	TS	−0.019	0.0637	0.7663			180				
	vWD	−0.0184	0.0175	0.2962			180				
	uWD	−0.0137	0.0201	0.4953			180				
	NEE	0.01	0.0266	0.7117			180				
	Random effects										
	Site							64.27			
	Year-month							$4.91e^{-07}$			

Code availability. The R code used for processing the EC and chamber CH_4 flux data, statistical analyses and producing the figures can be accessed via Zenodo (https://doi.org/10.5281/zenodo.20558238, Määttä, 2026).

Data availability. The timestamp-aligned data sets containing ecosystem and plot-scale CH_4 flux and environmental data at half-hourly, hourly, daily, weekly, monthly, and annual scales can be accessed via Zenodo (https://doi.org/10.5281/zenodo.17312404, Määttä et al., 2025).

Author contributions. TM, AM, SB, KD, AD, SF, EFC, RJ, SK, GM, LM, ZO, OS, MU, RV, EW, ZZ, AT, and MH conceptualized the study. Data was provided by AD, GB, JJ, AK, KK, LM, MN, SN, MP, KS, ET, MU, RV, JW, EW, and ZZ, and data curation was conducted by TM, AM, AD, GB, KD, EFC, JJ, SK, AK, KK, GM, MN, SN, MP, KS, ET, MU, RV, JW, EW, and ZZ. Formal analysis (data processing and statistical analyses) and visualization were done by TM. Investigation was conducted by TM and AM. AM supervised the study. Project administration was done by TM, AM and RJ. Funding acquisition for the study was done by AM and RJ. TM and AM prepared the original manuscript draft and TM, AM, AD, GB, SB, KD, SF, EFC, RJ, JJ, SK, LM, MN, ZO, MP, OS, ET, MU, RV, JW, EW, ZZ, AT, and MH contributed to the review and editing.

Competing interests. The contact author has declared that none of the authors has any competing interests.

Disclaimer. Publisher's note: Copernicus Publications remains neutral with regard to jurisdictional claims made in the text, published maps, institutional affiliations, or any other geographical representation in this paper. The authors bear the ultimate responsibility for providing appropriate place names. Views expressed in the text are those of the authors and do not necessarily reflect the views of the publisher.

Acknowledgements. We thank Kendalynn Morris for feedback on the manuscript. We acknowledge funding from the University of Zurich Stiftung für Wissenschaftliche Forschung (grant no. STWF-22-028) and the Swiss National Science Foundation (SNSF) (project (grant no. 200021_215214)) awarded to AM. This work was also supported by the COMPASS-FME project and an early career award (awarded to AM) by the U.S. Department of Energy, Office of Science, Biological and Environmental Research as part of the Environmental System Science Program. RBJ acknowledges support from the Gordon and Betty Moore Foundation through Grants GBMF5439 "Advancing Understanding of the Global Methane Cycle" and GBMF11519 "Advancing the understanding of methane emissions from tropical wetlands" to Stanford University and from the USGS Powell Synthesis Center (Scaling tropical wetland methane fluxes regionally and globally). SB was funded by the USGS Ecosystems Land Change Science Program and U.S. Department of Energy, Office of Science, Office of Biological and Environmental Research (grant no. DE-SC0023084). Any use of trade, firm, or product names is for descriptive purposes only and does not imply endorsement by the U.S. Government. MU was supported by the Arctic Challenge for Sustainability II and III (grant nos. JPMXD1420318865 and JPMXD1720251001). ZO was supported by the US Department of the Treasury (grant no. DISL-MESC-ALCOE-06). JJ, MBN and MP acknowledge financial support from the Swedish Research Council (VR) and SLU to ICOS-Sweden and SITES, and additional funding from VR (grant nos. 2019-04676 and 2018-03966) and the Kempe Foundation (grant nos. JCK-1108 and JCSMK23-0221). ARD acknowledges support for the US Dept of Energy Ameriflux Management Project support to ChEAS core site cluster. OS acknowledges financial support through the Canada Research Chair program (grant no. CRC-2018-00259) and the NSERC Discovery Grants program (grant no. DGPIN-2018-05743). EJW acknowledges support from the US Greenhouse Gas Center and the NASA Terrestrial Ecology Program. We thank Yang Qi for assistance in preliminary PlanetScope data processing.

Financial support. This research has been supported by the Swiss National Science Foundation (project no. 200021_215214) and University of Zurich Stiftung für Wissenschaftliche Forschung (grant no. STWF-22-028).

Review statement. This paper was edited by Ji-Hyung Park and reviewed by two anonymous referees.

References

Alduchov, O. A. and Eskridge, R.: Improved Magnus form approximation of saturation vapor pressure, J. Appl. Meteorol., 35, 601–609, https://doi.org/10.1175/1520-0450(1996)035<0601:IMFAOS>2.0.CO;2, 1996.

Alekseychik, P., Korrensalo, A., Mammarella, I., Launiainen, S., Tuittila, E.-S., Korpela, I., and Vesala, T.: Carbon balance of a Finnish bog: temporal variability and limiting factors based on 6 years of eddy-covariance data, Biogeosciences, 18, 4681–4704, https://doi.org/10.5194/bg-18-4681-2021, 2021.

Anthony, T. L. and Silver, W. L.: Hot moments drive extreme nitrous oxide and methane emissions from agricultural peatlands, Glob. Chang. Biol., 27, 5141–5153, https://doi.org/10.1111/gcb.15802, 2021.

Anthony, T. L. and Silver, W. L.: Hot spots and hot moments of greenhouse gas emissions in agricultural peatlands, Biogeochemistry, 167, 461–477, https://doi.org/10.1007/s10533-023-01095-y, 2023.

Aubinet, M.: Eddy covariance CO2 flux measurements in nocturnal conditions: an analysis of the problem, Ecol. Appl., 18, 1368–1378, https://doi.org/10.1890/06-1336.1, 2008.

Aubinet, M., Vesala, T., and Papale, D.: Eddy Covariance: A Practical Guide to Measurement and Data Analysis, Springer Science & Business Media, 438 pp., https://doi.org/10.1007/978-94-007-2351-1, 2012.

Baldocchi, D.: Assessing the eddy covariance technique for evaluating carbon dioxide exchange rates of ecosystems: past, present and future: carbon balance and eddy covariance,

Glob. Chang. Biol., 9, 479–492, https://doi.org/10.1046/j.1365-2486.2003.00629.x, 2003.

Baldocchi, D., Detto, M., Sonnentag, O., Verfaillie, J., Teh, Y. A., Silver, W., and Kelly, N. M.: The challenges of measuring methane fluxes and concentrations over a peatland pasture, Agric. For. Meteorol., 153, 177–187, https://doi.org/10.1016/j.agrformet.2011.04.013, 2012.

Bansal, S., Post van der Burg, M., Fern, R. R., Jones, J. W., Lo, R., McKenna, O. P., Tangen, B. A., Zhang, Z., and Gleason, R. A.: Large increases in methane emissions expected from North America's largest wetland complex, Sci. Adv., 9, eade1112, https://doi.org/10.1126/sciadv.ade1112, 2023a.

Bansal, S., Creed, I. F., Tangen, B. A., Bridgham, S. D., Desai, A. R., Krauss, K. W., Neubauer, S. C., Noe, G. B., Rosenberry, D. O., Trettin, C., Wickland, K. P., Allen, S. T., Arias-Ortiz, A., Armitage, A. R., Baldocchi, D., Banerjee, K., Bastviken, D., Berg, P., Bogard, M. J., Chow, A. T., Conner, W. H., Craft, C., Creamer, C., DelSontro, T., Duberstein, J. A., Eagle, M., Fennessy, M. S., Finkelstein, S. A., Göckede, M., Grunwald, S., Halabisky, M., Herbert, E., Jahangir, M. M. R., Johnson, O. F., Jones, M. C., Kelleway, J. J., Knox, S., Kroeger, K. D., Kuehn, K. A., Lobb, D., Loder, A. L., Ma, S., Maher, D. T., McNicol, G., Meier, J., Middleton, B. A., Mills, C., Mistry, P., Mitra, A., Mobilian, C., Nahlik, A. M., Newman, S., O'Connell, J. L., Oikawa, P., van der Burg, M. P., Schutte, C. A., Song, C., Stagg, C. L., Turner, J., Vargas, R., Waldrop, M. P., Wallin, M. B., Wang, Z. A., Ward, E. J., Willard, D. A., Yarwood, S., and Zhu, X.: Practical guide to measuring wetland carbon pools and fluxes, Wetlands (Wilmington), 43, 105, https://doi.org/10.1007/s13157-023-01722-2, 2023b.

Barba, J., Cueva, A., Bahn, M., Barron-Gafford, G. A., Bond-Lamberty, B., Hanson, P. J., Jaimes, A., Kulmala, L., Pumpanen, J., Scott, R. L., Wohlfahrt, G., and Vargas, R.: Comparing ecosystem and soil respiration: Review and key challenges of tower-based and soil measurements, Agric. For. Meteorol., 249, 434–443, https://doi.org/10.1016/j.agrformet.2017.10.028, 2018.

Bartoń, K.: MuMIn: Multi-Model Inference, https://doi.org/10.32614/CRAN.package.MuMIn, 2024.

Becker, R. A., Wilks, A. R., Brownrigg, R., Minka, T. P., and Deckmyn, A.: maps: Draw Geographical Maps, CRAN, https://doi.org/10.32614/CRAN.package.maps, 2023.

Bohrer, G., Ju, Y., Arend, K., Morin, T., Rey-Sanchez, C., Wrighton, K., and Villa, J.: Methane and CO_2 chamber fluxes and pore-water concentrations US-OWC Ameriflux wetland site, 2015–2018, AmeriFlux Management Project, ESS-DIVE repository, https://doi.org/10.15485/1568865, 2019.

Bohrer, G., Kerns, J., Morin, T., Rey-Sanchez, A., Villa, J., and Ju, Y.: FLUXNET-CH4 US-OWC Old Woman Creek, FLUXNET [data set], https://doi.org/10.18140/FLX/1669690, 2020.

Bond-Lamberty, B., Christianson, D. S., Malhotra, A., Pennington, S. C., Sihi, D., AghaKouchak, A., Anjileli, H., Altaf Arain, M., Armesto, J. J., Ashraf, S., Ataka, M., Baldocchi, D., Andrew Black, T., Buchmann, N., Carbone, M. S., Chang, S.-C., Crill, P., Curtis, P. S., Davidson, E. A., Desai, A. R., Drake, J. E., El-Madany, T. S., Gavazzi, M., Görres, C.-M., Gough, C. M., Goulden, M., Gregg, J., Gutiérrez Del Arroyo, O., He, J.-S., Hirano, T., Hopple, A., Hughes, H., Järveoja, J., Jassal, R., Jian, J., Kan, H., Kaye, J., Kominami, Y., Liang, N., Lipson, D., Macdonald, C. A., Maseyk, K., Mathes, K., Mauritz, M., Mayes, M. A., McNulty, S., Miao, G., Migliavacca, M., Miller, S., Miniat, C. F., Nietz, J. G., Nilsson, M. B., Noormets, A., Norouzi, H., O'Connell, C. S., Osborne, B., Oyonarte, C., Pang, Z., Peichl, M., Pendall, E., Perez-Quezada, J. F., Phillips, C. L., Phillips, R. P., Raich, J. W., Renchon, A. A., Ruehr, N. K., Sánchez-Cañete, E. P., Saunders, M., Savage, K. E., Schrumpf, M., Scott, R. L., Seibt, U., Silver, W. L., Sun, W., Szutu, D., Takagi, K., Takagi, M., Teramoto, M., Tjoelker, M. G., Trumbore, S., Ueyama, M., Vargas, R., Varner, R. K., Verfaillie, J., Vogel, C., Wang, J., Winston, G., Wood, T. E., Wu, J., Wutzler, T., Zeng, J., Zha, T., Zhang, Q., and Zou, J.: COSORE: A community database for continuous soil respiration and other soil-atmosphere greenhouse gas flux data, Glob. Chang. Biol., 26, 7268–7283, https://doi.org/10.1111/gcb.15353, 2020.

Bubier, J., Costello, A., Moore, T. R., Roulet, N. T., and Savage, K.: Microtopography and methane flux in boreal peatlands, northern Ontario, Canada, Can. J. Bot., 71, 1056–1063, https://doi.org/10.1139/b93-122, 1993.

Bubier, J. L.: The relationship of vegetation to methane emission and hydrochemical gradients in northern peatlands, J. Ecol., 83, 403–420, https://doi.org/10.2307/2261594, 1995.

Budishchev, A., Mi, Y., van Huissteden, J., Belelli-Marchesini, L., Schaepman-Strub, G., Parmentier, F. J. W., Fratini, G., Gallagher, A., Maximov, T. C., and Dolman, A. J.: Evaluation of a plot-scale methane emission model using eddy covariance observations and footprint modelling, Biogeosciences, 11, 4651–4664, https://doi.org/10.5194/bg-11-4651-2014, 2014.

Cernusak, L. A., Ubierna, N., Jenkins, M. W., Garrity, S. R., Rahn, T., Powers, H. H., Hanson, D. T., Sevanto, S., Wong, S. C., McDowell, N. G., and Farquhar, G. D.: Unsaturation of vapour pressure inside leaves of two conifer species, Sci. Rep., 8, 7667, https://doi.org/10.1038/s41598-018-25838-2, 2018.

Chaichana, N., Bellingrath-Kimura, S. D., Komiya, S., Fujii, Y., Noborio, K., Dietrich, O., and Pakoktom, T.: Comparison of Closed Chamber and Eddy Covariance Methods to Improve the Understanding of Methane Fluxes from Rice Paddy Fields in Japan, Atmosphere, 9, 356, https://doi.org/10.3390/atmos9090356, 2018.

Chamberlain, S. D., Verfaillie, J., Eichelmann, E., Hemes, K. S., and Baldocchi, D. D.: Evaluation of density corrections to methane fluxes measured by open-path eddy covariance over contrasting landscapes, Bound.-Lay. Meteorol., 165, 197–210, https://doi.org/10.1007/s10546-017-0275-9, 2017.

Chen, W., Zhang, F., Wang, B., Wang, J., Tian, D., Han, G., Wen, X., Yu, G., and Niu, S.: Diel and seasonal dynamics of ecosystem-scale methane flux and their determinants in an alpine meadow, J. Geophys. Res.-Biogeo., 124, 1731–1745, https://doi.org/10.1029/2019jg005011, 2019.

Chen, W., Wang, B., Zhang, F., Li, Z., Wang, J., Yu, G., Wen, X., and Niu, S.: Hysteretic relationship between plant productivity and methane uptake in an alpine meadow, Agric. For. Meteorol., 288–289, 107982, https://doi.org/10.1016/j.agrformet.2020.107982, 2020.

Cho, R., Schroth, M. H., and Zeyer, J.: Circadian methane oxidation in the root zone of rice plants, Biogeochemistry, 111, 317–330, https://doi.org/10.1007/s10533-011-9651-6, 2012.

Christiansen, J. R., Outhwaite, J., and Smukler, S. M.: Comparison of CO2, CH4 and N2O soil-atmosphere exchange measured in static chambers with cavity ring-down spectroscopy and gas chromatography, Agric. For. Meteorol., 211–212, 48–57, https://doi.org/10.1016/j.agrformet.2015.06.004, 2015.

Chu, H., Luo, X., Ouyang, Z., Chan, W. S., Dengel, S., Biraud, S. C., Torn, M. S., Metzger, S., Kumar, J., Arain, M. A., Arkebauer, T. J., Baldocchi, D., Bernacchi, C., Billesbach, D., Black, T. A., Blanken, P. D., Bohrer, G., Bracho, R., Brown, S., Brunsell, N. A., Chen, J., Chen, X., Clark, K., Desai, A. R., Duman, T., Durden, D., Fares, S., Forbrich, I., Gamon, J. A., Gough, C. M., Griffis, T., Helbig, M., Hollinger, D., Humphreys, E., Ikawa, H., Iwata, H., Ju, Y., Knowles, J. F., Knox, S. H., Kobayashi, H., Kolb, T., Law, B., Lee, X., Litvak, M., Liu, H., Munger, J. W., Noormets, A., Novick, K., Oberbauer, S. F., Oechel, W., Oikawa, P., Papuga, S. A., Pendall, E., Prajapati, P., Prueger, J., Quinton, W. L., Richardson, A. D., Russell, E. S., Scott, R. L., Starr, G., Staebler, R., Stoy, P. C., Stuart-Haëntjens, E., Sonnentag, O., Sullivan, R. C., Suyker, A., Ueyama, M., Vargas, R., Wood, J. D., and Zona, D.: Representativeness of Eddy-Covariance flux footprints for areas surrounding AmeriFlux sites, Agric. For. Meteorol., 301–302, 108350, https://doi.org/10.1016/j.agrformet.2021.108350, 2021.

Chu, H., Christianson, D. S., Cheah, Y.-W., Pastorello, G., O'Brien, F., Geden, J., Ngo, S.-T., Hollowgrass, R., Leibowitz, K., Beekwilder, N. F., Sandesh, M., Dengel, S., Chan, S. W., Santos, A., Delwiche, K., Yi, K., Buechner, C., Baldocchi, D., Papale, D., Keenan, T. F., Biraud, S. C., Agarwal, D. A., and Torn, M. S.: AmeriFlux BASE data pipeline to support network growth and data sharing, Sci. Data, 10, 614, https://doi.org/10.1038/s41597-023-02531-2, 2023.

Clark, W. A. and Avery, K. L.: The effects of data aggregation in statistical analysis, Geogr. Anal., 8, 428–438, https://doi.org/10.1111/j.1538-4632.1976.tb00549.x, 1976.

Clement, R. J., Verma, S. B., and Verry, E. S.: Relating chamber measurements to eddy correlation measurements of methane flux, J. Geophys. Res.-Atmos., 100, 21047–21056, https://doi.org/10.1029/95JD02196, 1995.

Davidson, E. A., Savage, K., Verchot, L. V., and Navarro, R.: Minimizing artifacts and biases in chamber-based measurements of soil respiration, Agric. For. Meteorol., 113, 21–37, https://doi.org/10.1016/s0168-1923(02)00100-4, 2002.

Davidson, S. J., Santos, M. J., Sloan, V. L., Reuss-Schmidt, K., Phoenix, G. K., Oechel, W. C., and Zona, D.: Upscaling CH_4 Fluxes Using High-Resolution Imagery in Arctic Tundra Ecosystems, Remote Sens.-Basel, 9, 1227, https://doi.org/10.3390/rs9121227, 2017.

Delwiche, K. B., Knox, S. H., Malhotra, A., Fluet-Chouinard, E., McNicol, G., Feron, S., Ouyang, Z., Papale, D., Trotta, C., Canfora, E., Cheah, Y.-W., Christianson, D., Alberto, Ma. C. R., Alekseychik, P., Aurela, M., Baldocchi, D., Bansal, S., Billesbach, D. P., Bohrer, G., Bracho, R., Buchmann, N., Campbell, D. I., Celis, G., Chen, J., Chen, W., Chu, H., Dalmagro, H. J., Dengel, S., Desai, A. R., Detto, M., Dolman, H., Eichelmann, E., Euskirchen, E., Famulari, D., Fuchs, K., Goeckede, M., Gogo, S., Gondwe, M. J., Goodrich, J. P., Gottschalk, P., Graham, S. L., Heimann, M., Helbig, M., Helfter, C., Hemes, K. S., Hirano, T., Hollinger, D., Hörtnagl, L., Iwata, H., Jacotot, A., Jurasinski, G., Kang, M., Kasak, K., King, J., Klatt, J., Koebsch, F., Krauss, K. W., Lai, D. Y. F., Lohila, A., Mammarella, I., Belelli Marchesini, L., Manca, G., Matthes, J. H., Maximov, T., Merbold, L., Mitra, B., Morin, T. H., Nemitz, E., Nilsson, M. B., Niu, S., Oechel, W. C., Oikawa, P. Y., Ono, K., Peichl, M., Peltola, O., Reba, M. L., Richardson, A. D., Riley, W., Runkle, B. R. K., Ryu, Y., Sachs, T., Sakabe, A., Sanchez, C. R., Schuur, E. A., Schäfer, K. V. R., Sonnentag, O., Sparks, J. P., Stuart-Haëntjens, E., Sturtevant, C., Sullivan, R. C., Szutu, D. J., Thom, J. E., Torn, M. S., Tuittila, E.-S., Turner, J., Ueyama, M., Valach, A. C., Vargas, R., Varlagin, A., Vazquez-Lule, A., Verfaillie, J. G., Vesala, T., Vourlitis, G. L., Ward, E. J., Wille, C., Wohlfahrt, G., Wong, G. X., Zhang, Z., Zona, D., Windham-Myers, L., Poulter, B., and Jackson, R. B.: FLUXNET-CH_4: a global, multi-ecosystem dataset and analysis of methane seasonality from freshwater wetlands , Earth Syst. Sci. Data, 13, 3607–3689, https://doi.org/10.5194/essd-13-3607-2021, 2021.

Desai, A. R.: AmeriFlux BASE US-Los Lost Creek, Ver. 33–5, AmeriFlux AMP [data set], https://doi.org/10.17190/AMF/1246071, 2025a.

Desai, A. R.: In Situ Carbon Dioxide and Methane Flux Measurements Using Opaque Chambers in a Sedge Fen Wetland (US-Los Lost Creek AmeriFlux Site, Wisconsin, Summer 2015) ver 1, Environmental Data Initiative [data set], https://doi.org/10.6073/pasta/fc48a416ab7c580f2fd0d5450668a23a, 2025b.

Desai, A. R. and Thom, J.: FLUXNET-CH4 US-Los Lost Creek, FLUXNET [data set], https://doi.org/10.18140/FLX/1669682, 2020.

Desai, A. R., Xu, K., Tian, H., Weishampel, P., Thom, J., Baumann, D., Andrews, A. E., Cook, B. D., King, J. Y., and Kolka, R.: Landscape-level terrestrial methane flux observed from a very tall tower, Agric. For. Meteorol., 201, 61–75, https://doi.org/10.1016/j.agrformet.2014.10.017, 2015.

Detto, M., Verfaillie, J., Anderson, F., Xu, L., and Baldocchi, D.: Comparing laser-based open- and closed-path gas analyzers to measure methane fluxes using the eddy covariance method, Agric. For. Meteorol., 151, 1312–1324, https://doi.org/10.1016/j.agrformet.2011.05.014, 2011.

Deventer, M. J., Griffis, T. J., Roman, D. T., Kolka, R. K., Wood, J. D., Erickson, M., Baker, J. M., and Millet, D. B.: Error characterization of methane fluxes and budgets derived from a long-term comparison of open- and closed-path eddy covariance systems, Agric. For. Meteorol., 278, 107638, https://doi.org/10.1016/j.agrformet.2019.107638, 2019.

Dinno, A.: conover.test: Conover-Iman Test of Multiple Comparisons Using Rank Sums, CRAN [code], https://doi.org/10.32614/CRAN.package.conover.test, 2024.

Erkkilä, K.-M., Ojala, A., Bastviken, D., Biermann, T., Heiskanen, J. J., Lindroth, A., Peltola, O., Rantakari, M., Vesala, T., and Mammarella, I.: Methane and carbon dioxide fluxes over a lake: comparison between eddy covariance, floating chambers and boundary layer method, Biogeosciences, 15, 429–445, https://doi.org/10.5194/bg-15-429-2018, 2018.

Forbrich, I., Kutzbach, L., Hormann, A., and Wilmking, M.: A comparison of linear and exponential regression for estimating diffusive CH4 fluxes by closed-chambers in peatlands, Soil Biol. Biochem., 42, 507–515, https://doi.org/10.1016/j.soilbio.2009.12.004, 2010.

Forbrich, I., Kutzbach, L., Wille, C., Becker, T., Wu, J., and Wilmking, M.: Cross-evaluation of measurements of peatland methane emissions on microform and ecosystem scales using high-resolution landcover classification and source weight modelling, Agric. For. Meteorol., 151, 864–874, https://doi.org/10.1016/j.agrformet.2011.02.006, 2011.

Fox, J. and Weisberg, S.: An R companion to applied regression, 3rd edn., SAGE Publications, Thousand Oaks, CA, 608 pp., https://www.john-fox.ca/Companion/ (last access: 15 February 2026), 2018.

Griebel, A., Bennett, L. T., Metzen, D., Cleverly, J., Burba, G., and Arndt, S. K.: Effects of inhomogeneities within the flux footprint on the interpretation of seasonal, annual, and interannual ecosystem carbon exchange, Agric. For. Meteorol., 221, 50–60, https://doi.org/10.1016/j.agrformet.2016.02.002, 2016.

Grossiord, C., Buckley, T. N., Cernusak, L. A., Novick, K. A., Poulter, B., Siegwolf, R. T. W., Sperry, J. S., and McDowell, N. G.: Plant responses to rising vapor pressure deficit, New Phytol., 226, 1550–1566, https://doi.org/10.1111/nph.16485, 2020.

Hargreaves, K. J., Fowler, D., Pitcairn, C. E. R., and Aurela, M.: Annual methane emission from Finnish mires estimated from eddy covariance campaign measurements, Theor. Appl. Climatol., 70, 203–213, https://doi.org/10.1007/s007040170015, 2001.

Hartley, I. P., Hill, T. C., Wade, T. J., Clement, R. J., Moncrieff, J. B., Prieto-Blanco, A., Disney, M. I., Huntley, B., Williams, M., Howden, N. J. K., Wookey, P. A., and Baxter, R.: Quantifying landscape-level methane fluxes in subarctic Finland using a multiscale approach, Glob. Chang. Biol., 21, 3712–3725, https://doi.org/10.1111/gcb.12975, 2015.

Heusinkveld, B. G., Jacobs, A. F. G., and Holtslag, A. A. M.: Effect of open-path gas analyzer wetness on eddy covariance flux measurements: A proposed solution, Agric. For. Meteorol., 148, 1563–1573, https://doi.org/10.1016/j.agrformet.2008.05.010, 2008.

Hill, A. C. and Vargas, R.: Carbon dioxide and methane chamber flux data from temperate S. alterniflora salt-marsh, Figshare [data set], https://doi.org/10.6084/M9.FIGSHARE.20099321.V1, 2022a.

Hill, A. C. and Vargas, R.: Methane and carbon dioxide fluxes in a temperate tidal salt marsh: Comparisons between plot and ecosystem measurements, J. Geophys. Res.-Biogeo., 127, https://doi.org/10.1029/2022jg006943, 2022b.

Hollinger, D. Y. and Richardson, A. D.: Uncertainty in eddy covariance measurements and its application to physiological models, Tree Physiol., 25, 873–885, https://doi.org/10.1093/treephys/25.7.873, 2005.

Holm, G., Perez, B., McWhorter, D., Krauss, K., Raynie, R., and Killebrew, C.: FLUXNET-CH4 US-LA1 Pointe-aux-Chenes Brackish Marsh, FLUXNET [data set], https://doi.org/10.18140/FLX/1669680, 2020a.

Holm, G., Perez, B., McWhorter, D., Krauss, K., Raynie, R., and Killebrew, C.: FLUXNET-CH4 US-LA2 Salvador WMA Freshwater Marsh, FLUXNET [data set], https://doi.org/10.18140/FLX/1669681, 2020b.

Intergovernmental Panel on Climate Change (IPCC): Climate Change 2021 – the physical science basis, Cambridge University Press, https://doi.org/10.1017/9781009157896, 2023.

Irvin, J., Zhou, S., McNicol, G., Lu, F., Liu, V., Fluet-Chouinard, E., Ouyang, Z., Knox, S. H., Lucas-Moffat, A., Trotta, C., Papale, D., Vitale, D., Mammarella, I., Alekseychik, P., Aurela, M., Avati, A., Baldocchi, D., Bansal, S., Bohrer, G., Campbell, D. I., Chen, J., Chu, H., Dalmagro, H. J., Delwiche, K. B., Desai, A. R., Euskirchen, E., Feron, S., Goeckede, M., Heimann, M., Helbig, M., Helfter, C., Hemes, K. S., Hirano, T., Iwata, H., Jurasinski, G., Kalhori, A., Kondrich, A., Lai, D. Y. F., Lohila, A., Malhotra, A., Merbold, L., Mitra, B., Ng, A., Nilsson, M. B., Noormets, A., Peichl, M., Rey-Sanchez, A. C., Richardson, A. D., Runkle, B. R. K., Schäfer, K. V. R., Sonnentag, O., Stuart-Haëntjens, E., Sturtevant, C., Ueyama, M., Valach, A. C., Vargas, R., Vourlitis, G. L., Ward, E. J., Wong, G. X., Zona, D., Alberto, M. C. R., Billesbach, D. P., Celis, G., Dolman, H., Friborg, T., Fuchs, K., Gogo, S., Gondwe, M. J., Goodrich, J. P., Gottschalk, P., Hörtnagl, L., Jacotot, A., Koebsch, F., Kasak, K., Maier, R., Morin, T. H., Nemitz, E., Oechel, W. C., Oikawa, P. Y., Ono, K., Sachs, T., Sakabe, A., Schuur, E. A., Shortt, R., Sullivan, R. C., Szutu, D. J., Tuittila, E.-S., Varlagin, A., Verfaillie, J. G., Wille, C., Windham-Myers, L., Poulter, B., and Jackson, R. B.: Gap-filling eddy covariance methane fluxes: Comparison of machine learning model predictions and uncertainties at FLUXNET-CH4 wetlands, Agric. For. Meteorol., 308–309, 108528, https://doi.org/10.1016/j.agrformet.2021.108528, 2021.

Iwata, H., Kosugi, Y., Ono, K., Mano, M., Sakabe, A., Miyata, A., and Takahashi, K.: Cross-validation of open-path and closed-path eddy-covariance techniques for observing methane fluxes, Bound.-Lay. Meteorol., 151, 95–118, https://doi.org/10.1007/s10546-013-9890-2, 2014.

Iwata, H., Ueyama, M., and Harazono, Y.: FLUXNET-CH4 US-Uaf University of Alaska, Fairbanks, FLUXNET [data set], https://doi.org/10.18140/FLX/1669701, 2020.

Järveoja, J., Nilsson, M. B., Gažovič, M., Crill, P. M., and Peichl, M.: Partitioning of the net CO_2 exchange using an automated chamber system reveals plant phenology as key control of production and respiration fluxes in a boreal peatland, Glob. Chang. Biol., 24, 3436–3451, https://doi.org/10.1111/gcb.14292, 2018.

Jentzsch, K., van Delden, L., Fuchs, M., and Treat, C. C.: An expert survey on chamber measurement techniques and data handling procedures for methane fluxes, Earth Syst. Sci. Data, 17, 2331–2372, https://doi.org/10.5194/essd-17-2331-2025, 2025.

Juselius-Rajamäki, T., Piilo, S., Salminen-Paatero, S., Tuomaala, E., Virtanen, T., Korhola, A., Autio, A., Marttila, H., Ala-Aho, P., Lohila, A., and Väliranta, M.: External and internal drivers behind the formation, vegetation succession, and carbon balance of a subarctic fen margin, Biogeosciences, 22, 3047–3071, https://doi.org/10.5194/bg-22-3047-2025, 2025.

Knapp, A. K. and Yavitt, J. B.: Evaluation of a closed-chamber method for estimating methane emissions from aquatic plants, Tellus B, 44, 63–71, https://doi.org/10.1034/j.1600-0889.1992.00006.x, 1992.

Knox, S. H., Matthes, J. H., Sturtevant, C., Oikawa, P. Y., Verfaillie, J., and Baldocchi, D.: Biophysical controls on interannual variability in ecosystem-scale CO_2 and CH_4 exchange in a California rice paddy: Interannual variability rice CH_4 fluxes, J. Geophys. Res.-Biogeo., 121, 978–1001, https://doi.org/10.1002/2015jg003247, 2016.

Knox, S. H., Jackson, R. B., Poulter, B., McNicol, G., Fluet-Chouinard, E., Zhang, Z., Hugelius, G., Bousquet, P., Canadell, J. G., Saunois, M., Papale, D., Chu, H., Keenan, T. F., Baldocchi, D., Torn, M. S., Mammarella, I., Trotta, C., Aurela, M., Bohrer, G., Campbell, D. I., Cescatti, A., Chamberlain, S., Chen, J., Chen, W., Dengel, S., Desai, A. R., Euskirchen, E., Friborg, T., Gasbarra, D., Goded, I., Goeckede, M., Heimann, M., Helbig, M., Hirano, T., Hollinger, D. Y., Iwata, H., Kang, M., Klatt, J., Krauss, K. W., Kutzbach, L., Lohila, A., Mitra, B., Morin, T. H., Nilsson, M. B., Niu, S., Noormets, A., Oechel, W. C., Peichl,

M., Peltola, O., Reba, M. L., Richardson, A. D., Runkle, B. R. K., Ryu, Y., Sachs, T., Schäfer, K. V. R., Schmid, H. P., Shurpali, N., Sonnentag, O., Tang, A. C. I., Ueyama, M., Vargas, R., Vesala, T., Ward, E. J., Windham-Myers, L., Wohlfahrt, G., and Zona, D.: FLUXNET-CH4 Synthesis Activity: Objectives, Observations, and Future Directions, Bull. Am. Meteorol. Soc., 100, 2607–2632, https://doi.org/10.1175/BAMS-D-18-0268.1, 2019.

Knox, S. H., Bansal, S., McNicol, G., Schafer, K., Sturtevant, C., Ueyama, M., Valach, A. C., Baldocchi, D., Delwiche, K., Desai, A. R., Euskirchen, E., Liu, J., Lohila, A., Malhotra, A., Melling, L., Riley, W., Runkle, B. R. K., Turner, J., Vargas, R., Zhu, Q., Alto, T., Fluet-Chouinard, E., Goeckede, M., Melton, J. R., Sonnentag, O., Vesala, T., Ward, E., Zhang, Z., Feron, S., Ouyang, Z., Alekseychik, P., Aurela, M., Bohrer, G., Campbell, D. I., Chen, J., Chu, H., Dalmagro, H. J., Goodrich, J. P., Gottschalk, P., Hirano, T., Iwata, H., Jurasinski, G., Kang, M., Koebsch, F., Mammarella, I., Nilsson, M. B., Ono, K., Peichl, M., Peltola, O., Ryu, Y., Sachs, T., Sakabe, A., Sparks, J. P., Tuittila, E.-S., Vourlitis, G. L., Wong, G. X., Windham-Myers, L., Poulter, B., and Jackson, R. B.: Identifying dominant environmental predictors of freshwater wetland methane fluxes across diurnal to seasonal time scales, Glob. Chang. Biol., 27, 3582–3604, https://doi.org/10.1111/gcb.15661, 2021.

Koebsch, F., Jurasinski, G., Koch, M., Hofmann, J., and Glatzel, S.: Controls for multi-scale temporal variation in ecosystem methane exchange during the growing season of a permanently inundated fen, Agric. For. Meteorol., 204, 94–105, https://doi.org/10.1016/j.agrformet.2015.02.002, 2015.

Korkiakoski, M., Tuovinen, J.-P., Aurela, M., Koskinen, M., Minkkinen, K., Ojanen, P., Penttilä, T., Rainne, J., Laurila, T., and Lohila, A.: Methane exchange at the peatland forest floor – automatic chamber system exposes the dynamics of small fluxes, Biogeosciences, 14, 1947–1967, https://doi.org/10.5194/bg-14-1947-2017, 2017.

Korrensalo, A., Männistö, E., Alekseychik, P., Mammarella, I., Rinne, J., Vesala, T., and Tuittila, E.-S.: Small spatial variability in methane emission measured from a wet patterned boreal bog, Biogeosciences, 15, 1749–1761, https://doi.org/10.5194/bg-15-1749-2018, 2018.

Krauss, K. W., Holm, G. O., Perez, B. C., McWhorter, D. E., Cormier, N., Moss, R. F., Johnson, D. J., Neubauer, S. C., and Raynie, R. C.: Component greenhouse gas fluxes and radiative balance from two deltaic marshes in Louisiana: Pairing chamber techniques and eddy covariance, J. Geophys. Res.-Biogeo., 121, 1503–1521, https://doi.org/10.1002/2015JG003224, 2016.

Kroon, P. S., Hensen, A., Jonker, H. J. J., Zahniser, M. S., van 't Veen, W. H., and Vermeulen, A. T.: Suitability of quantum cascade laser spectroscopy for CH_4 and N_2O eddy covariance flux measurements, Biogeosciences, 4, 715–728, https://doi.org/10.5194/bg-4-715-2007, 2007.

Kroon, P. S., Hensen, A., Jonker, H. J. J., Ouwersloot, H. G., Vermeulen, A. T., and Bosveld, F. C.: Uncertainties in eddy covariance flux measurements assessed from CH_4 and N_2O observations, Agric. For. Meteorol., 150, 806–816, https://doi.org/10.1016/j.agrformet.2009.08.008, 2010.

Kuhn, M. A., Varner, R. K., Bastviken, D., Crill, P., MacIntyre, S., Turetsky, M., Walter Anthony, K., McGuire, A. D., and Olefeldt, D.: BAWLD-CH_4: a comprehensive dataset of methane fluxes from boreal and arctic ecosystems, Earth Syst. Sci. Data, 13, 5151–5189, https://doi.org/10.5194/essd-13-5151-2021, 2021.

Kutzbach, L., Wagner, D., and Pfeiffer, E.-M.: Effect of microrelief and vegetation on methane emission from wet polygonal tundra, Lena Delta, Northern Siberia, Biogeochemistry, 69, 341–362, https://doi.org/10.1023/B:BIOG.0000031053.81520.db, 2004.

Lai, D. Y. F., Roulet, N. T., Humphreys, E. R., Moore, T. R., and Dalva, M.: The effect of atmospheric turbulence and chamber deployment period on autochamber CO_2 and CH_4 flux measurements in an ombrotrophic peatland, Biogeosciences, 9, 3305–3322, https://doi.org/10.5194/bg-9-3305-2012, 2012.

Langensiepen, M., Kupisch, M., van Wijk, M. T., and Ewert, F.: Analyzing transient closed chamber effects on canopy gas exchange for optimizing flux calculation timing, Agric. For. Meteorol., 164, 61–70, https://doi.org/10.1016/j.agrformet.2012.05.006, 2012.

Lawrence, M. G.: The relationship between relative humidity and the dewpoint temperature in moist air: A simple conversion and applications, Bull. Am. Meteorol. Soc., 86, 225–234, https://doi.org/10.1175/bams-86-2-225, 2005.

Levy, P. E., Gray, A., Leeson, S. R., Gaiawyn, J., Kelly, M. P. C., Cooper, M. D. A., Dinsmore, K. J., Jones, S. K., and Sheppard, L. J.: Quantification of uncertainty in trace gas fluxes measured by the static chamber method, Eur. J. Soil Sci., 62, 811–821, https://doi.org/10.1111/j.1365-2389.2011.01403.x, 2011.

Liu, X., Zhu, D., Zhan, W., Chen, H., Zhu, Q., Zhang, J., Wu, N., and He, Y.: Dominant influence of non-thawing periods on annual CO_2 emissions from Zoige peatlands: Five-year eddy covariance analysis, Ecol. Indic., 129, 107913, https://doi.org/10.1016/j.ecolind.2021.107913, 2021.

Livingston, G. P. and Hutchinson, G. L.: Enclosure-based measurement of trace gas exchange: applications and sources of error, in: Methods in ecology: biogenic trace gas emissions from soil and water, Blackwell Scientific Publications Inc., 14–51, ISBN 978-1-444-31381-9, 1995.

Long, K. D., Flanagan, L. B., and Cai, T.: Diurnal and seasonal variation in methane emissions in a northern Canadian peatland measured by eddy covariance, Glob. Chang. Biol., 16, 2420–2435, https://doi.org/10.1111/j.1365-2486.2009.02083.x, 2010.

Määttä, T.: tiia-maa/Cross-site-comparison-of-ecosystem-and-plot-scale-methane-fluxes-across-multiple-sites: Cross site comparison of ecosystem and plot scale methane fluxes across multiple timescales v1 (v), Zenodo [code], https://doi.org/10.5281/zenodo.20558238, 2026.

Määttä, T., Desai, A., Ueyama, M., Vargas, R., Ward, E. J., Zhang, Z., Bohrer, G., Delwiche, K., Fluet-Chouinard, E., Järveoja, J., Knox, S., Melling, L., Nilsson, M. B., Peichl, M., Tang, A. C. I., Tuittila, E.-S., Wang, J., Bansal, S., Feron, S., Helbig, M., Korrensalo, A., Krauss, K. W., McNicol, G., Niu, S., Ouyang, Z., Savage, K., Sonnentag, O., Jackson, R., and Malhotra, A.: Cross-site comparison of ecosystem- and plot-scale methane fluxes from wetlands and uplands (Version v1), Zenodo [data set], https://doi.org/10.5281/zenodo.17312404, 2025.

Männistö, E., Korrensalo, A., Alekseychik, P., Mammarella, I., Peltola, O., Vesala, T., and Tuittila, E.-S.: Multi-year methane ebullition measurements from water and bare peat surfaces of a patterned boreal bog, Biogeosciences, 16, 2409–2421, https://doi.org/10.5194/bg-16-2409-2019, 2019.

Marushchak, M. E., Friborg, T., Biasi, C., Herbst, M., Johansson, T., Kiepe, I., Liimatainen, M., Lind, S. E., Martikainen, P. J., Virtanen, T., Soegaard, H., and Shurpali, N. J.: Methane dynamics in the subarctic tundra: combining stable isotope analyses, plot- and ecosystem-scale flux measurements, Biogeosciences, 13, 597–608, https://doi.org/10.5194/bg-13-597-2016, 2016.

McGuire, A. D., Christensen, T. R., Hayes, D., Heroult, A., Euskirchen, E., Kimball, J. S., Koven, C., Lafleur, P., Miller, P. A., Oechel, W., Peylin, P., Williams, M., and Yi, Y.: An assessment of the carbon balance of Arctic tundra: comparisons among observations, process models, and atmospheric inversions, Biogeosciences, 9, 3185–3204, https://doi.org/10.5194/bg-9-3185-2012, 2012.

McNicol, G., Fluet-Chouinard, E., Ouyang, Z., Knox, S., Zhang, Z., Aalto, T., Bansal, S., Chang, K.-Y., Chen, M., Delwiche, K., Feron, S., Goeckede, M., Liu, J., Malhotra, A., Melton, J. R., Riley, W., Vargas, R., Yuan, K., Ying, Q., Zhu, Q., Alekseychik, P., Aurela, M., Billesbach, D. P., Campbell, D. I., Chen, J., Chu, H., Desai, A. R., Euskirchen, E., Goodrich, J., Griffis, T., Helbig, M., Hirano, T., Iwata, H., Jurasinski, G., King, J., Koebsch, F., Kolka, R., Krauss, K., Lohila, A., Mammarella, I., Nilson, M., Noormets, A., Oechel, W., Peichl, M., Sachs, T., Sakabe, A., Schulze, C., Sonnentag, O., Sullivan, R. C., Tuittila, E.-S., Ueyama, M., Vesala, T., Ward, E., Wille, C., Wong, G. X., Zona, D., Windham-Myers, L., Poulter, B., and Jackson, R. B.: Upscaling wetland methane emissions from the FLUXNET-CH4 eddy covariance network (UpCH4 v1.0): Model development, network assessment, and budget comparison, AGU Adv., 4, https://doi.org/10.1029/2023av000956, 2023.

Meijide, A., Manca, G., Goded, I., Magliulo, V., di Tommasi, P., Seufert, G., and Cescatti, A.: Seasonal trends and environmental controls of methane emissions in a rice paddy field in Northern Italy, Biogeosciences, 8, 3809–3821, https://doi.org/10.5194/bg-8-3809-2011, 2011.

Metzger, S.: Surface-atmosphere exchange in a box: Making the control volume a suitable representation for in-situ observations, Agric. For. Meteorol., 255, 68–80, https://doi.org/10.1016/j.agrformet.2017.08.037, 2018.

Montaldo, N. and Oren, R.: The way the wind blows matters to ecosystem water use efficiency, Agric. For. Meteorol., 217, 1–9, https://doi.org/10.1016/j.agrformet.2015.11.002, 2016.

Morin, T. H.: Advances in the eddy covariance approach to CH_4 monitoring over two and a half decades, J. Geophys. Res.-Biogeo., 124, 453–460, https://doi.org/10.1029/2018jg004796, 2019.

Morin, T. H., Bohrer, G., Frasson, R. P. d., Naor-Azreli, L., Mesi, S., Stefanik, K. C., and Schäfer, K. V. R.: Environmental drivers of methane fluxes from an urban temperate wetland park, J. Geophys. Res.-Biogeo., 119, 2188–2208, https://doi.org/10.1002/2014JG002750, 2014.

Morin, T. H., Bohrer, G., Stefanik, K. C., Rey-Sanchez, A. C., Matheny, A. M., and Mitsch, W. J.: Combining eddy-covariance and chamber measurements to determine the methane budget from a small, heterogeneous urban floodplain wetland park, Agric. For. Meteorol., 237–238, 160–170, https://doi.org/10.1016/j.agrformet.2017.01.022, 2017.

Nadeau, D. F., Rousseau, A. N., Coursolle, C., Margolis, H. A., and Parlange, M. B.: Summer methane fluxes from a boreal bog in northern Quebec, Canada, using eddy covariance measurements, Atmos. Environ., 81, 464–474, https://doi.org/10.1016/j.atmosenv.2013.09.044, 2013.

Nakano, T.: A comparison of regression methods for estimating soil–atmosphere diffusion gas fluxes by a closed-chamber technique, Soil Biol. Biochem., 36, 107–113, https://doi.org/10.1016/j.soilbio.2003.07.005, 2004.

Nilsson, M. and Peichl, M.: FLUXNET-CH4 SE-Deg Degero, FLUXNET [data set], https://doi.org/10.18140/FLX/1669659, 2020.

Niu, S. and Chen, W.: FLUXNET-CH4 CN-Hgu Hongyuan, FLUXNET [data set], https://doi.org/10.18140/FLX/1669632, 2020.

Niu, S., Luo, Y., Fei, S., Montagnani, L., Bohrer, G., Janssens, I. A., Gielen, B., Rambal, S., Moors, E., and Matteucci, G.: Seasonal hysteresis of net ecosystem exchange in response to temperature change: patterns and causes: Seasonal hysteresis ofnet ecosystem exchange, Glob. Chang. Biol., 17, 3102–3114, https://doi.org/10.1111/j.1365-2486.2011.02459.x, 2011.

Oikawa, P. Y., Sihi, D., Forbrich, I., Fluet-Chouinard, E., Najarro, M., Thomas, O., Shahan, J., Arias-Ortiz, A., Russell, S., Knox, S. H., McNicol, G., Wolfe, J., Windham-Myers, L., Stuart-Haentjens, E., Bridgham, S. D., Needelman, B., Vargas, R., Schäfer, K., Ward, E. J., Megonigal, P., and Holmquist, J.: A new coupled biogeochemical modeling approach provides accurate predictions of methane and carbon dioxide fluxes across diverse tidal wetlands, J. Geophys. Res.-Biogeo., 129, https://doi.org/10.1029/2023jg007943, 2024.

Parmentier, F. J. W., van Huissteden, J., van der Molen, M. K., Schaepman-Strub, G., Karsanaev, S. A., Maximov, T. C., and Dolman, A. J.: Spatial and temporal dynamics in eddy covariance observations of methane fluxes at a tundra site in northeastern Siberia, J. Geophys. Res., 116, https://doi.org/10.1029/2010jg001637, 2011.

Peltola, O., Hensen, A., Helfter, C., Belelli Marchesini, L., Bosveld, F. C., van den Bulk, W. C. M., Elbers, J. A., Haapanala, S., Holst, J., Laurila, T., Lindroth, A., Nemitz, E., Röckmann, T., Vermeulen, A. T., and Mammarella, I.: Evaluating the performance of commonly used gas analysers for methane eddy covariance flux measurements: the InGOS intercomparison field experiment, Biogeosciences, 11, 3163–3186, https://doi.org/10.5194/bg-11-3163-2014, 2014.

Peltola, O., Vesala, T., Gao, Y., Räty, O., Alekseychik, P., Aurela, M., Chojnicki, B., Desai, A. R., Dolman, A. J., Euskirchen, E. S., Friborg, T., Göckede, M., Helbig, M., Humphreys, E., Jackson, R. B., Jocher, G., Joos, F., Klatt, J., Knox, S. H., Kowalska, N., Kutzbach, L., Lienert, S., Lohila, A., Mammarella, I., Nadeau, D. F., Nilsson, M. B., Oechel, W. C., Peichl, M., Pypker, T., Quinton, W., Rinne, J., Sachs, T., Samson, M., Schmid, H. P., Sonnentag, O., Wille, C., Zona, D., and Aalto, T.: Monthly gridded data product of northern wetland methane emissions based on upscaling eddy covariance observations, Earth Syst. Sci. Data, 11, 1263–1289, https://doi.org/10.5194/essd-11-1263-2019, 2019.

Peterson, R.: Finding optimal normalizing transformations via bestNormalize, R J., 13, 310, https://doi.org/10.32614/rj-2021-041, 2021.

Phillips, C. L., Bond-Lamberty, B., Desai, A. R., Lavoie, M., Risk, D., Tang, J., Todd-Brown, K., and Vargas, R.: The value of soil respiration measurements for interpreting and

modeling terrestrial carbon cycling, Plant Soil, 413, 1–25, https://doi.org/10.1007/s11104-016-3084-x, 2017.

Pihlatie, M. K., Christiansen, J. R., Aaltonen, H., Korhonen, J. F. J., Nordbo, A., Rasilo, T., Benanti, G., Giebels, M., Helmy, M., Sheehy, J., Jones, S., Juszczak, R., Klefoth, R., Lobo-do-Vale, R., Rosa, A. P., Schreiber, P., Serça, D., Vicca, S., Wolf, B., and Pumpanen, J.: Comparison of static chambers to measure CH4 emissions from soils, Agric. For. Meteorol., 171–172, 124–136, https://doi.org/10.1016/j.agrformet.2012.11.008, 2013.

Pinheiro, J., Bates, D., and R Core Team: nlme: Linear and Nonlinear Mixed Effects Models, CRAN [code], https://doi.org/10.32614/CRAN.package.nlme, 2023.

Pinheiro, J. C. and Bates, D. M.: Mixed-Effects Models in S and S-PLUS, Springer, New York, https://doi.org/10.1007/b98882, 2000.

Pollet, T. V., Stulp, G., Henzi, S. P., and Barrett, L.: Taking the aggravation out of data aggregation: A conceptual guide to dealing with statistical issues related to the pooling of individual-level observational data, Am. J. Primatol., 77, 727–740, https://doi.org/10.1002/ajp.22405, 2015.

Pugh, C. A., Reed, D. E., Desai, A. R., and Sulman, B. N.: Wetland flux controls: how does interacting water table levels and temperature influence carbon dioxide and methane fluxes in northern Wisconsin?, Biogeochemistry, 137, 15–25, https://doi.org/10.1007/s10533-017-0414-x, 2018.

Pumpanen, J., Kolari, P., Ilvesniemi, H., Minkkinen, K., Vesala, T., Niinistö, S., Lohila, A., Larmola, T., Morero, M., Pihlatie, M., and Janssens, I.: Comparison of different chamber techniques for measuring soil CO2 efflux, Agric. For. Meteorol., 123, 159–176, https://doi.org/10.1016/j.agrformet.2003.12.001, 2004.

R Core Team: R: A Language and Environment for Statistical Computing, R Foundation for Statistical Computing, Vienna, Austria, https://www.R-project.org (last access: 15 February 2026), 2024.

Räsänen, A., Manninen, T., Korkiakoski, M., Lohila, A., and Virtanen, T.: Predicting catchment-scale methane fluxes with multi-source remote sensing, Landsc. Ecol., 36, 1177–1195, https://doi.org/10.1007/s10980-021-01194-x, 2021.

Rebmann, C., Göckede, M., Foken, T., Aubinet, M., Aurela, M., Berbigier, P., Bernhofer, C., Buchmann, N., Carrara, A., Cescatti, A., Ceulemans, R., Clement, R., Elbers, J. A., Granier, A., Grünwald, T., Guyon, D., Havránková, K., Heinesch, B., Knohl, A., Laurila, T., Longdoz, B., Marcolla, B., Markkanen, T., Miglietta, F., Moncrieff, J., Montagnani, L., Moors, E., Nardino, M., Ourcival, J.-M., Rambal, S., Rannik, Ü., Rotenberg, E., Sedlak, P., Unterhuber, G., Vesala, T., and Yakir, D.: Quality analysis applied on eddy covariance measurements at complex forest sites using footprint modelling, Theor. Appl. Climatol., 80, 121–141, https://doi.org/10.1007/s00704-004-0095-y, 2005.

Rey-Sanchez, C., Morin, T. H., Stefanik, K. C., Wrighton, K., and Bohrer, G.: Determining total emissions and environmental drivers of methane flux in a Lake Erie estuarine marsh, Ecol. Eng., 114, 7–15, https://doi.org/10.1016/j.ecoleng.2017.06.042, 2018.

Rey-Sanchez, C., Arias-Ortiz, A., Kasak, K., Chu, H., Szutu, D., Verfaillie, J., and Baldocchi, D.: Detecting hot spots of methane flux using footprint-weighted flux maps, J. Geophys. Res.-Biogeo., 127, e2022JG006977, https://doi.org/10.1029/2022JG006977, 2022.

Rey-Sanchez, C., Arias-Ortiz, A., Kasak, K., Shortt, R., Szutu, D., Verfaillie, J., Lorenson, T., Liira, M., Somelar, P., Espenberg, M., and Baldocchi, D.: Explaining hot spots of methane flux in a restored wetland: the role of water level, soil disturbance, and methanotrophy, Environ. Res. Lett., 20, 074064, https://doi.org/10.1088/1748-9326/ade45b, 2025.

Richardson, A. D. and Hollinger, D.: FLUXNET-CH4 US-Ho1 Howland Forest (main tower), FLUXNET [data set], https://doi.org/10.18140/FLX/1669675, 2020.

Richardson, A. D., Hollinger, D. Y., Burba, G. G., Davis, K. J., Flanagan, L. B., Katul, G. G., William Munger, J., Ricciuto, D. M., Stoy, P. C., Suyker, A. E., Verma, S. B., and Wofsy, S. C.: A multi-site analysis of random error in tower-based measurements of carbon and energy fluxes, Agric. For. Meteorol., 136, 1–18, https://doi.org/10.1016/j.agrformet.2006.01.007, 2006.

Richardson, A. D., Mahecha, M. D., Falge, E., Kattge, J., Moffat, A. M., Papale, D., Reichstein, M., Stauch, V. J., Braswell, B. H., Churkina, G., Kruijt, B., and Hollinger, D. Y.: Statistical properties of random CO2 flux measurement uncertainty inferred from model residuals, Agric. For. Meteorol., 148, 38–50, https://doi.org/10.1016/j.agrformet.2007.09.001, 2008.

Richardson, A. D., Hollinger, D. Y., Shoemaker, J. K., Hughes, H., Savage, K., and Davidson, E. A.: Six years of ecosystem-atmosphere greenhouse gas fluxes measured in a sub-boreal forest, Sci. Data, 6, 117, https://doi.org/10.1038/s41597-019-0119-1, 2019.

Rinne, J., Riutta, T., Pihlatie, M., Aurela, M., Haapanala, S., Tuovinen, J.-P., Tuittila, E.-S., and Vesala, T.: Annual cycle of methane emission from a boreal fen measured by the eddy covariance technique, Tellus B, 59, https://doi.org/10.3402/tellusb.v59i3.17009, 2007.

Riutta, T., Laine, J., Aurela, M., Rinne, J., Vesala, T., Laurila, T., Haapanala, S., Pihlatie, M., and Tuittila, E.-S.: Spatial variation in plant community functions regulates carbon gas dynamics in a boreal fen ecosystem, Tellus B, 59, 838, https://doi.org/10.1111/j.1600-0889.2007.00302.x, 2007.

Rößger, N., Wille, C., Holl, D., Göckede, M., and Kutzbach, L.: Scaling and balancing carbon dioxide fluxes in a heterogeneous tundra ecosystem of the Lena River Delta, Biogeosciences, 16, 2591–2615, https://doi.org/10.5194/bg-16-2591-2019, 2019.

Sachs, T., Wille, C., Boike, J., and Kutzbach, L.: Environmental controls on ecosystem-scale CH_4 emission from polygonal tundra in the Lena River Delta, Siberia, J. Geophys. Res., 113, https://doi.org/10.1029/2007jg000505, 2008.

Saunois, M., Martinez, A., Poulter, B., Zhang, Z., Raymond, P. A., Regnier, P., Canadell, J. G., Jackson, R. B., Patra, P. K., Bousquet, P., Ciais, P., Dlugokencky, E. J., Lan, X., Allen, G. H., Bastviken, D., Beerling, D. J., Belikov, D. A., Blake, D. R., Castaldi, S., Crippa, M., Deemer, B. R., Dennison, F., Etiope, G., Gedney, N., Höglund-Isaksson, L., Holgerson, M. A., Hopcroft, P. O., Hugelius, G., Ito, A., Jain, A. K., Janardanan, R., Johnson, M. S., Kleinen, T., Krummel, P. B., Lauerwald, R., Li, T., Liu, X., McDonald, K. C., Melton, J. R., Mühle, J., Müller, J., Murguia-Flores, F., Niwa, Y., Noce, S., Pan, S., Parker, R. J., Peng, C., Ramonet, M., Riley, W. J., Rocher-Ros, G., Rosentreter, J. A., Sasakawa, M., Segers, A., Smith, S. J., Stanley, E. H., Thanwerdas, J., Tian, H., Tsuruta, A., Tubiello, F. N., Weber, T. S., van der Werf, G. R., Worthy, D. E. J., Xi, Y., Yoshida, Y., Zhang, W., Zheng, B., Zhu, Q., Zhu, Q., and Zhuang, Q.: Global

Methane Budget 2000–2020, Earth Syst. Sci. Data, 17, 1873–1958, https://doi.org/10.5194/essd-17-1873-2025, 2025.

Schrier-Uijl, A. P., Kroon, P. S., Hensen, A., Leffelaar, P. A., Berendse, F., and Veenendaal, E. M.: Comparison of chamber and eddy covariance-based CO_2 and CH_4 emission estimates in a heterogeneous grass ecosystem on peat, Agric. For. Meteorol., 150, 825–831, https://doi.org/10.1016/j.agrformet.2009.11.007, 2010.

Sha, C., Mitsch, W. J., Mander, Ü., Lu, J., Batson, J., Zhang, L., and He, W.: Methane emissions from freshwater riverine wetlands, Ecol. Eng., 37, 16–24, https://doi.org/10.1016/j.ecoleng.2010.07.022, 2011.

Smeets, C. J. P. P., Holzinger, R., Vigano, I., Goldstein, A. H., and Röckmann, T.: Eddy covariance methane measurements at a Ponderosa pine plantation in California, Atmos. Chem. Phys., 9, 8365–8375, https://doi.org/10.5194/acp-9-8365-2009, 2009.

Stewart, G. A., Sharp, S. J., Taylor, A. K., Williams, M. R., and Palmer, M. A.: High spatial variability in wetland methane fluxes is tied to vegetation patch types, Biogeochemistry, https://doi.org/10.1007/s10533-024-01188-2, 2024.

Subke, J.-A., Kutzbach, L., and Risk, D.: Soil chamber measurements, in: Springer Handbook of Atmospheric Measurements, Springer International Publishing, Cham, 1603–1624, https://doi.org/10.1007/978-3-030-52171-4_60, 2021.

Tokida, T., Miyazaki, T., Mizoguchi, M., Nagata, O., Takakai, F., Kagemoto, A., and Hatano, R.: Falling atmospheric pressure as a trigger for methane ebullition from peatland, Global Biogeochem. Cycles, 21, https://doi.org/10.1029/2006GB002790, 2007.

Treat, C. C., Bloom, A. A., and Marushchak, M. E.: Nongrowing season methane emissions – a significant component of annual emissions across northern ecosystems, Glob. Change Biol., 24, 3331–3343, https://doi.org/10.1111/gcb.14137, 2018.

Tuovinen, J.-P., Aurela, M., Hatakka, J., Räsänen, A., Virtanen, T., Mikola, J., Ivakhov, V., Kondratyev, V., and Laurila, T.: Interpreting eddy covariance data from heterogeneous Siberian tundra: land-cover-specific methane fluxes and spatial representativeness, Biogeosciences, 16, 255–274, https://doi.org/10.5194/bg-16-255-2019, 2019.

Turetsky, M. R., Kotowska, A., Bubier, J., Dise, N. B., Crill, P., Hornibrook, E. R. C., Minkkinen, K., Moore, T. R., Myers-Smith, I. H., Nykänen, H., Olefeldt, D., Rinne, J., Saarnio, S., Shurpali, N., Tuittila, E.-S., Waddington, J. M., White, J. R., Wickland, K. P., and Wilmking, M.: A synthesis of methane emissions from 71 northern, temperate, and subtropical wetlands, Glob. Chang. Biol., 20, 2183–2197, https://doi.org/10.1111/gcb.12580, 2014.

Ueyama, M., Iwata, H., and Harazono, Y.: CO2 and CH4 fluxes data based on an automated-closed chamber system for a black spruce forest on permafrost in Fairbanks, Alaska, Arctic Data archive System (ADS) [data set], https://doi.org/10.17592/001.2021093001, 2022.

Ueyama, M., Iwata, H., Endo, R., and Harazono, Y.: Methane and carbon dioxide emissions from the forest floor of a black spruce forest on permafrost in interior Alaska, Polar Sci., 35, 100921, https://doi.org/10.1016/j.polar.2022.100921, 2023a.

Ueyama, M., Knox, S. H., Delwiche, K. B., Bansal, S., Riley, W. J., Baldocchi, D., Hirano, T., McNicol, G., Schafer, K., Windham-Myers, L., Poulter, B., Jackson, R. B., Chang, K.-Y., Chen, J., Chu, H., Desai, A. R., Gogo, S., Iwata, H., Kang, M., Mammarella, I., Peichl, M., Sonnentag, O., Tuittila, E.-S., Ryu, Y., Euskirchen, E. S., Göckede, M., Jacotot, A., Nilsson, M. B., and Sachs, T.: Modeled production, oxidation, and transport processes of wetland methane emissions in temperate, boreal, and Arctic regions, Glob. Chang. Biol., 29, 2313–2334, https://doi.org/10.1111/gcb.16594, 2023b.

van den Berg, M., van den Elzen, E., Ingwersen, J., Kosten, S., Lamers, L. P. M., and Streck, T.: Contribution of plant-induced pressurized flow to CH4 emission from a Phragmites fen, Sci. Rep., 10, 12304, https://doi.org/10.1038/s41598-020-69034-7, 2020.

van der Nat, F.-F. W. A., Middelburg, J. J., Van Meteren, D., and Wielemakers, A.: Diel methane emission patterns from Scirpus lacustris and Phragmites australis, Biogeochemistry, 41, 1–22, https://doi.org/10.1023/a:1005933100905, 1998.

Vargas, R.: AmeriFlux US-StJ St Jones Reserve, AmeriFlux, University of Delaware [data set], https://doi.org/10.17190/AMF/1480316, 2018.

Vargas, R. and Le, V. H.: The paradox of assessing greenhouse gases from soils for nature-based solutions, Biogeosciences, 20, 15–26, https://doi.org/10.5194/bg-20-15-2023, 2023.

Vázquez-Lule, A. and Vargas, R.: Biophysical drivers of net ecosystem and methane exchange across phenological phases in a tidal salt marsh, Agric. For. Meteorol., 300, 108309, https://doi.org/10.1016/j.agrformet.2020.108309, 2021.

Venterea, R. T., Spokas, K. A., and Baker, J. M.: Accuracy and precision analysis of chamber-based nitrous oxide gas flux estimates, Soil Sci. Soc. Am. J., 73, 1087–1093, https://doi.org/10.2136/sssaj2008.0307, 2009.

Vesala, T., Kljun, N., Rannik, U., Rinne, J., Sogachev, A., Markkanen, T., Sabelfeld, K., Foken, T., and Leclerc, M. Y.: Flux and concentration footprint modelling: state of the art, Environ. Pollut., 152, 653–666, https://doi.org/10.1016/j.envpol.2007.06.070, 2008.

Vesala, T., Tuittila, E.-S., Mammarella, I., and Alekseychik, P.: FLUXNET-CH4 FI-Si2 Siikaneva-2 Bog, FLUXNET [data set], https://doi.org/10.18140/FLX/1669639, 2020.

Villa, J. A., Ju, Y., Stephen, T., Rey-Sanchez, C., Wrighton, K. C., and Bohrer, G.: Plant-mediated methane transport in emergent and floating-leaved species of a temperate freshwater mineral-soil wetland, Limnol. Oceanogr., 65, 1635–1650, 2020.

Villa, J. A., Ju, Y., Yazbeck, T., Waldo, S., Wrighton, K. C., and Bohrer, G.: Ebullition dominates methane fluxes from the water surface across different ecohydrological patches in a temperate freshwater marsh at the end of the growing season, Sci. Total Environ., 767, 144498, https://doi.org/10.1016/j.scitotenv.2020.144498, 2021.

Virkkala, A.-M., Virtanen, T., Lehtonen, A., Rinne, J., and Luoto, M.: The current state of CO_2 flux chamber studies in the Arctic tundra: A review, Progress in Physical Geography: Earth and Environment, 42, 162–184, https://doi.org/10.1177/0309133317745784, 2018.

Voigt, C., Virkkala, A.-M., Hould Gosselin, G., Bennett, K. A., Black, T. A., Detto, M., Chevrier-Dion, C., Guggenberger, G., Hashmi, W., Kohl, L., Kou, D., Marquis, C., Marsh, P., Marushchak, M. E., Nesic, Z., Nykänen, H., Saarela, T., Sauheitl, L., Walker, B., Weiss, N., Wilcox, E. J., and Sonnentag, O.: Arctic soil methane sink increases with drier conditions and

higher ecosystem respiration, Nat. Clim. Chang., 13, 1095–1104, https://doi.org/10.1038/s41558-023-01785-3, 2023.

Vroom, R. J. E., van den Berg, M., Pangala, S. R., van der Scheer, O. E., and Sorrell, B. K.: Physiological processes affecting methane transport by wetland vegetation – A review, Aquat. Bot., 182, 103547, https://doi.org/10.1016/j.aquabot.2022.103547, 2022.

Waddington, J. M. and Roulet, N. T.: Carbon balance of a boreal patterned peatland, Glob. Change Biol., 6, 87–97, https://doi.org/10.1046/j.1365-2486.2000.00283.x, 2000.

Wang, J., Luo, Y., Quan, Q., Ma, F., Tian, D., Chen, W., Wang, S., Yang, L., Meng, C., and Niu, S.: Effects of warming and clipping on CH_4 and N_2O fluxes in an alpine meadow, Agric. For. Meteorol., 297, 108278, https://doi.org/10.1016/j.agrformet.2020.108278, 2021.

Wang, J. M., Murphy, J. G., Geddes, J. A., Winsborough, C. L., Basiliko, N., and Thomas, S. C.: Methane fluxes measured by eddy covariance and static chamber techniques at a temperate forest in central Ontario, Canada, Biogeosciences, 10, 4371–4382, https://doi.org/10.5194/bg-10-4371-2013, 2013.

Whiting, G. J. and Chanton, J. P.: Control of the diurnal pattern of methane emission from emergent aquatic macrophytes by gas transport mechanisms, Aquat. Bot., 54, 237–253, https://doi.org/10.1016/0304-3770(96)01048-0, 1996.

Wille, C., Kutzbach, L., Sachs, T., Wagner, D., and Pfeiffer, E.-M.: Methane emission from Siberian arctic polygonal tundra: eddy covariance measurements and modeling: methane emission from Siberian arctic tundra, Glob. Chang. Biol., 14, 1395–1408, https://doi.org/10.1111/j.1365-2486.2008.01586.x, 2008.

Xu, K., Metzger, S., and Desai, A. R.: Surface-atmosphere exchange in a box: Space-time resolved storage and net vertical fluxes from tower-based eddy covariance, Agric. For. Meteorol., 255, 81–91, https://doi.org/10.1016/j.agrformet.2017.10.011, 2018.

Yeo, I. and Johnson, R. A.: A new family of power transformations to improve normality or symmetry, Biometrika, 87, 954–959, https://doi.org/10.1093/BIOMET/87.4.954, 2000.

Yu, L., Wang, H., Wang, G., Song, W., Huang, Y., Li, S.-G., Liang, N., Tang, Y., and He, J.-S.: A comparison of methane emission measurements using Eddy Covariance and manual and automated chamber-based techniques in Tibetan Plateau alpine wetland, Environ. Pollut., 181, 81–90, https://doi.org/10.1016/j.envpol.2013.06.018, 2013.

Yuan, K., Li, F., McNicol, G., Chen, M., Hoyt, A., Knox, S., Riley, W. J., Jackson, R., and Zhu, Q.: Boreal-Arctic wetland methane emissions modulated by warming and vegetation activity, Nat. Clim. Chang., 14, 282–288, https://doi.org/10.1038/s41558-024-01933-3, 2024.

Zhang, Y., Sachs, T., Li, C., and Boike, J.: Upscaling methane fluxes from closed chambers to eddy covariance based on a permafrost biogeochemistry integrated model, Glob. Chang. Biol., 18, 1428–1440, https://doi.org/10.1111/j.1365-2486.2011.02587.x, 2012.

Zhao, K., Ma, B., Xu, Y., Stirling, E., and Xu, J.: Light exposure mediates circadian rhythms of rhizosphere microbial communities, ISME J., 15, 2655–2664, https://doi.org/10.1038/s41396-021-00957-3, 2021.

Zhu, Q., Yuan, K., Li, F., Riley, W. J., Hoyt, A., Jackson, R., McNicol, G., Chen, M., Knox, S. H., Briner, O., Beerling, D., Gedney, N., Hopcroft, P. O., Ito, A., Jain, A. K., Jensen, K., Kleinen, T., Li, T., Liu, X., McDonald, K. C., Melton, J. R., Miller, P. A., Müller, J., Peng, C., Poulter, B., Qin, Z., Peng, S., Tian, H., Xu, X., Yao, Y., Xi, Y., Zhang, Z., Zhang, W., Zhu, Q., and Zhuang, Q.: Critical needs to close monitoring gaps in pantropical wetland CH_4 emissions, Environ. Res. Lett., 19, 114046, https://doi.org/10.1088/1748-9326/ad8019, 2024.